



Methyl rotor analysis as a function of electronic state, conformation and functionality in indoles and stilbenes

by Sonja Sue Siewert

A thesis submitted in partial fulfillment of the requirements for the degree of Doctor of Philosophy in Chemistry

Montana State University

© Copyright by Sonja Sue Siewert (1994)

Abstract:

A normal mode and methyl torsional analysis as a function of electronic state, substituent effects and extent of conjugation has been performed using one and two-photon fluorescence excitation and dispersed fluorescence techniques. The methyl rotor barrier is used as a probe of the local π electron density and is found to be very sensitive to substituents ten carbons away, along with the nature of the electronic state.

3-methylindole, 3-trideuterio-methylindole, and 5-methylindole were examined for their methyl rotor structure. The indoles have two close-lying electronic states, 1La and 1Lb. The 5MI 1Lb methyl barrier is $V_3 = 80 \text{ cm}^{-1}$ with a V_6 contribution of -21 cm^{-1} . Methyl barriers were also found for complexes of 5MI with water and helium, which aid in identifying the site of complexation. The barrier for 3MI for 1Lb is $V_3 = 306.6 \text{ cm}^{-1}$, $V_6 = -10.9 \text{ cm}^{-1}$, with a ground state barrier of 443.2 cm^{-1} .

Substituted trans-stilbenes were examined because the extent of conjugation allows the study of electronic effects rather than steric interferences for the methyl group. The trans-stilbenes examined, are: p-methyl-trans-stilbene, p-methoxy-trans-stilbene, p'-methoxy-p-methyl-trans-stilbene, p'-chloro-p-methyl-trans-stilbene, p'-fluoro-p-methyl-trans-stilbene and p'-chloro-m-methyl-trans-stilbene. The molecules were chosen for the electron donating and withdrawing capabilities of the substituents. The low-frequency skeletal modes, torsional transitions, and the methyl barriers for the S0 and S1 states are assigned. The spectra for the methoxy-stilbenes displays two electronic origins, indicating the presence of two preferred conformers for the methoxy group. The methyl barriers for the two p'-methoxy-p-methyl-trans-stilbene conformers differ by 12 cm^{-1} , showing extreme sensitivity to the conformation of the methoxy group ten carbons away, different by 12 cm^{-1} . The excited state torsional barrier for p-methyl-trans-stilbene is 150 cm^{-1} , and the barrier decreases for every substituted trans-stilbene examined, indicating that the methyl hyperconjugation is extremely sensitive to π electronic effects through the extended conjugated system.

METHYL ROTOR ANALYSIS AS A FUNCTION OF ELECTRONIC STATE,
CONFORMATION AND FUNCTIONALITY IN INDOLES AND STILBENES

by

Sonja Sue Siewert

A thesis submitted in partial fulfillment
of the requirements for the degree

of

Doctor of Philosophy

in

Chemistry

MONTANA STATE UNIVERSITY
Bozeman, Montana

April 1994

D378
Si 195

APPROVAL

of a thesis submitted by

Sonja Sue Siewert

This thesis has been read by each member of the thesis committee and has been found to be satisfactory regarding content, English usage, format, citations, bibliographic style, and consistency, and is ready for submission to the College of Graduate Studies.

4/21/94
Date

Lee H. Brangler
Chairperson, Graduate Committee

Approved for the Major Department

4/21/94
Date

David M. Dooley
Head, Major Department

Approved for the College of Graduate Studies

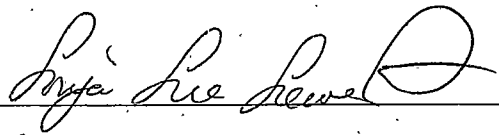
4/28/94
Date

R. Brown
Graduate Dean

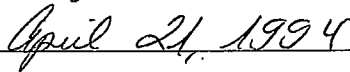
STATEMENT OF PERMISSION TO USE

In presenting this thesis in partial fulfillment of the requirements for a doctoral degree at Montana State University, I agree that the Library shall make it available to borrowers under rules of the Library. I further agree that copying of this thesis is allowable only for scholarly purposes, consistent with "fair use" as prescribed in the U.S. Copyright Law. Requests for extensive copying or reproduction of this thesis should be referred to University Microfilms International, 300 North Zeeb Road, Ann Arbor, Michigan 48106, to whom I have granted "the exclusive right to reproduce and distribute my dissertation for sale in and from microform or electronic format, along with the right to reproduce and distribute my abstract in any format in whole or in part."

Signature



Date



ACKNOWLEDGMENTS

I would like to express my appreciation to all of the people who have supported me during the past four and a half years here at Montana State University. I wish to thank my advisor Dr. Lee H. Spangler for his support in my development as a physical chemist. The members of my committee have been supportive, with special thanks to Dr. Patrik Callis. I wish to thank Dr. David Sammeth for convincing me that I really could do this, and not to be intimidated. He gave me the trust that I needed to go ahead and try new things. Several Spangler and Callis group members have made my time here interesting, from friendships to incredible science discussions, special thanks to Dr. Pedro Muino, Mr. Jim Vivian, Mr. Brian Metzger and the other members of the physical chemistry division. The collaborative efforts and friendships with the other chemists in the department are much appreciated.

I would also like to thank those special people who know what real friendships are about. My memories from graduate school here in Bozeman will be mostly positive due to you. Most of all I would like to thank my parents and family for believing in me and supporting me in this endeavor. They instilled in me the fact at an early age that it is possible to accomplish one's goals in life.

TABLE OF CONTENTS

	Page
1. INTRODUCTION	1
Statement of the Problem	3
2. METHYL ROTOR THEORY AND HISTORY	6
3. EXPERIMENTAL PROCEDURES	18
Compounds	18
Sample Preparation	20
1hv and 2hv Theory	23
Experimental Apparatus	25
4. EXPERIMENTAL RESULTS: INDOLES	35
5-methylindole Experimental Results	36
3-methylindole and 3-CD ₃ -indole	39
5. DISCUSSION: METHYLINDOLES	42
5-methylindole	42
3-methylindole	51
6. EXPERIMENTAL RESULTS: STILBENES	58
Experimental Results	61
p-methyl-trans-stilbene	61
p-methoxy-trans-stilbene	67
p'-methoxy-p-methyl-trans-stilbene	75
p'-chloro-p-methyl-trans-stilbene	84
p'-fluoro-p-methyl-trans-stilbene	90
p'-chloro-m-methyl-trans-stilbene	95

TABLE OF CONTENTS-Continued

	Page
7. DISCUSSION: STILBENES	103
p-methyl-trans-stilbene	104
The Methoxy Conformation in para-methoxy-stilbenes	106
Comparison of Vibrations	113
Methyl Rotor Analysis	119
8. CONCLUSION	123
REFERENCES CITED	126

LIST OF TABLES

Table	Page
1. The G_6 molecular symmetry table	8
2. The internal rotation angular momentum quantum number relating to the symmetry of the torsional state with G_6 symmetry	10
3. The melting points and temperature in $^{\circ}\text{C}$ needed to obtain sufficient vapor pressure.	22
4. Calculated barriers and experimental and calculated transition frequencies for 5-methylindole and complexes.	46
5. Calculated frequencies and intensities for the 1L_b of 3-methylindole using two different ground-state barriers. ($V_3 = 307.6 \text{ cm}^{-1}$, $V_6 = -10.9 \text{ cm}^{-1}$ and $B = 5.30 \text{ cm}^{-1}$)	55
6. The symmetry correlation between C_{2h} and C_s	61
7. Torsional frequencies for p-methyl-trans-stilbene.	63
8. The major vibrational frequencies for the S_1 states of p-methoxy-trans-stilbene.	71
9. The torsional and vibrational frequencies for S_0 and S_1 of the A and B conformers of p'-methoxy-p-methyl-trans-stilbene. The ground state frequencies are expressed as combination differences.	83
10. The experimental and calculated frequencies and intensities for the A and B conformers in S_1 for p'-methoxy-p-methyl-trans-stilbene.	84

LIST OF TABLES: continued

Table	Page
11. The experimental and calculated frequencies/intensities for p'-chloro-p-methyl-trans-stilbene. ($V'_3 = 104.3 \text{ cm}^{-1}$, $V'_6 = 4.9 \text{ cm}^{-1}$, 60° conformation change.)	88
12. The calculated and experimental torsional frequencies for p'-fluoro-p-methyl-trans-stilbene. ($V'_3 = 100.5 \text{ cm}^{-1}$, $V'_6 = 12 \text{ cm}^{-1}$)	91
13. The experimental and calculated frequencies and intensities for the A isomer of p'-chloro-m-methyl-trans-stilbene.	98
14. The experimental and calculated frequencies and intensities for the B isomer of p'-chloro-m-methyl-trans-stilbene.	99
15. Experimental and calculated frequencies and intensities for the S_1 state of p-methyl-trans-stilbene. The 60° and 30° refer to the conformation change of the methyl group upon excitation.	106
16. Heats of formation calculated for p-methoxy-trans-stilbene from AMPAC AM1.	108
17. Relative intensities for the torsional progressions in p'-methoxy-p-methyl-trans-stilbene. (each progression lists relative intensities to each origin progression.)	113
18. The ground state low-frequency vibrational assignments for trans-stilbenes. Expressed as cm^{-1} above the vibrationless level.	114
19. The excited state low-frequency vibrational assignments for trans-stilbenes. Expressed as cm^{-1} above 0_0^0	117
20. Dimensionless displacements for ν_{25} in the stilbene analogues.	118
21. Methyl rotor barriers and conformation changes upon excitation for stilbene analogues.	121

LIST OF FIGURES

Figure		Page
1.	The indole and stilbene analogues examined in this study.	4
2.	Methyl rotor splitting as a function of V_3 barrier height.	11
3.	The potential barrier for S_0 and S_1 for the hindered methyl rotor in p-methyl-trans-stilbene.	14
4.	The supersonic jet expansions	22
5.	The process of fluorescence for isolated molecules.	23
6.	The process of dispersed fluorescence.	25
7.	The apparatus for 1hv fluorescence excitation experiments	27
8.	The apparatus for dispersed fluorescence experiments utilizing the CCD detection system.	30
9.	Comparison of the scanning 0.25 meter monochromator dispersed fluorescence apparatus versus the CCD/0.5 meter monochromator system from exciting the B origin of p-methoxy-trans-stilbene.	32
10.	The experimental apparatus for 2hv fluorescence spectroscopy.	33
11.	The 1hv fluorescence excitation spectrum of 5-methylindole.	38
12.	The 1hv fluorescence excitation spectrum of 3-methylindole.	40
13.	The 1hv fluorescence excitation spectrum of 3-trideuterio-methylindole.	41

LIST OF FIGURES: continued

Figure	Page
14. The low frequency region of the 5-methylindole spectrum (top). Two-photon contours of the first four transitions using both linearly and circularly polarized light are shown at the bottom. These contours span 9 cm^{-1} with tic marks appearing every 0.5 cm^{-1} .	43
15. Torsional progression for 5-methylindole helium complexes, with a water complex progression on the bottom trace. The torsional levels show a measurable change in their relative frequencies.	48
16. Comparison of the weak peaks in the low frequency region of the 3MI and 3MI- CD_3 spectra. The transitions correlate as indicated by the tie lines.	52
17. Plots of excited-state combination differences (same as relative frequencies) vs. a V_3 barrier height. The corresponding 3MI spectra are shown plotted to the same frequency scale indicating the assignment of the torsional transitions and the approximate barrier height.	54
18. Low frequency modes of trans-stilbene.	60
19. The $1h\nu$ fluorescence excitation spectrum of p-methyl-trans-stilbene.	62
20. $1h\nu$ fluorescence excitation spectra of p-methyl-trans-stilbene under different expansion conditions.	64
21. The linearly polarized $2h\nu$ contour of the origin of p-methyl-trans-stilbene on the top trace with the fluorescence excitation contour below.	66
22. The $1h\nu$ fluorescence excitation spectrum of p-methoxy-trans-stilbene.	68
23. A vs. B conformer spectra for p-methoxy-trans-stilbene.	69
24. The dispersed fluorescence from the origins of the A and B conformers of p-methoxy-trans-stilbene.	72
25. The dispersed fluorescence spectra of the low-frequency vibrations for the A and B conformers of p-methoxy-trans-stilbene.	74

LIST OF FIGURES: continued

Figure		Page
26.	The 1hv FE spectrum of p'-methoxy-p-methyl-trans-stilbene. The conformer origins are identified with labels A and B.	77
27.	The first 300 cm ⁻¹ of the 1hv FE spectrum for each conformer. Note that the B conformer origin has been placed directly under the A origin for comparison purposes.	78
28.	The DE from the A conformer torsional features of p'-methoxy-p-methyl-trans-stilbene.	80
29.	The DE from the 0a ₁ , 1e, 2e and 3a ₁ transitions for the B conformer of p'-methoxy-p-methyl-trans-stilbene.	82
30.	The 1hv FE spectrum of p'-chloro-p-methyl-trans-stilbene.	86
31.	The DE of the 0 ₀ ⁰ methyl rotor structure for p'-chloro-p-methyl-trans-stilbene.	89
32.	The 1hv FE spectrum of p'-fluoro-p-methyl-trans-stilbene.	92
33.	The DF of the rotor levels for p'-fluoro-p-methyl-trans-stilbene.	93
34.	The DF from 24 ¹ and 25 ¹ for p'-fluoro-p-methyl-trans-stilbene.	94
35.	The 1hv FE spectrum of p'-chloro-m-methyl-trans-stilbene. The first isomer is labeled A and the second isomer is labeled B. Tie lines indicate torsional structure.	96
36.	The DE for the A isomer of p'-chloro-m-methyl-trans-stilbene.	100
37.	The DE for the B origin of p'-chloro-m-methyl-trans-stilbene.	101
38.	Dispersed fluorescence from the "X" transitions of p-methoxy-trans-stilbene.	110
39.	The B-25 ¹ ₀ 37 ² ₀ Fermi resonance of p-methoxy-trans-stilbene. The 1hv trace is on the top, the dispersed fluorescence from both transitions below.	112

ABSTRACT

A normal mode and methyl torsional analysis as a function of electronic state, substituent effects and extent of conjugation has been performed using one and two-photon fluorescence excitation and dispersed fluorescence techniques. The methyl rotor barrier is used as a probe of the local π electron density and is found to be very sensitive to substituents ten carbons away, along with the nature of the electronic state.

3-methylindole, 3-trideuterio-methylindole, and 5-methylindole were examined for their methyl rotor structure. The indoles have two close-lying electronic states, 1L_a and 1L_b . The 5MI 1L_b methyl barrier is $V_3 = 80 \text{ cm}^{-1}$ with a V_6 contribution of -21 cm^{-1} . Methyl barriers were also found for complexes of 5MI with water and helium, which aid in identifying the site of complexation. The barrier for 3MI for 1L_b is $V_3 = 306.6 \text{ cm}^{-1}$, $V_6 = -10.9 \text{ cm}^{-1}$, with a ground state barrier of 443.2 cm^{-1} .

Substituted trans-stilbenes were examined because the extent of conjugation allows the study of electronic effects rather than steric interferences for the methyl group. The trans-stilbenes examined are: p-methyl-trans-stilbene, p-methoxy-trans-stilbene, p'-methoxy-p-methyl-trans-stilbene, p'-chloro-p-methyl-trans-stilbene, p'-fluoro-p-methyl-trans-stilbene and p'-chloro-m-methyl-trans-stilbene. The molecules were chosen for the electron donating and withdrawing capabilities of the substituents. The low-frequency skeletal modes, torsional transitions, and the methyl barriers for the S_0 and S_1 states are assigned. The spectra for the methoxy-stilbenes displays two electronic origins, indicating the presence of two preferred conformers for the methoxy group. The methyl barriers for the two p'-methoxy-p-methyl-trans-stilbene conformers differ by 12 cm^{-1} , showing extreme sensitivity to the conformation of the methoxy group ten carbons away, different by 12 cm^{-1} . The excited state torsional barrier for p-methyl-trans-stilbene is 150 cm^{-1} , and the barrier decreases for every substituted trans-stilbene examined, indicating that the methyl hyperconjugation is extremely sensitive to π electronic effects through the extended conjugated system.

CHAPTER ONE

INTRODUCTION

Spectroscopy is the study of the interaction of electromagnetic radiation with matter.¹ The broad range of energies in the electromagnetic spectrum allows scientists to examine the fundamental chemistry and physics of matter. The work in this thesis utilizes the visible and ultraviolet region. In this wavelength region, the interaction of light with matter is known as electronic spectroscopy, where the higher energy light promotes the redistribution of electrons in the molecule. Molecules and atoms absorb the ultraviolet and visible light at a resonant energy, and then the energy is lost through fluorescence or phosphorescence. Fluorescence is detected in the research presented here, and from the resulting spectra, the molecular structure and chemical reactivity can be examined. With the advent of moderate resolution tunable dye lasers and supersonic expansions, several issues that previously could not be examined can now be addressed.

One area which can now be examined is the internal rotation of methyl groups. The torsion of a methyl group is interesting since it is intrinsically different in its behavior than other normal modes of vibration, and often is the driving force of many of the dynamics for molecules.²⁻⁴ Vibrations, such as the stretching and bending motions of functional groups common in organic chemistry, are commonly examined using infrared spectroscopy. The

methyl group is unique in that it is an internal rotation of low frequency and large amplitude. The internal modes are typically anharmonic in behavior, making spectral analysis more challenging. Before the advent of supersonic expansions to introduce the sample to the exciting radiation, these low frequency torsional transitions were often unresolvable in the electronic spectrum due to spectral congestion. The expansion forces the vibrational and rotational temperatures to be dramatically reduced, thus only the lowest levels of the ground state molecule are populated prior to excitation, making the excitation spectrum much less congested.

The potential energy surface that describes the torsional coordinates often changes upon electronic excitation. The methyl group will frequently have a conformational (or phase) change upon excitation, typically 30° or 60° due to the the three equivalent hydrogens and the resulting symmetry. The light hydrogens and low barriers of the methyl group result in torsional tunneling, and because of this rigid molecular point group symmetry cannot be used to describe this internal motion, and instead non-rigid group theoretical methods are utilized.

The methyl group typically does not rotate freely, the motion is usually hindered. This barrier to internal motion was originally examined using microwave spectroscopy⁵ (which obtains ground state information), and with the improved technology available for electronic spectroscopy, the examination of the methyl barrier in excited states is possible. The contributing factors to these barriers have been under examination for several years and is the topic of this thesis. The interactions of the methyl group with the π molecular orbitals is one contribution to the barrier, and is strongly influenced by the local π electron density.

Statement of the Problem

The goal of this research is to examine the sensitivity of the methyl group to the local π electron density in molecules with more than a single aromatic ring. The sensitivity of the methyl group to the local π electron density has been studied in several single ring systems,^{2, 6-11} however it has not been examined in extended conjugated systems. In single ring systems, steric effects can be a strong factor in hindering the methyl torsion. By expanding the studies to extended conjugated systems, the methyl group should be more strongly influenced by electronic effects than steric effects. This thesis presents a study of the analysis of the barrier to internal rotation for the methyl group as a function of electronic state and conformational changes, site of the methyl rotor, substituent effects and van der Waals complexes for several indole and stilbene analogues. The barrier to internal rotation is obtained by analyzing the fluorescence spectra for all of these molecules, and conclusions will be made regarding the above effects on the barrier to internal rotation. With further understanding of the methyl group and the effects of the local π electron density upon its rotation, it is hoped that the methyl group can be used as a probe of the local π electron density in aromatic compounds.

Figure one shows the indole and stilbene derivatives that will be examined in this study. The specific reasons why these molecules were chosen will be discussed in their respective chapters. Briefly, indole is the chromophore of the amino acid tryptophan, and has two-close lying electronic states. Information regarding these electronic states is important because tryptophan is responsible for the majority of the fluorescence in proteins.¹² The indole analogues examined in this thesis are 5-methylindole, 3-methylindole, and 3-trideuterio-

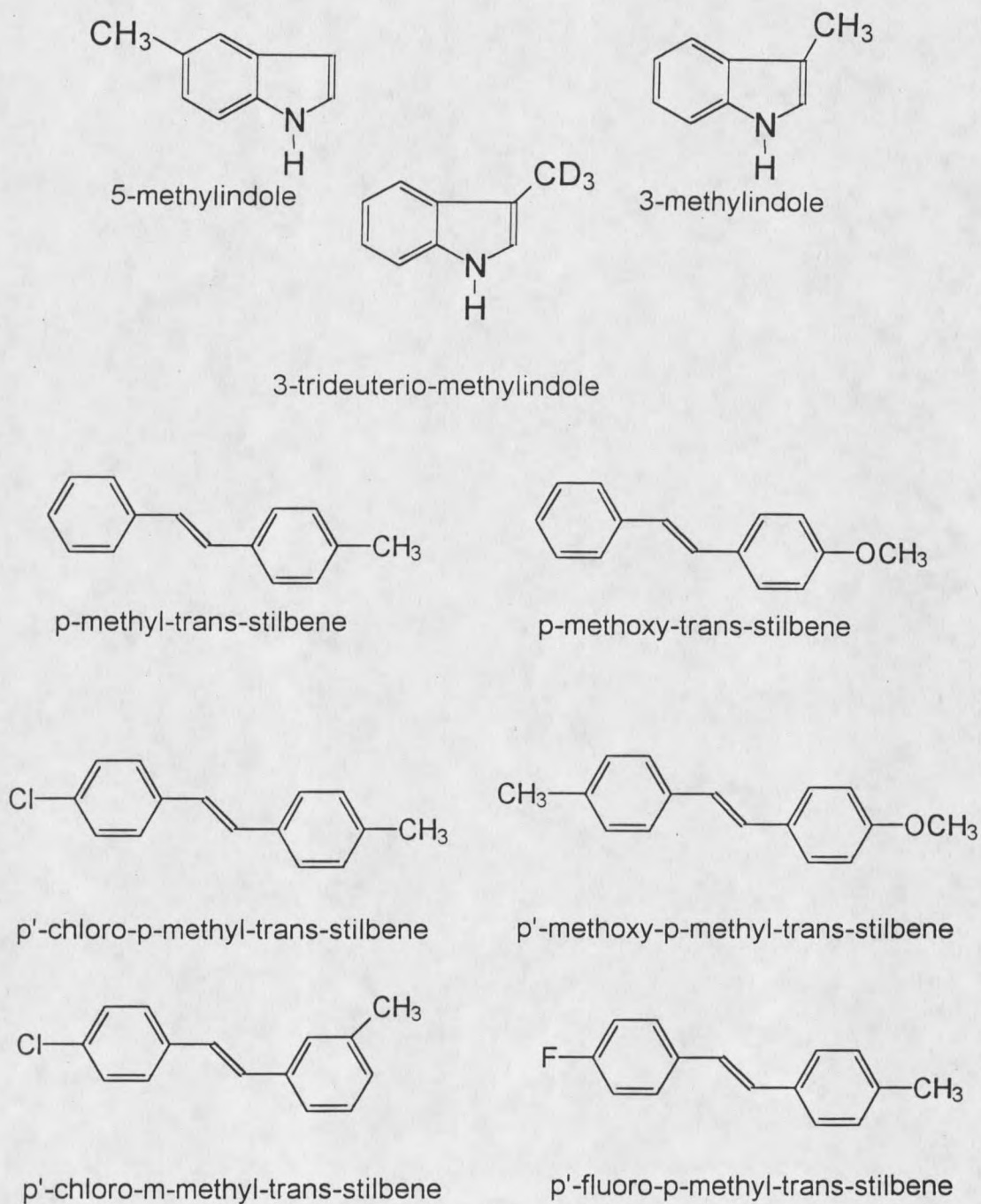


Figure 1: The indole and stilbene analogues examined in this study.

methylindole. The spectra of these methylated indoles exhibit characteristics due to hindered internal rotation of the methyl group along with dynamics driven by the methyl group.

The second group of molecules examined are the stilbenes. Stilbene is the prototypical model for the study of reaction dynamic in the gas phase, and undergoes cis/trans photoisomerization.¹³ Stilbene has an extended π conjugated system which makes it an ideal system to examine electronic effects since the π system is delocalized, even more so in the excited state, and it should allow substituents on one phenyl ring to affect the π electron density on the other phenyl ring. These effects can then be measured by the methyl barrier. Spectral analysis in stilbenes is made more difficult by several low-frequency vibrations, and these vibrational assignments will be made for the stilbene analogues. The stilbenes examined in this study are also shown in Figure one and are: p-methyl-trans-stilbene, p-methoxy-trans-stilbene, p'-methoxy-p-methyl-trans-stilbene, p'-chloro-p-methyl-trans-stilbene, p'-chloro-m-methyl-trans-stilbene and p'-fluoro-p-methyl-trans-stilbene.

CHAPTER TWO

METHYL ROTOR THEORY AND HISTORY

Methyl groups are attached to their parent molecule by a single bond resulting in a possibility for internal rotation. This rotation is not necessarily free and several factors can contribute to the barrier including steric and π electronic effects. Microwave spectroscopy⁵ results were used for many years to determine the barrier in the ground state, however, the advent of supersonic jet molecular laser spectroscopy has allowed the investigation of the methyl group in other electronic states by reducing the spectral congestion. The barriers obtained for ground and excited electronic states and in different molecules can then be compared to examine how functionality, conformation, the extent of conjugation, and other factors effect the barrier. The barrier therefore can be utilized as a probe of the local electron density in the molecule.¹⁴

If the methyl group is treated as a rigid body, able to rotate freely with fixed bond angles and distances, the Hamiltonian is that of a particle-in-a-ring, where ϕ is the internal rotation angle.

$$H = -B \frac{d^2}{d\phi^2}$$

The eigenvalues for this Hamiltonian are m^2B , where $m = 0, \pm 1, \pm 2, \dots$, and B is the internal rotation constant $B = \hbar^2/2I_\phi$, where I_ϕ is the reduced moment of inertia $I_\phi = [(I_{\text{CH}_3}I_{\text{frame}})/(I_{\text{CH}_3} + I_{\text{frame}})]$.^{4,5} In most of the molecules with methyl rotors, there is at least a small barrier to internal rotation. The barrier can be describe using a Fourier series of $\cos(n3\phi)$ terms where $n = 1, 2, \dots$, ϕ is the internal rotation angle, and the 3 comes from the threefold rotational symmetry of the methyl group. The Schrödinger equation for torsional motion is

$$-B \frac{d^2 \Psi}{d\phi^2} + V\phi = E \Psi$$

The appropriate basis set is the free rotor representation:

$$\Psi = \frac{1}{\sqrt{2\pi}} e^{im\phi}, \quad m = 0, \pm 1, \pm 2, \dots$$

The potential energy of the torsional motion can be described using the following expression.

$$H_1 = V(\phi) = \frac{V_3}{2}(1 - \cos 3\phi) + \frac{V_6}{2}(1 - \cos 6\phi) + \dots$$

The first non-zero term in this series will depend on the number of equivalent conformations. For example, in toluene¹⁵ the methyl has threefold symmetry about the rotor axis (phenyl-methyl bond) and the ring has twofold symmetry about the same axis giving rise to six equivalent conformations. Therefore, V_6 will be the first non-zero term. In the molecules studied here, V_3 will typically be the dominant term. V_3 will determine the height

of the potential, while V_6 will determine the shape of the wells. Contributions from V_9 are minimal.

Owing to the multiple minima along the CH_3 torsional coordinate, the relatively low barriers, and the low mass of the hydrogen atoms involved, tunneling can occur between the wells, which makes point-group theory inadequate in treating the symmetry of these non-rigid molecules.^{16,17} The tunneling represents an exchange or permutation of nuclei, and the molecular symmetry groups developed by Longuet-Higgins and Bunker must be used. If all possible nuclear permutations and inversions are used, the group used is the complete nuclear permutation and inversion (CNPI) group. Many of the CNPI operations are physically unlikely and can be discarded, resulting in the molecular symmetry group. In every molecule examined in this study, the CH_3 groups can best be described using G_6 symmetry, which is isomorphic with the C_{2v} group. See Table 1 for the G_6 symmetry table.

Table 1: The G_6 molecular symmetry table.

G_6	E	(123)	(23)*
		(321)	(12)*
			(31)*
	[1]	[2]	[3]
A_1	1	1	1
A_2	1	1	-1
E	2	-1	0

In the case of low-medium barriers ($1-300 \text{ cm}^{-1}$), the tunneling interaction of the rotor wave functions splits the triply degenerate levels from the harmonic oscillator basis set (which describes an infinitely high barrier with triply degenerate levels compared to the free rotor where the torsional levels are as $E = m^2B$) into singly and doubly degenerate levels (a_1 or a_2 and e). The energy levels of the methyl rotor will be labeled by the above internal rotation angular momentum quantum number m and the symmetry of the level. See Table 2 for a description of how the internal rotation angular momentum quantum number relates to the symmetry of the torsional state. In terms increasing energy the torsional levels for the methyl rotor are: $0a_1, 1e, 2e, 3a_2, 3a_1, 4e, 5e, \dots$ ¹⁴ These labels will be used throughout as identification of the methyl rotor levels. To identify the torsional levels, the basis set used is the free rotor representation shown above, and it can be solved where:

$$e^{+im\theta} + e^{-im\theta} = \cos(m\theta) + i \sin(m\theta) + \cos(m\theta) - i \sin(m\theta) = 2 \cos(m\theta)$$

The use of a supersonic jet expansion, discussed in chapter three, to introduce the sample ensures that we will be populating only the lowest levels for the methyl rotor, these being the $0a_1$ and $1e$ levels. Torsional selection rules for electronic transitions state that in transitions for the methyl rotor, like must go to like. Therefore, transitions starting in the $1e$ level can only go to other E levels, A_1 to A_1 levels. The A_1 and E species are different nuclear spin isomers of the same molecule, and the differences in their selection rules are useful in interpreting a spectrum.⁵ Another difference is that A levels are nondegenerate and the E levels are doubly degenerate. In G_6 , the A_1 and A_2 torsions have A_1 nuclear spin symmetry and have a statistical weight of 8. Torsions with E symmetry must have a nuclear spin symmetry

statistical weight of 4. Hence, the A_1 and E levels cannot cool into one another in the expansion resulting in two spin isomers and simplifying the identification of spectra through fluorescence excitation and dispersed fluorescence work.⁴

Table 2: The internal rotation angular momentum quantum number relating to the symmetry of the torsional state with G_6 symmetry.

	E	(123)	(23)*	
	$\tau_{\Theta=0}$	$\tau+240$	τ	
m	$2\cos m\Theta$	$2\cos m\Theta$		
0	1	1	1	A_1
± 1	2	-1	0	E
± 2	2	-1	0	E
± 3	2	2	0	$A_1 + A_2$
± 4	2	-1	0	E
± 5	2	-1	0	E
± 6	2	2	0	$A_1 + A_2$

For levels with A symmetry, the internal motion resembles a vibration, a torsional oscillation localized in the potential wells. The internal motion of the E states has more of the character of free rotation passing from one potential well to another by tunneling. The degeneracy of the free rotor remains for the E states which is related to the two possible directions of internal rotation. Overall rotation of the molecule slightly splits the E degeneracy via angular momentum coupling, and if the perturbation is strong enough, the E contours will appear to be broader than the A_1 contours. In the spectra obtained in this study, for both the methyl indoles and stilbenes, the E levels in fact are broader, aiding in their

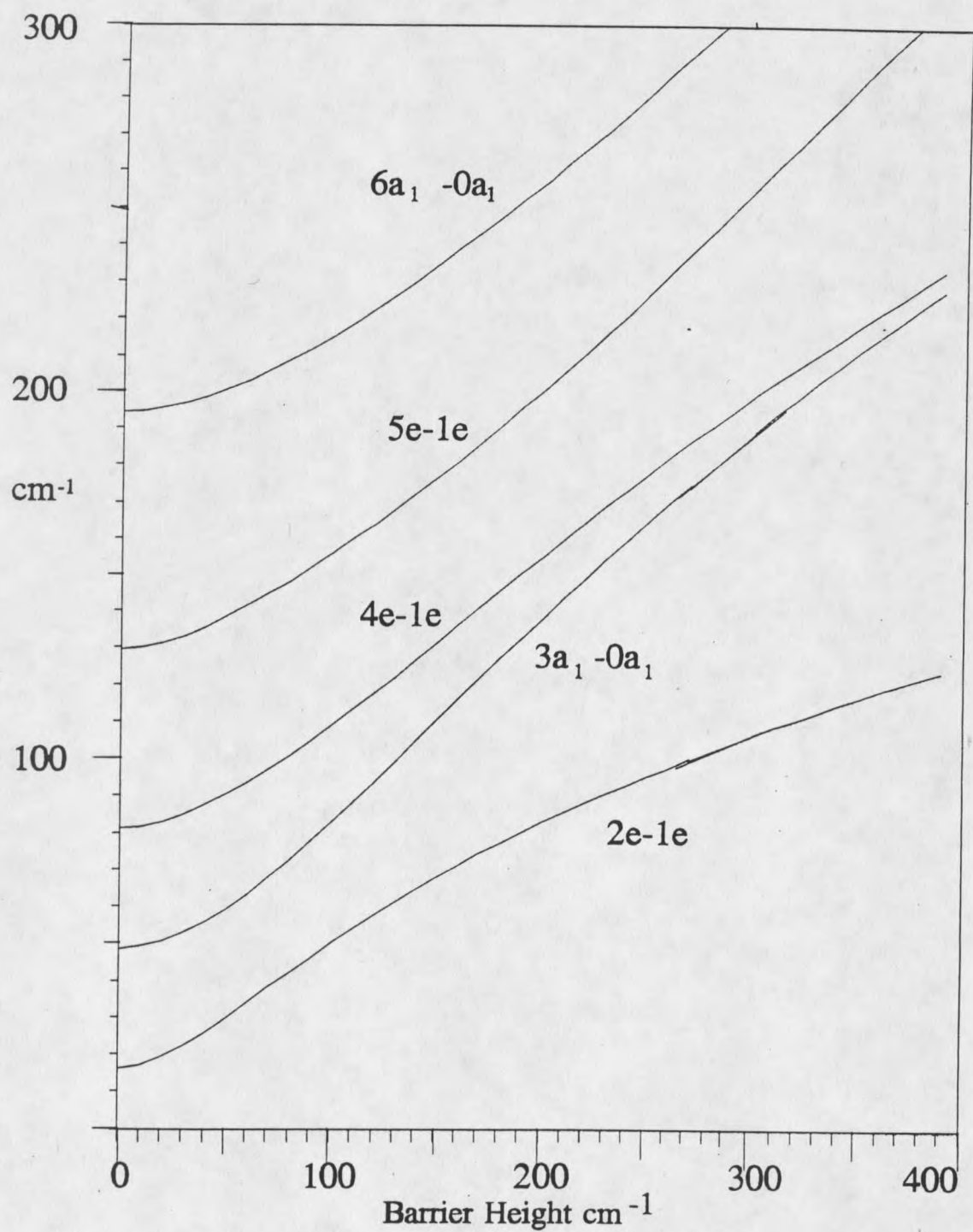


Figure 2: Methyl rotor splitting as a function of V_3 barrier height.

identification. Once these E and A_1 levels have been identified in a spectrum, their frequencies and intensities are used to determine a value for a potential barrier. (See Figure 2)¹⁸ By identifying the first few members of the torsional progression in a spectrum, the higher transitions can often be located by comparison with the calculated frequencies.

The first step in determining the potential barrier for the methyl group from experimental data is to use a FORTRAN program, VNCOS, written by Laane and coworkers.¹⁹ This program calculates the eigenvalues for a potential function of the type $\sum_n (V_n/2)(1-\cos nx)$. Based on the frequency differences of the rotor levels, the V_3 and V_6 terms are optimized to reflect the barriers. There is one other factor in the calculation which is optimized, B , the internal rotation constant. For CH_3 , this value typically ranges from 5.2-5.4 cm^{-1} . Using the VNCOS program, we can then obtain the potential terms for the ground and excited state barriers if we have experimental data available. Transitions higher than $3a_1$ are typically above the barrier and are not as well fit by VNCOS.

VNCOS was written to calculate IR transitions for a single electronic state. While it can be used to determine barriers for both the ground and excited states, it cannot calculate intensities in excitation or dispersed emission spectra. A program written by Spangler²⁰ known as INROT calculates the frequency of a transition and its intensity based on the barriers previously calculated from VNCOS for the ground and excited states. These values can then be optimized to find barriers that would yield the observed intensities and frequencies. The intensities are calculated from the Franck-Condon factors. The Franck-

$$S_{v'v} = \int \psi_{v'}^* \psi_v d\tau_N$$

Condon factors are determined by an integral^{1,21} which is the overlap of vibrational wave functions of the ground and excited electronic state, occasionally expressed as the integral squared to reflect the probability. A change in conformational preference, displacement of the potential energy surface, barrier shape and height all contribute to the observed intensities. If many transitions in the methyl rotor progression have intensity in a spectrum, the conformation change is typically 30°-60°, while if only the origin has significant intensity (98%), there is no conformation change between the two states.

An example of the hindered internal rotation potential barriers for the methyl group are the potentials for p-methyl-trans-stilbene. These barriers were assigned previously by Zwier and Spangler.¹⁴ The barriers for the ground and excited states, reflecting the conformation change for the methyl group, are shown in Figure 3, with $V_3'' = 28 \text{ cm}^{-1}$ and $V_3' = 150 \text{ cm}^{-1}$, and the internal rotation constant is $B = 5.35 \text{ cm}^{-1}$ for both states. This molecule was previously assigned with a 35° conformation change. The conformation change was modified to 60° upon reassignment of the $3a_2$ level as discussed in chapter seven. The barrier for rotation increased 5-times upon excitation, indicating that the methyl group in this molecule is very sensitive to changes in the electronic structure.

There are many possible causes for the barrier that hinders the internal rotation of the methyl group. An early example of internal rotation in the excited state was work by Ito, in the mid-1980's. He examined this in fluorotoluene as a function of *ortho*, *meta* and *para* substitution.² For *o*-fluorotoluene the ground state barrier is 228 cm^{-1} and reduces to 21.8 cm^{-1} upon excitation. The *ortho* position can make steric factors the dominant factor hindering the rotation. In the ground state for both *meta* and *para* fluorotoluene the barrier

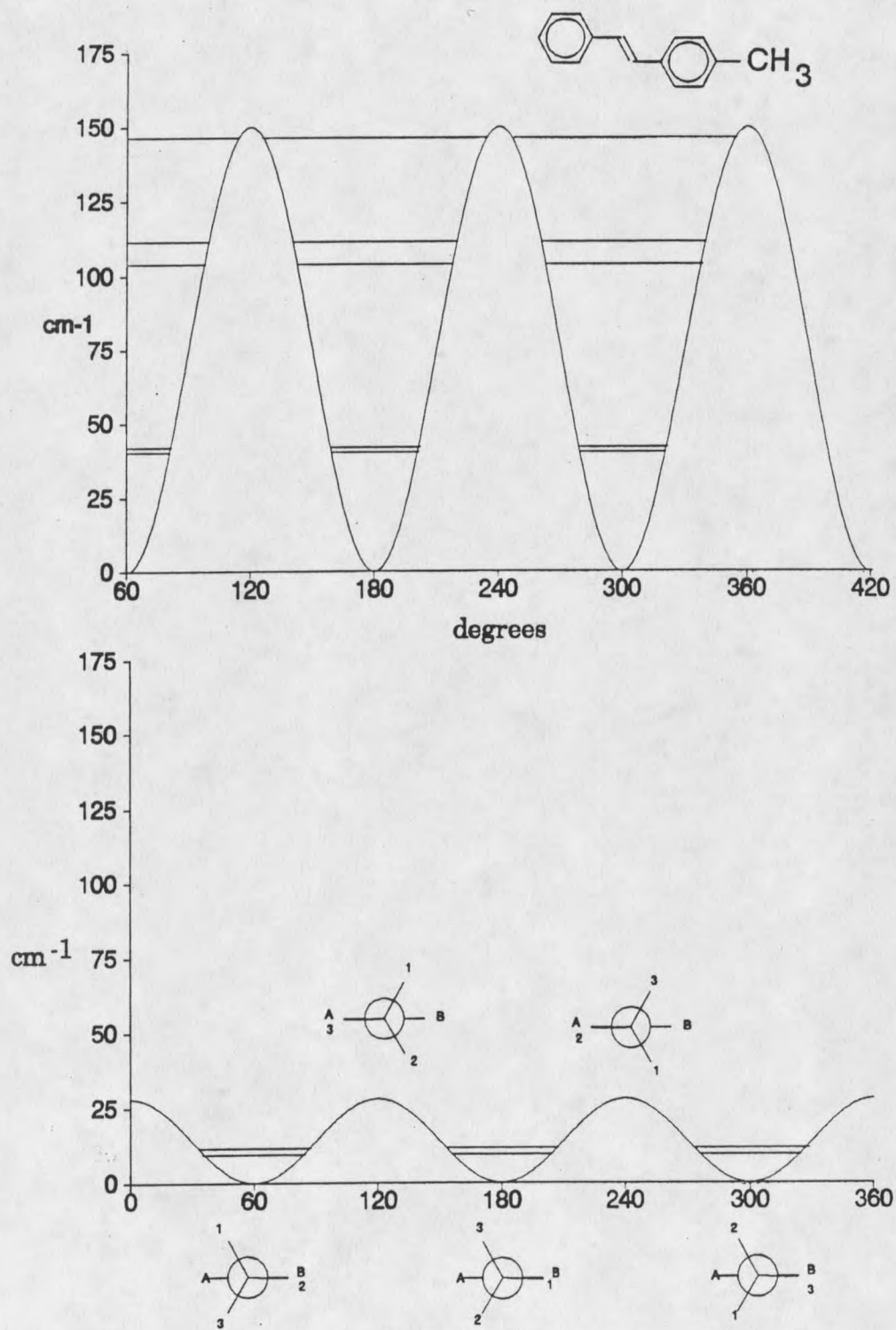


Figure 3: The potential barriers for S_0 and S_1 for the hindered methyl rotor in p-methyl-trans-stilbene.

is very low, but for *m*-fluorotoluene it increases dramatically upon excitation. This group of molecules is one of the best starting points for looking at π electronic effects in phenyl ring systems since it systematically looks at the different positions around the phenyl ring. There have been many other comprehensive examinations of methylated single ring systems such as pyrimidines^{10,11}, toluenes^{2,9}, cresols^{22,23}, anilines²⁴ and styrenes¹⁰⁻¹². As discussed in later chapters, the study of methylated stilbenes will show that π electronic effects are a contributing factor to the barrier to internal rotation, as steric effects are ruled out by the large separation of the substituents.

The role of hyperconjugation in relation to the barrier has been a point of contention for many years. Hyperconjugation is a resonance stabilization due to delocalization of a σ bond with the adjacent π orbitals.²⁵ Over the past several decades, several different models of hyperconjugation have been developed. Hehre states that the interactions between a methyl group and the π electron system of the molecule to which the methyl group is attached to can be explained by considering the π and π^* orbitals of a double bond and the π -like orbitals of the CH_3 group.²⁶ There are four different interactions that can contribute to hyperconjugation, and the preferred staggered or eclipsed conformation depends upon the orbital interactions. If an electronic excitation takes place, the staggered conformer would be favored over the eclipsed for two of the interactions (propene is an example) but the contributions from the other two interactions must be taken into consideration. For small molecules this theory does explain the experimental evidence, however, in larger molecules many more interactions must be taken into consideration.

A theoretical approach to hyperconjugation involves looking at the methyl group such as in propylene ($C_1=C_2-C_3-H_{1,2,3}$), where $H_{1,2,3}$ are the three methyl hydrogens.²⁷ The wavefunction is a set of 3 C-H bond functions, each being a linear combination of a hydrogen 1s orbital and a C sp^3 orbital. These are used to form group orbitals as a linear combination of the three H orbitals. These are mutually orthogonal if overlap integrals are neglected.

$$\phi_1 = \frac{1}{\sqrt{3}}(\phi_{H_1} + \phi_{H_2} + \phi_{H_3})$$

$$\phi_2 = \frac{1}{\sqrt{6}}(2\phi_{H_1} - \phi_{H_2} - \phi_{H_3})$$

$$\phi_3 = \frac{1}{\sqrt{2}}(\phi_{H_2} - \phi_{H_3})$$

The function ϕ_1 has no node and can overlap with whatever 2s and $2p_x$ orbital of C_3 that is "left over" from the σ bond to carbon 2. The function ϕ_2 has a nodal plane roughly approximate to the nodal plane of $2p_z$, and ϕ_3 has a nodal plane in the xz plane, with orbital overlap occurring with the carbon p_y orbital. Therefore, the C_3-2p_z orbitals and the ϕ_2 group orbital can by symmetry join the π -lattice, which is the 2 electrons in the C_3-H_3 π -type bond, and are now treated as part of the π system. There are two other models of hyperconjugation in the literature. One is the Pauling model, which is described in terms of an inductive model and in which conjugation is neglected. The other is the Matsen and Stevenson Heteroatom Model, in which the electrons in a methyl group behave as a single electron pair contribution to the π system.

The model that we feel best represents hyperconjugation is the first model which contributes π electron density from the C-H bonds to the π system. There are many influences which affect the hyperconjugation when the methyl group is attached to aromatic systems along with other functional groups. The methyl group is shown to be sensitive to π electronic effects from the functionality of substituent effects, as will be shown in this thesis for the substituted stilbenes.

CHAPTER THREE

EXPERIMENTAL PROCEDURES

The details of the experimental procedures developed and used in this thesis work are presented in this chapter. The main experimental technique, supersonic jet laser spectroscopy, has been developed extensively over the past decades.^{2-4,6-15,22-24,28} When the need has arisen, new procedures were developed in the laboratory to obtain more information, including the application of a charged coupled device (CCD) to take exposures of the dispersed fluorescence. The origination and/or synthesis of the molecules used in this study will be presented first. The experimental setups for 1hv, 2hv, and dispersed fluorescence will then be presented, along with discussions pertaining to the theory and use of these methods.

Compounds

The indole compounds used for the methyl rotor studies came from a variety of sources. 5-methylindole was obtained from Aldrich Chemical, while the 3-methyl-indole was obtained from Sigma Chemical. Both were used without further purification with a stated purity of >98%. 3-trideutero-methyl-indole was synthesized by Dr. C.J. Lee as discussed in the thesis of David Sammeth.²⁹

The stilbene analogues were obtained from several different sources. The p-methyl-trans-stilbene was synthesized for the earlier studies performed at Calvin College and was obtained from T.S. Zwier now at Purdue University. The p-methoxy-trans-stilbene was obtained from the Sigma Chemical Company and was used without further purification. P'-methoxy-p-methyl-trans-stilbene was synthesized in our research group by reacting 0.03 moles of the Arbusov product, $\text{CH}_3\text{-C}_6\text{H}_4\text{-CH}_2\text{-P=O(Et)}$ dissolved in 0.06 moles NaH in 1,2-dimethoxyethane (DME), into which was added 0.03 moles p-anisaldehyde. This solution was refluxed at 70°C for 0.5 hours during which time H_2 gas was produced by the reaction, indicative of formation of the stilbene. The reaction was quenched with water, and the resulting stilbene crystals were collected and recrystallized twice in ethanol and then dried. The yield was approximately 75%, and the melting point is 158° Celsius. The compound was examined with $^1\text{H-NMR}$ and FTIR, and compared to the commercially available p-methoxy-trans-stilbene.

The three halogenated methylstilbenes were prepared in a similar manner. They are p'-chloro-p-methyl-trans-stilbene, p'-chloro-m-methyl-trans-stilbene and p'-fluoro-p-methyl-trans-stilbene. The Arbusov product used above was replaced with the appropriate phosphinate obtained from Lancaster Chemical, along with the proper halogenated aldehyde compound. The p'-chloro-p-methyl-trans-stilbene and the p'-chloro-m-methyl-trans-stilbene were synthesized originally as a project in Dr. Arnold Craig's organic 206 laboratory, and further work was done by our research group, Brian Pagenkopf, and Susan Sheehan. A version of the Wittig reaction is utilized, involving the transfer of an alkylidene-phosphorane, derived from an alkyl triphenylphosphonium salt, to a carbonyl compound with displacement

of the carbonyl oxygen.³⁰ This synthesis results in the majority of the compound to be of trans stereochemistry. The formation of cis isomers does not affect the experiments performed in this project as cis-stilbene in jets has a fluorescence spectrum that is broad and featureless, and absorbs in a different wavelength region than trans-stilbenes.¹³ One equivalent of n-BuLi was used as a base, then it was reacted with 3-(or 4)-methylbenzyltriphenyl-phosphonium chloride in THF as a solvent. One equivalent of 4-chloro-benzaldehyde was added and the solution was refluxed. The product was filtered, recrystallized in ethanol, and dried on a high-vacuum line. ¹H-NMR, FTIR and gas chromatography were used to test for purity and identification.

The p'-fluoro-p-methyl-trans-stilbene was prepared in a similar manner by Brian Pagenkopf. One equivalent of 4-methylbenzyl-triphenylphosphonium bromide was dissolved in THF and one equivalent n-BuLi. 4-fluoro-benzaldehyde was added and the solution was refluxed. The product was recrystallized in ethanol and the solvent removed. Once again the sample was examined for purity with gas chromatography, and analyzed with ¹H-NMR and FTIR.

Sample Preparation

The vapor pressure of these compounds is very low at room temperature, therefore the samples are heated to get adequate concentration in the expansion. The indoles were heated to approximately 100° Celsius, while the stilbene had to be heated to 125° Celsius, near the temperature limit of the sample system. See Table 3 for specific sample temperatures. The stilbenes were placed into a Pyrex beaker inside of a stainless steel sample

chamber to help inhibit polymerization. This also made for easier sample recovery. Glass wool was occasionally used inside of the sample chamber to raise the sample closer to the outtake tube.

As mentioned above, the samples were introduced via a supersonic jet expansion. Without cooling the sample via the expansion, the spectrum would be very congested due to hot bands, which are transitions that begin from higher vibrational levels of the ground state, and the low-frequency modes that are examined in this work would be difficult to observe. A seeded jet is used, in which vaporized sample is entrained in helium and the gas mixture is flowed through a pulsed nozzle. The cooling occurs when gas from a high pressure reservoir is discharged into a low pressure region through a small nozzle. The seeded molecule is embedded in a translationally cold environment which cools the internal degrees of freedom through collisional energy transfer. At the point where the gas density becomes too low to support collisions, the final temperature becomes fixed. During the expansion the gas acquires a net flow velocity which exceeds the local speed of sound.³¹ With our system, optimal cooling was achieved with a He backing pressure of 5-7 bars. This allows a sufficient quantity of sample made available for excitation. With this pressure, the molecules rotational temperature is near 5K while the vibrational temperatures are typically less than 50K. In order to increase the thermal population of higher vibrational levels of the electronic ground state to identify hot bands, the helium backing pressure can be reduced to 0.4 barr He. See Figure 4 for a diagram showing the expansion conditions necessary to obtain supersonic jet-cooling. In the figure, P_0 refers to the helium backing pressure at temperature T_0 , which goes through a nozzle with a diameter D , where it expands into a low pressure (P_1) chamber

maintained at 10^{-5} torr by a diffusion pump. The stilbenes and indoles in this study show a high tendency to form complexes with helium, therefore different backing pressures were used to examine hot bands, complexes and to differentiate them from low-frequency modes.

Table 3: The melting points and temperatures in $^{\circ}\text{C}$ needed to obtain sufficient vapor pressure.

	melting point $^{\circ}\text{C}$	1hv sampling temp	DE sampling temp
3-methylindole	95	110	
3(CD_3)methylindole		85	
5-methylindole	60	45	
p-methyl-trans-stilbene		110	
p-methoxy-trans-stilbene		120	125
p'-methoxy-p-methyl-trans-stilbene	158	120	125
p'-chloro-p-methyl-trans-stilbene		110	125
p'-chloro-m-methyl-trans-stilbene	105	90	100
p'-fluoro-p-methyl-trans-stilbene		90	115

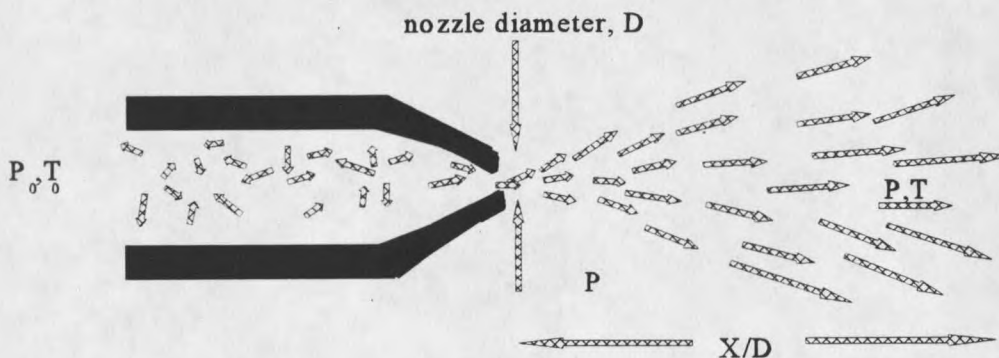


Figure 4: The supersonic jet expansion.

1hv and 2hv theory

The low sample concentration in a jet requires sensitive spectroscopic techniques. Instead of absorption spectroscopy, fluorescence excitation (FE) is used to probe absorption characteristics. In a one-photon (1hv) FE, the total fluorescence from an excited level is examined. Fluorescence involves transitions through $S_1 - S_0$ states, and is rapid. The lifetime of fluorescence is typically on the order of tens of nanoseconds.³² See Figure 5 for a general diagram showing the process of fluorescence.

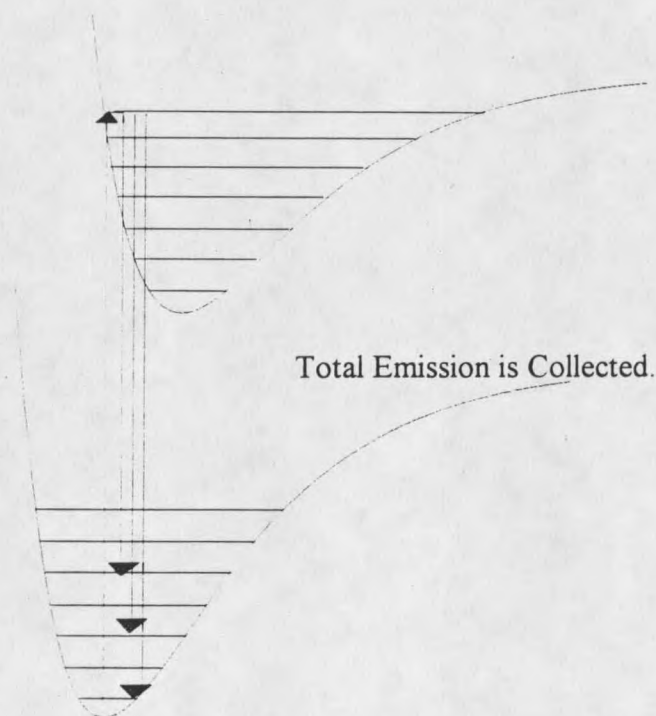


Figure 5: The process of fluorescence for isolated molecules.

In 1hv FE, only one photon of exciting radiation is used to reach the desired state. Because of the quantized nature of all systems, one must have exactly the right wavelength of light to probe the desired transition. The frequency of an observed spectral line is given by $h\nu = E' - E''$, where E' and E'' are term energy values containing separable electronic, vibrational, and rotational contributions. All observed transitions must follow symmetry selection rules. At our coldest conditions (with $P_0 = 6$ bar He) the transitions typically have a bandwidth of 3-4 cm^{-1} . A frequency region of approximately 1000 cm^{-1} is scanned to obtain the spectrum of the S_1 state. In stilbenes, after 1000 cm^{-1} , combination bands create significant spectral congestion, making it difficult to identify individual transitions.

In dispersed fluorescence (DF), instead of scanning over a region, only one excitation frequency is used, set for a known S_1 vibronic transition. The subsequent emission is then dispersed using a monochromator and the ground state levels to which emission occurs can be identified from the frequencies of the transitions in the resulting spectrum. The emission spectrum is dependent on the vibrational character of the initially prepared S_1 level and this technique allows improved identification and understanding of energy levels, Franck-Condon factors, and dynamical issues.³³ See Figure 6 for a diagram explaining the process of dispersed fluorescence.

A two photon fluorescence excitation utilizes two photons of visible light to probe an excited transition. One photon is used to reach a virtual state, and simultaneously the second photon takes the molecule from the virtual state to the excited state. There are factors in the two photon process which lead to experimental difficulties. Two photon absorption cross sections are typically 10^6 smaller than one photon cross sections making it much more difficult

to attain adequate S/N. As a result of the intensity dependence, $2h\nu$ absorptions are normalized by dividing the signal by the average laser intensity squared. Even though $2h\nu$ absorptions are more difficult to obtain, there is a difference in the selection rules between $1h\nu$ and $2h\nu$ processes that makes $2h\nu$ data desirable. This difference in the rotational selection rules can yield useful information, as is discussed in the literature.^{5,14,34,35}

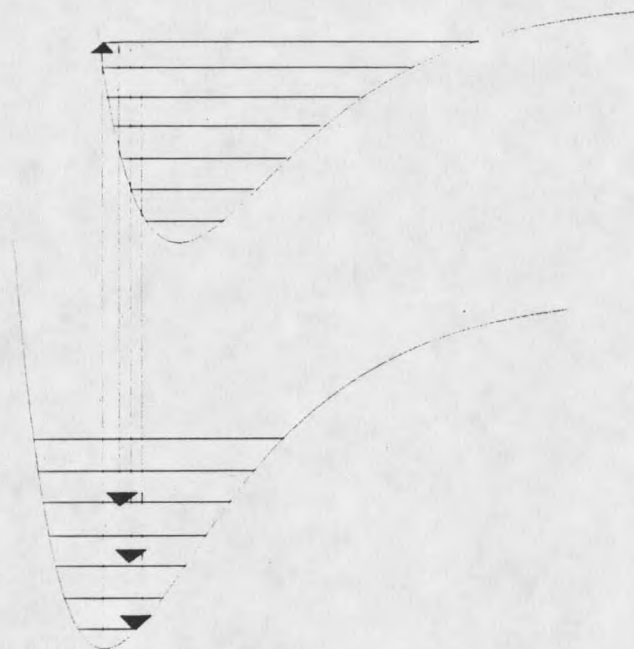


Figure 6: The process of dispersed fluorescence.

Experimental Apparatus

The apparatus for the $1h\nu$ FE experiments is shown in Figure 7. In all experiments, a Lumonics Nd:YAG 750 laser, pulsed at 20Hz, was used as the pump source for the dye

laser. It is usually operated at the second harmonic of 532 nm, with a typical energy output of 276 mJ running near optimum conditions. For the methyl indole work, the wavelength region required utilizes the third harmonic of 355 nm light with a typical power of 173 mJ/pulse. Each pulse is 8-10 nanoseconds in duration. This beam pumps a Lumonics HD-300 tunable dye laser, with a resolution of 0.07 cm^{-1} in the visible region. It is equipped with a Bethune cell for the amplifier which creates a circular beam with uniform intensity, as opposed to the comet-shaped output of a standard dye cell. This Bethune cell has a lower conversion efficiency than a standard cell, requiring the high power achieved with the Nd:YAG 750 laser. For the methylindoles, Exciton's Coumarin-540A dye was used with the dye curve extending from 523-590 nm. The stilbenes analyzed required different wavelength regions. The following stilbenes were analyzed using DCM in propylene carbonate and methanol, which covers the wavelength region of $29,600 \text{ cm}^{-1}$ to $32,400 \text{ cm}^{-1}$: p-methoxy-trans-stilbene, p'-methoxy-p-methyl-trans-stilbene, p'-chloro-p-methyl-trans-stilbene, p'-chloro-m-methyl-trans-stilbene, and p'-fluoro-p-methyl-trans-stilbene. P-methyl-trans-stilbene was analyzed using R640 in methanol with acid added to red-shift the dye region.

For the dispersed emission experiments and the one-photon work, monochromatic visible light from the dye was frequency doubled in BBO using a Lumonics Hypertrack 1000. The dye curve was set in $\approx 300 \text{ cm}^{-1}$ increments to optimize the doubling angle of the BBO crystal. A set of prisms was originally used to pass the UV light, but they were removed when problems arose with the beam "walking" with changing wavelength, and the appropriate Schott filters were used to remove the visible light. The beam is then passed through a spatial filter and a focusing lens. For all of the stilbenes, a one-meter focusing lens was used

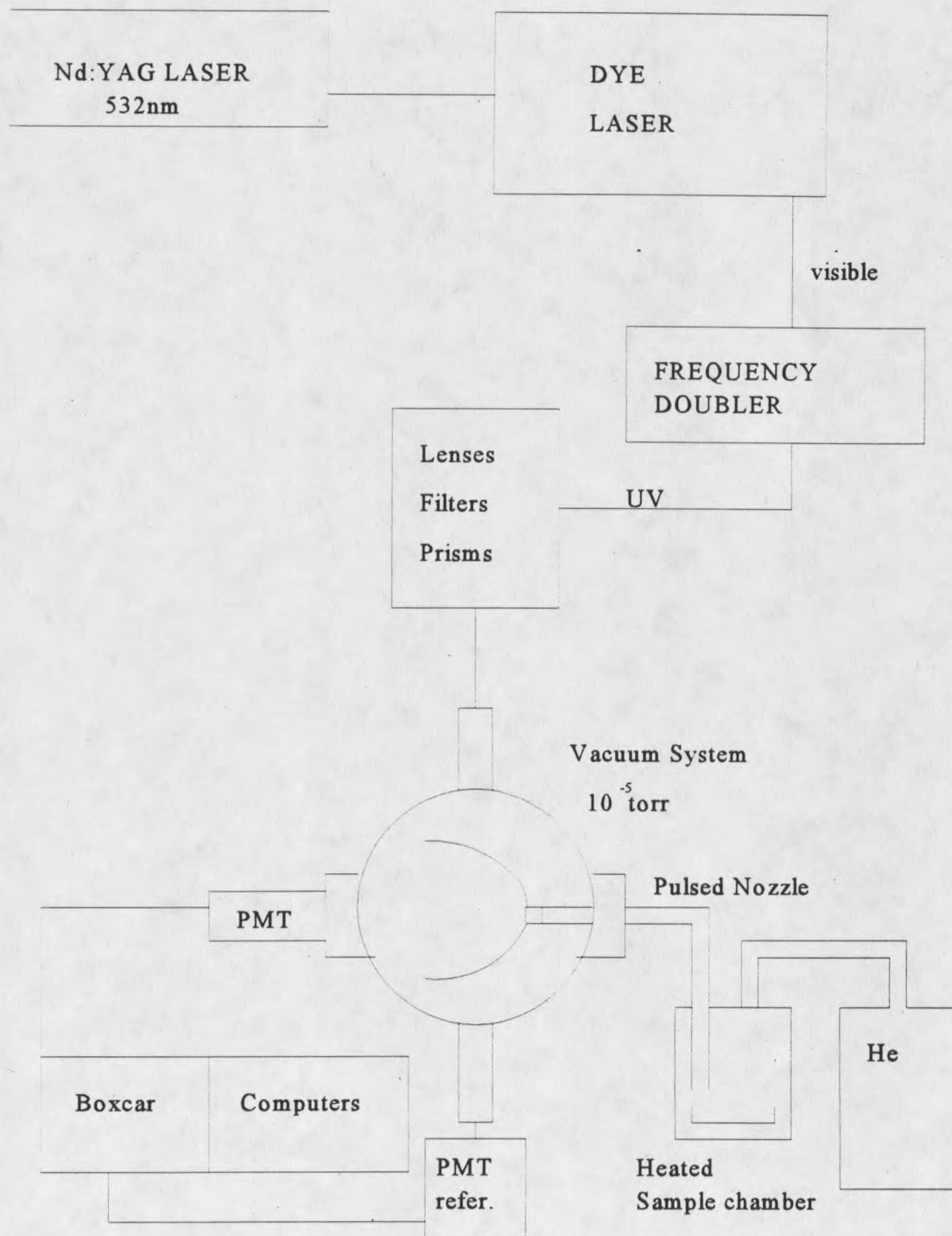


Figure 7: The apparatus for 1hv fluorescence excitation experiments.

at the appropriate distance from the excitation region. Two prisms are then used to raise the laser beam to the level of the excitation chamber.

The jet apparatus utilizes a General Valve Series 9 pulsed nozzle with a 0.8 mm orifice, which expands the sample into a six inch nominal, six-way cross evacuated by a Varian VHS-6 diffusion pump which is backed by a Varian mechanical pump. A pressure of 5×10^{-5} torr can be maintained under experimental conditions. Samples are heated to the desired temperatures as described in Table 3 and entrained in 0.2-7 bar helium. The jet axis and laser axis cross at 90° . The fluorescence is collected and focused onto the cathode of an EMI 9813QB photomultiplier tube (PMT) by a Melles Griot REM 0.14 ellipsoidal reflector, which captures more than 70% of the emitted light. An adjustable iris with an aperture of approximately 2 mm is placed in front of the PMT to spatially discriminate against the scattered light. The resulting signal is fed to a Stanford Research Systems SRS250 boxcar integrator, digitized, and stored on a computer. A 1450Ω resistor is used to terminate the signal on each boxcar. Laser power is monitored by using a Rhodamine 590 solution as a quantum counter and detecting the dye emission with a second PMT with the resulting signal sent to another boxcar system. Correction for laser power variations are made in the long-rang 1hv scans. The 1hv spectra presented in the following chapters are an average of three scans, normalized, with a resolution of 0.15 cm^{-1} unless otherwise noted.

The dispersed fluorescence experiments are very similar to the 1hv fluorescence excitation experiments. The dye laser is held at one frequency instead of being in the scanning mode. A single electronic transition is excited, and the fluorescence is collected with the same ellipsoidal reflector as described above. Two different methods were used to obtain dispersed

fluorescence data during the course of this study. The first method used a 0.25 meter Oriel monochromator with a 2400 line/mm grating, with entrance and exit slits typically set at 200 microns giving a resolution of $\approx 15 \text{ cm}^{-1}$ in the dispersed fluorescence spectrum. An Oriel scanning control unit rotates the grating to obtain a spectrum. The same PMT and data acquisition system was used as described above. To improve signal/noise, several scans requiring over an hour in acquisition time had to be averaged for every probed transition. Because several of the desired transitions in the ground state could not be resolved with the relatively poor dispersion and S/N of this system, another procedure was implemented.

The majority of the dispersed fluorescence spectra obtained in this research was obtained with a new dispersed emission system. A Spex 0.5 meter monochromator with a 3600 line/mm grating and an entrance slit of 100-200 microns was used for the majority of the dispersed emission. (See Figure 8.) Additionally, a Princeton Instruments liquid nitrogen cooled charge-coupled device (CCD) detector was used to collect the dispersed fluorescence. No exit slit is required on the monochromator as the full dispersed fluorescence is collected with the CCD, although we are limited to approximately 1400 cm^{-1} in this wavelength region as dictated by the CCD chip size. A CCD is a silicon solid-state multichannel detector which integrates signal information as the light strikes it, similar to taking an exposure with a camera. One of the biggest benefits from using a CCD compared to other detectors is by their ability to transfer the photogenerated signal from the photoactive element to an on-chip amplifier, which allows for a very high signal-to-noise output.^{36,37} Other advantages of using a CCD include very low detector noise, approximately 1 count/pixel/hour, and binning, which is a process of summing the charge contained in multiple elements on the detector before

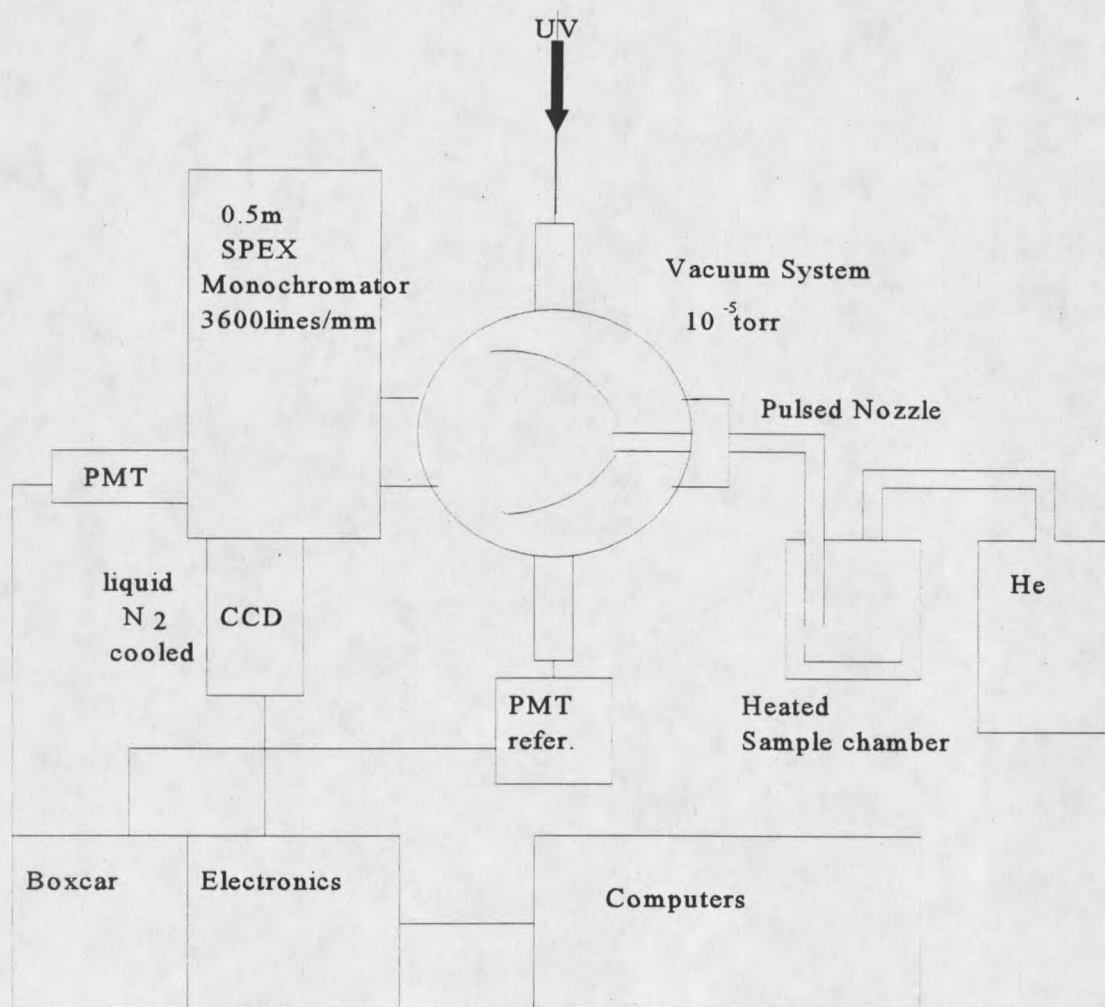


Figure 8: The apparatus for dispersed fluorescence experiments utilizing the CCD detection system.

sensing the total charge. The CCD chip used in this system is a 1024 X 256 pixel chip with a UV coating, with each pixel having a width of 26 microns. The 256 pixels in the vertical direction are binned to improve S/N. With an entrance slit of 100 microns on the monochromator, we are limited to a grating resolution of $1.38 \text{ cm}^{-1}/\text{pixel}$, with an overall resolution of $\approx 5.5 \text{ cm}^{-1}$ in this frequency region. This is adequate resolution to obtain good ground state vibrational and torsional frequencies for most transitions. The detector quantum efficiency is also very high, and is very sensitive to low light levels.

A comparison of the experimental data obtained for the two dispersed fluorescence methods is shown in Figure 9. A dispersed fluorescence spectrum of the second electronic origin of p-methoxy-trans-stilbene acquired with the scanning monochromator system took 2.5 hours as compared to two minutes with the CCD method. This reduction in acquisition time is important because of limited sample quantity. There is also a large improvement in the resolution. The decrease in acquisition time along with the improvement in resolution allows the frequency of low-frequency modes in S_0 to be found with greater precision, and dispersion of weaker transitions more feasible.

The other spectroscopic technique used in this study for the methylindoles and for p-methyl-trans-stilbene and p'-chloro-p-methyl-trans-stilbene is two-photon ($2h\nu$) spectroscopy. The doubler is removed from the system, allowing the visible light to be the exciting beam. An important feature of $2h\nu$ spectroscopy is the dependence on the polarization of the exciting radiation. See Figure 10 for the layout of the $2h\nu$ experimental apparatus. As described in the thesis of David Sammeth²⁹, the visible light is passed through a Glan-Foucault

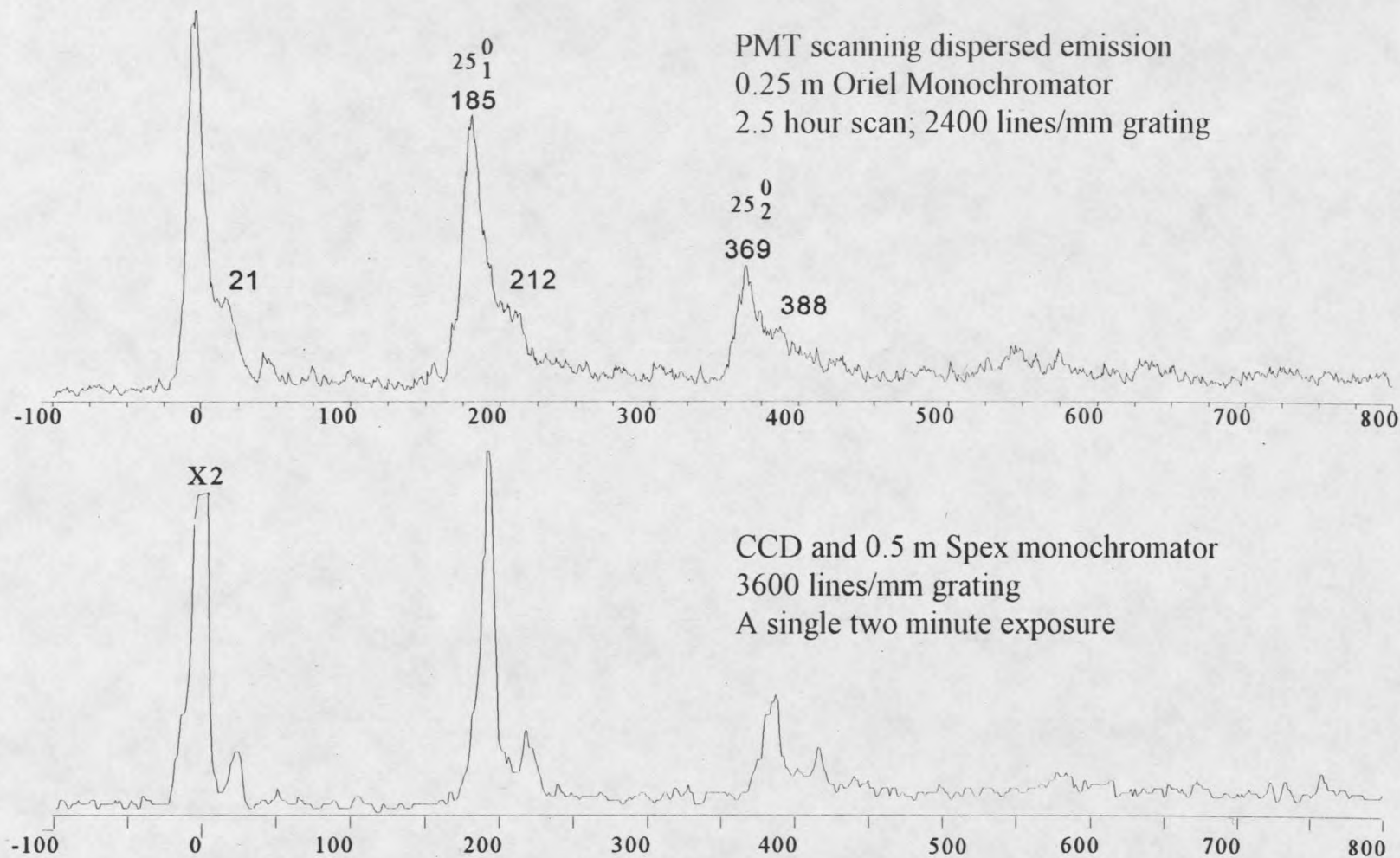


Figure 9: Comparison of the scanning 0.25 meter monochromator dispersed fluorescence apparatus versus the CCD/0.5 meter monochromator system from exciting the B origin of p-methoxy-trans-stilbene.

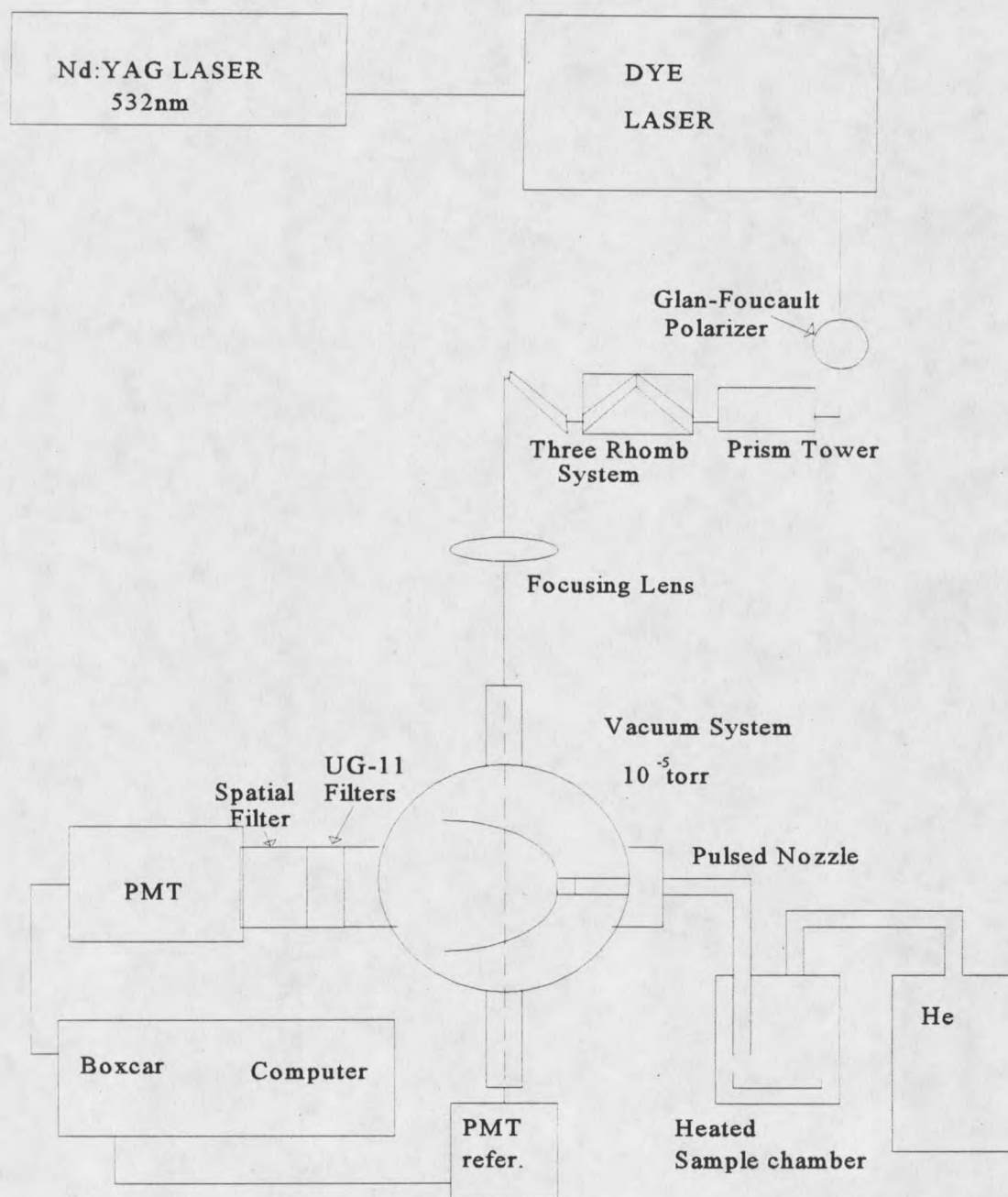


Figure 10: The experimental apparatus for 2hv fluorescence spectroscopy.

polarizer which allows only vertical linearly polarized light from the dye laser to pass. Two prisms are then used to raise the laser beam to the axis of the jet chamber. A three rhomb system for light polarization control is placed after the prism tower. A lens is placed in the beam path to focus it down for greater power density. The polarization is changed by rotating the double rhomb assembly manually. The fluorescence is collected with the same ellipsoidal reflector used in the 1hv work. All scattered light is due to scattered visible light, while the wavelength of interest is in the UV, so several Schott UG11 UV bandpass filters are placed in front of the PMT to eliminate all scattered laser light, and the spatial aperture can be removed. The PMT voltage can be increased for high sensitivity, along with various boxcar adjustments.

Any special parameters that were utilized for specific molecules will be described in chapter four and six, which contain the experimental results.

CHAPTER FOUR

EXPERIMENTAL RESULTS: INDOLES

The indole molecule and its derivatives have been investigated spectroscopically for many years because indole is the chromophore of the amino acid tryptophan, which is responsible for the majority of the fluorescence for proteins.¹² Two electronic states, 1L_a and 1L_b (Platt notation) are close lying in frequency and are sensitive both to the environment and substitution. Polarized two-photon fluorescence excitation spectroscopy has been used to distinguish the two electronic states in solution and more recently in the jet.³⁸

The spectra of methylated indole derivatives exhibit characteristics due to hindered internal rotation of the methyl group. 5-methylindole and 3-methylindole are examined in this work to investigate the dependence of methyl behavior on both the position and the electronic state. Previous solution work on these two molecules suggested that the electronic states become widely separated when the methyl is in the 5 position but move together when the substitution is in the three position.³⁹⁻⁴¹ Sammeth et.al. showed that the 1L_a and 1L_b electronic states for the isolated indole molecule remain separated in energy and distinguishable via two-photon spectroscopy.³⁸ The 1L_a and 1L_b states can also be distinguished for the methylindoles examined in this research. The study of the methylindoles includes torsional assignments, barriers, dynamical behavior, and solvent and rare gas complexes. A discussion of the

assignment of the electronic character of various vibronic transitions as determined by two-photon spectroscopy is presented elsewhere.²⁹ This work will deal with how the electronic nature of the states affects the methyl group.

The indole itself was examined by previous members of the Callis and Spangler research groups and lays the foundation for the work on the methylindoles. To distinguish the electronic nature of transitions, 2h ν fluorescence excitation scans were taken for transitions with both circular and linearly polarized light. Ω values are then measured, where Ω is the ratio of the intensity with circularly polarized light compared to that for linearly polarized light. It has been found that $\Omega(^1L_b)$ is ≈ 1.35 , while $\Omega(^1L_a)$ is ≈ 0.5 . The first intense transition observed is assigned as the origin for 1L_b , while transitions that show 1L_a character and may be the 1L_a origin begin at +455 and +480 cm^{-1} above the 1L_b origin.³⁸

5-methylindole Experimental Results

The one-photon fluorescence excitation spectrum of 5-methylindole is shown in Figure 11.¹² The absolute frequency of the first intense transition is at 35,353 cm^{-1} , and this has been assigned as the 1L_b origin from 2h ν studies. There are several more transitions observed in this spectrum than in indole, owing to the distribution of the intensity over a prominent methyl rotor progression. In order to observe a torsional progression with this much intensity, there must be a conformational change for the methyl group upon excitation. Wallace and coworkers previously reported the assignments of the torsional progression and the barrier to internal rotation⁴², however we have reassigned the higher torsional features and discovered many interesting effects related to the methyl group. The torsional pattern is also

observed in combination with all of the skeletal modes of this molecule, however, there are significant variations from the expected relative intensity patterns. The first transitions that have an Ω value indicative of the 1L_a state appear approximately 1400 cm^{-1} above the 1L_b origin. All 5-methylindole torsional structure in Figure 11 belongs to the 1L_b state. A discussion of the assignments of the methyl rotor transitions will follow in chapter five, along with the calculations of the potential barrier for the hindered internal rotor.

Close examination of the low frequency region of the $1h\nu$ fluorescence excitation spectrum reveals that there are weaker satellite transitions, usually to the blue of each torsional member. These lines are due to the carrier gas helium forming van der Waals complexes with 5-methylindole. This was confirmed by changing the backing pressure of the helium and observing the intensity dependence of these transitions as a function of the amount the helium concentration. One and two helium complexes are observed and identified in this manner. The methyl rotor barrier has been fit for each complex and the implications of this barrier will be discussed in chapter five.

At 150 cm^{-1} to the red of the 1L_b origin another torsional progression is observed. This progression lost intensity over the course of the experiments, and is due to atmospheric contamination of the sample with water. Previous work gave similar red-shifts for indole + water and 3-methylindole + water⁴³, verifying this assignment in 5-methylindole. A barrier has been fit for the 5-methylindole + water complex, and this will also be discussed in chapter five.



Figure 11: The $1h\nu$ fluorescence excitation spectrum of 5-methylindole.

3-methylindole and 3-CD₃-indole

The one-photon fluorescence excitation spectrum of 3-methylindole (3MI) is shown in Figure 12⁴⁴, with the origin truncated at ~ 0.3 of its correct relative intensity. The absolute frequency of the origin is 34,876 cm⁻¹. 3-CD₃-indole was also examined to identify vibrations and the torsional structure via the deuterium effect (see Figure 13). The low-frequency region of the 1hν fluorescence excitation spectrum of 3-CD₃-indole will be presented in chapter five as it pertains to the 3MI assignments.

The spectrum of 3MI does not show a long progression for the methyl torsion⁴⁴⁻⁴⁶, indicating that there is no conformational change upon excitation for the methyl group. Examination of the low-frequency region of 3MI and the deuterio compound does allow assignment of transitions due to the methyl rotor progression. The spectrum is fairly complicated as there is the existence of a second, low-lying electronic state, the ¹L_a. The intense origin is assigned as the ¹L_b origin, however, most of the other transitions in the spectrum appear to contain ¹L_a character. Several low frequency transitions have inconclusive Ω values concerning the nature of the electronic state. The methyl barrier can be fit from the experimental data for S₀ and the ¹L_b state, and the ¹L_a barrier can be estimated from observed splittings of transitions with ¹L_a character, as will be discussed in the following chapter.

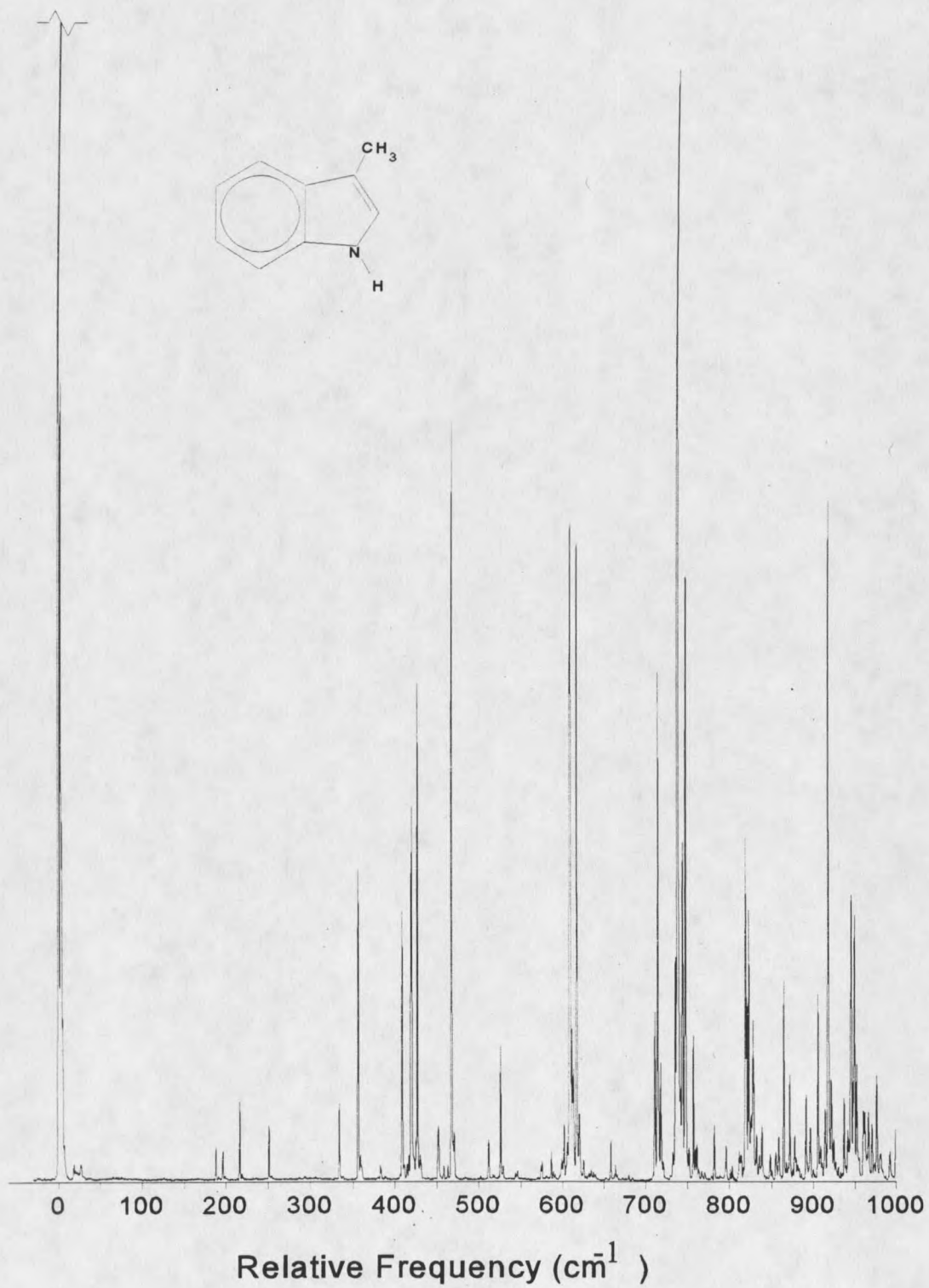


Figure 12: The 1hν fluorescence excitation spectrum of 3-methylindole.

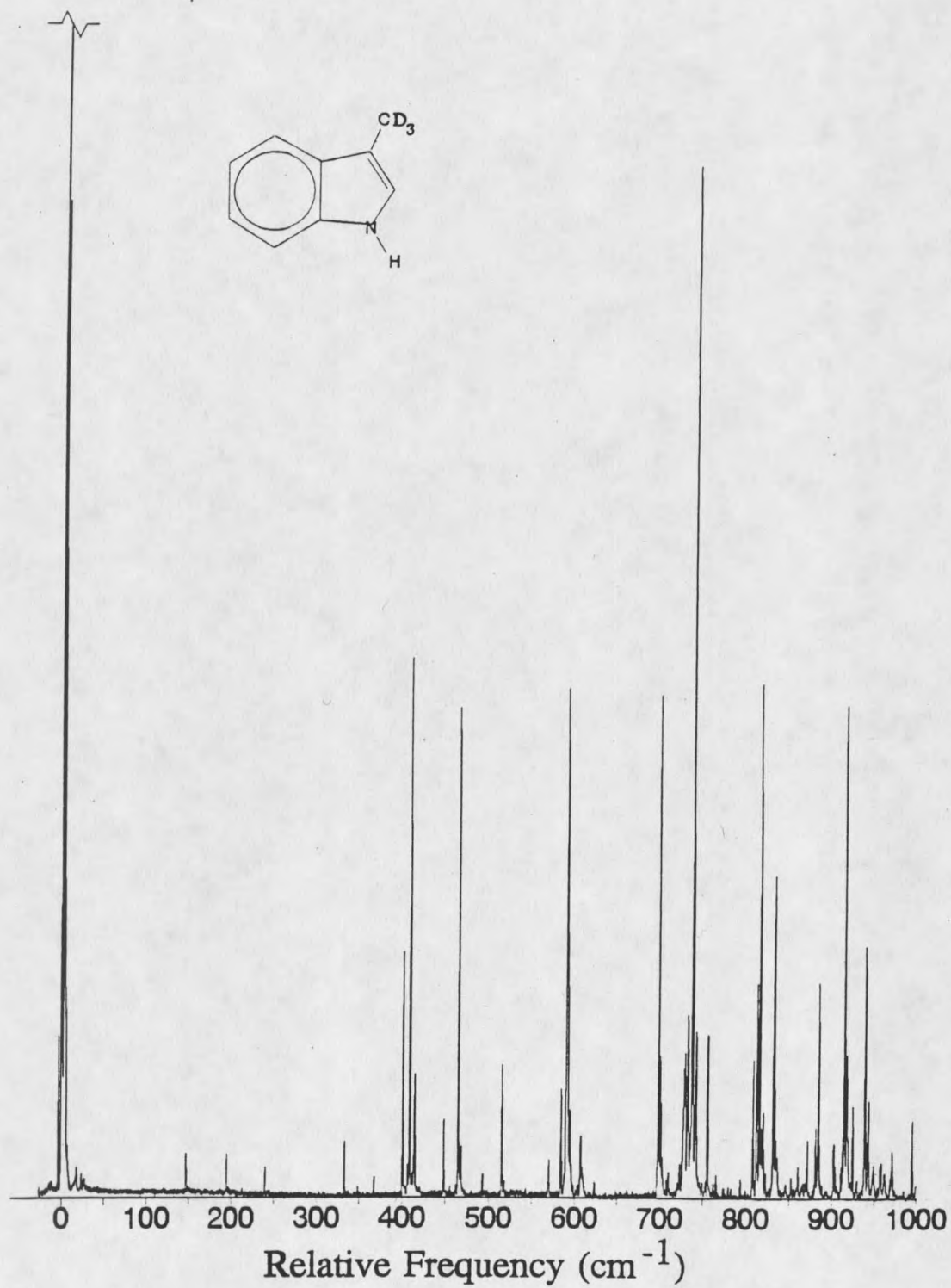


Figure 13: The 1hν fluorescence excitation spectrum of 3-trideuterio-methylindole.

CHAPTER FIVE

DISCUSSION: METHYLINDOLES

The goal of this research is to examine how different electronic effects influence the methyl group. For the methylindoles, this is done by examining the nature of the electronic states, 1L_a and 1L_b , in relation to the potential barrier for hindered internal rotation. The assignments of the torsional features and the calculated barriers for each molecule in its electronic states will be presented individually, along with discussions of special issues relating to that molecule such as the complexes and dynamical issues. At the conclusion of this chapter there will be a comparison of the barriers to internal rotation for the methylindoles.

5-methylindole

The $1h\nu$ fluorescence excitation low frequency spectrum (first 250 cm^{-1}) of 5-methylindole (5MI) is presented in the top trace of Figure 14.¹² On the bottom half of Figure 14 are the linearly and circularly polarized two-photon contours of the first four transitions, which are part of the methyl rotor progression. Each two-photon contour spans 9 cm^{-1} , with the circularly polarized contour on the top trace, and the linearly polarized contour on the bottom. As mentioned previously, these transitions all belong to the 1L_b electronic state.

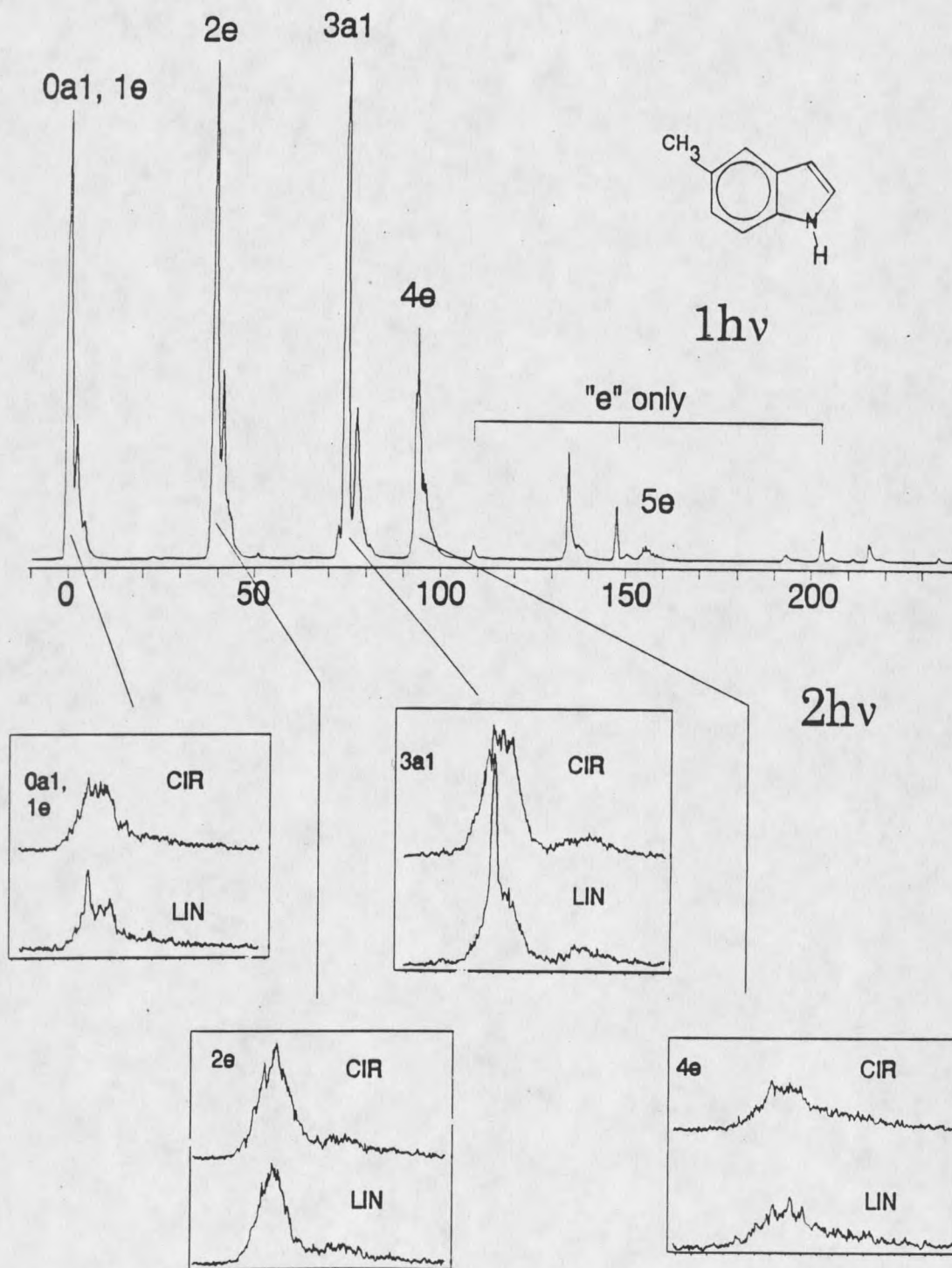


Figure 14: The low frequency region of the 5-methylindole spectrum (top). Two-photon contours of the first four transitions using both linearly and circularly polarized light are shown at the bottom. These contours span 9 cm⁻¹ with tic marks appearing every 0.5 cm⁻¹.

There is an internal-overall rotation interaction in 5MI that affects the E contours. As discussed in Gordy and Cook based on work originally done with microwave spectroscopy, the angular momentum due to internal rotation of the CH_3 can couple with the angular momentum due to overall rotation of the molecule, and this coupling is significant if the CH_3 top axis lies near the symmetric top axis.^{5,12} 5MI has been calculated from AMPAC calculations to be a near prolate top, $\kappa = -0.82$ with the A axis passing between the 5 and 6 positions near the methyl axis. The interaction is also increased when the methyl motion is closer to a true internal rotation as opposed to a torsional vibration. This distinguishes the A_1 from the E levels. The E level wavefunctions show a larger amplitude inside the barrier than do the A_1 wavefunctions, thus the E wavefunctions more strongly resemble an internal rotation allowed by tunneling through the barrier. The overall rotation in the system will slightly split the E degeneracy, and with sufficient resolution, each rotational level of the E transitions will appear as a doublet. At the resolution in these experiments, these effects cause the E contours to appear broader than the A_1 contours.

This broadening of the E contours manifests itself in 5MI in the $2e$, $4e$ and $5e$ contours. The $1h\nu$ contours are observed to be broader than A_1 contours. The two-photon contours manifests this by giving a narrow ${}^{\text{Q}}$ branch in the linearly polarized contours for the A_1 transitions but not for the E transitions.

The electronic origin contains the torsional intensity for both the $0a_1$ and the $1e$ members of the torsional progression. An approximate $0a_1$ - $1e$ splitting can be determined from the $2h\nu$ contour of these transitions. Since the $0a_1$ will have a narrow ${}^{\text{Q}}$ branch and the $1e$ will be broader, the red-most part of the origin is assigned as the $0a_1$ frequency, with

the $1e$ being $+1.2 \text{ cm}^{-1}$, which is close to the calculated value. The $2e$ and $3a_1$ assignments agree with that of Wallace and coworkers⁴². These transitions occur at $+39.5 \text{ cm}^{-1}$ and $+74.6 \text{ cm}^{-1}$ respectively.

The best fit for the torsional structure for the $5\text{MI } ^1L_b$ electronic state is shown in Table 4. This table includes the calculated barrier and experimental and calculated transition frequencies for 5-methylindole and observed complexes. The best fit was obtained by using INROT and VNCOS, and differs from Wallace's assignment in three ways: the relative frequencies are slightly different, the assignments of $5e$ and $6a_1$ are different, and the internal rotational constant used is more appropriate for this molecule. The resulting potential barrier is very similar to Wallace's with a moderate V_3 potential height and a significant negative V_6 term which gives rise to unusually wide wells and narrow barriers. The wide wells aid in the strong internal-overall rotation interaction which cause the observed broadening in the E levels. Adding a V_9 term to the calculation does not improve the fit. The barrier can be best fit with the following values: $B' = 5.30 \text{ cm}^{-1}$, $V_3 = 80 \pm 5 \text{ cm}^{-1}$, and $V_6 = -21 \pm 5 \text{ cm}^{-1}$. The intensities of the torsional progressions can be best described using a 60° conformational change for the methyl group upon excitation.

The reassignment of the $5e$ level is based upon the following information. The assigned $4e$ is observed at $+94.4 \text{ cm}^{-1}$ and is broad, and thus the $5e$ would also be expected to be fairly broad, especially since it is calculated to be above the barrier. There is a transition that appears with the expected broadening and expected intensity at $+155.5 \text{ cm}^{-1}$, and is thus assigned as the $5e$. There is a transition at the calculated frequency of $+147.1 \text{ cm}^{-1}$ that is narrow. The $+155 \text{ cm}^{-1}$ transition is also observed in other progressions that

appear in combination with skeletal modes, while the $+147\text{ cm}^{-1}$ transitions does not. Since the $4e$ has an experimental frequency different than the calculated frequency, it would be expected that the $5e$ would also deviate from the calculated frequency. Above the barrier the pure hindered rotor Hamiltonian used to fit the levels in the calculations is inadequate. This is because for the unbound levels, the angular momentum couples too strongly to other sources of angular momentum to allow reasonable separation of the Hamiltonian.

Table 4: Calculated barriers and experimental and calculated transition frequencies for 5-methylindole and complexes.

	5MI		5MI + He		5MI + 2He		5MI + H ₂ O	
	$V'_3 = 80.8\text{ cm}^{-1}$		$V'_3 = 85.3\text{ cm}^{-1}$		$V'_3 = 76.9\text{ cm}^{-1}$		$V'_3 = 92.5\text{ cm}^{-1}$	
	$V'_6 = -21.4\text{ cm}^{-1}$		$V'_6 = -23.5\text{ cm}^{-1}$		$V'_6 = -2.8\text{ cm}^{-1}$		$V'_6 = -23.9\text{ cm}^{-1}$	
	expt	calc	expt	calc	expt	calc	expt	calc
$0a_1$	0	0	0	0	0	0	0	0
$1e$	~1.2	1.7		1.5		1.6		1.35
$2e$	39.5	39.5	40.6	40.6	41.3	41.6	42.8	42.8
$3a_2$	52	52.1		52.4		56.9		53.7
$3a_1$	74.6	74.4	76.6	76.6	70.6	70.6	79.9	79.9
$4e$	94.4	100.7		102.2		99.9		104.7
$5e$	156	147.1		148.5		146.5		150.8
$6a_1$	203	205		206.4		204		208.7

The $3a_2$ level is forbidden in first order but can obtain allowed character through the internal-overall rotation interaction. From the discussion above concerning the broadening of E levels, there is an internal-overall rotation interaction taking place. Using the VNCOS

and INROT programs, the $0a_1'' \rightarrow 3a_2'$ transition is calculated to be at $+52 \text{ cm}^{-1}$, although calculated intensity is $10^{-17}\%$ of the origins intensity. There is a very weak, reproducible transition at this frequency.

Several transitions 1400 cm^{-1} above the 1L_b origin are possible members of a 1L_a torsional progression. Attempts to calculate a barrier from the observed frequencies gave calculated frequencies $2-8 \text{ cm}^{-1}$ from the observed. This is compared to $\pm 0.5 \text{ cm}^{-1}$ differences for the torsional progressions of the 1L_b origin. Even though we are unsuccessful in fitting a torsional barrier for the 1L_a state, these transitions cannot be ruled out as being torsional levels as the high density of nearby 1L_b states may be perturbing the 1L_a levels.

As mentioned in chapter four, the members of the torsional progression have satellite peaks that have been identified as 5MI complexes with helium. See Figure 15 for an expanded view of the origin progression with the corresponding He complexes. Tie lines are used to illustrate the 5MI + He complexes torsional progressions. Under the different expansion conditions used in identifying these transitions, the intensities of the members of each progression labeled as a He complex scaled with one another, aiding in their identification. The second helium complex has an additional shift in frequency. The torsional progressions can be fit for both the 5MI + 1He and 5MI + 2He complexes, and these fits are shown in Table 4.

The barriers for the helium complexes are similar to those of the bare molecule, but the differences can give us information concerning the site where the helium attaches to indole. The torsional progression and calculated barrier for 5MI + 1He are very similar to that of the bare molecule. The barrier for the 5MI + 2He has different torsional frequencies, with

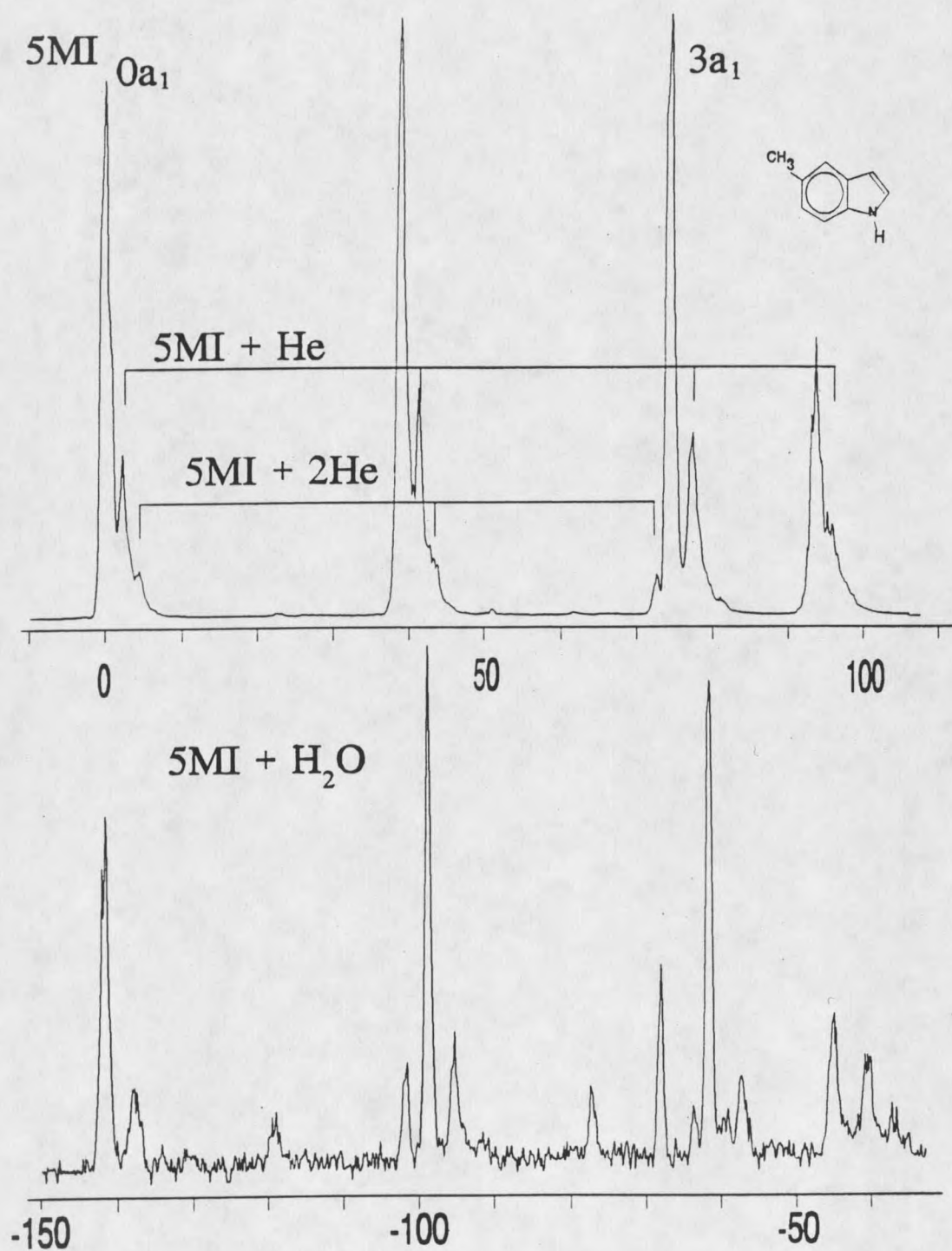


Figure 15: Torsional progressions for 5-methylindole Helium complexes, with a water complex progression on the bottom trace. The torsional levels show a measurable change in their relative frequencies.

the 3α , red-shifting in frequency. The barrier for the 2He complex has a similar V_3 barrier height, however the width of the well has changed significantly, with V_6 changing from -25 cm^{-1} to -2.8 cm^{-1} . The decrease in the width of the well also means less tunneling interaction. The small perturbation caused by the first He may indicate that it attaches to the five membered ring, relatively distant from the methyl. The change in barrier for the 2He complex means that the second He is significantly increasing the perturbation experienced by the CH_3 , and thus the He is attaching at a site closer to the CH_3 , likely the six-membered ring.

Another complex observed in these experiments is that of 5MI with water. (See the bottom trace of Figure 15.) Its progression lies $\sim 150 \text{ cm}^{-1}$ to the red of the bare molecule origin and its assignment as the $5\text{MI} + 1\text{H}_2\text{O}$ complex is supported by work on other indole complexes.⁴²⁻⁴⁶ Because this spectrum was obtained only with water due to atmospheric contamination, the signal to noise ratio is fairly low. The rotor progression is similar to the other complexes, but the levels have increased in frequency relative to the bare molecule, indicative of a higher barrier. The barrier height has increased to 92.5 cm^{-1} , similar in magnitude to how much the barrier decreased for the 2He complex. Wide potential wells also give a large V_6 value. The water molecule has a permanent dipole, therefore it should cause a larger electronic perturbation than the addition of two helium. The $\sim 150 \text{ cm}^{-1}$ red-shift of the $5\text{MI} + \text{H}_2\text{O}$ complex is evidence of this increased perturbation, compared to the 2.2 cm^{-1} blue shift of $5\text{MI} + 2\text{He}$. The perturbation in the local electron density where the H_2O complexes should also be larger than the perturbation created by the 2He complex. Since the perturbation on the methyl rotor is similar between the water and 2He complex, the

water likely is attaching to the five-membered ring. The nitrogen acts as a hydrogen bonding site, and therefore we would expect the water to complex there.

There is one other area to be discussed in terms of electronic effects on the methyl rotor in 5MI, and this is how an 109 cm^{-1} out of plane skeletal mode affects its torsional progression. The low-frequency region of 5MI shown in Figure 14 shows a weak progression beginning at 109 cm^{-1} that is missing the $3a_1$ transition, and also has reduced intensity in the first member. Transitions belonging to this progression appear at 109 , 148 and 203 cm^{-1} , identified as the $1e$, $2e$, and $4e$ members of the torsional progression. Intensities are correct for the E levels, however this does not explain the absence of the A_1 levels. Using the G_6 molecular symmetry group as discussed in chapter two and the symmetry of the out of plane modes, the cause of the missing A_1 levels can be explained. Out of plane modes are nondegenerate and are non-totally symmetric, so they are of A_2 symmetry in G_6 . This means that for molecules containing E torsional levels, the torsional \otimes vibrational symmetry will be $E \otimes A_2 = E$ and the transition is symmetry allowed. Even though it is symmetry allowed, it most likely will be extremely weak. For molecules with A levels, only the $0a_1$ level has significant population in the jet and the symmetry of an out of plane vibrational level will be $A_1 \otimes A_2 = A_2$ and will be forbidden. This would explain the observation of a weak progression of E levels only for an out of plane mode. There is a possibility that the $3a_2$ level could have intensity, but as observed from the origin progression, it is extremely low and is unobserved in this out of plane torsional progression.

There is one other low frequency vibration at $+135\text{ cm}^{-1}$ that cannot be fit using any of the above assignments. The transitions appears in combination with many of the skeletal

modes but cannot be accounted for in the origin progression. In p-methyl-trans-stilbene¹⁴ there is a similar frequency transition assigned as the combination band $3\alpha_2 + 37_0^1$. This 135 cm^{-1} band in 5MI could be a combination band involving $3\alpha_2$ and a vibration that directly affects the methyl potential and breaks the planar symmetry of the molecule in the vicinity of the CH_3 group. Skeletal modes which fit this description are the out of plane methyl wag or puckering of the five membered ring. Since the $3\alpha_2$ frequency in 5MI is 52 cm^{-1} , the A_2 vibrational mode required to make the combination band allowed would have a frequency of $\sim 83 \text{ cm}^{-1}$.

3-methylindole

The assignments for the methyl rotor progression in 3-methylindole⁴⁴ (3MI) are more difficult to make as the spectrum does not contain an intense torsional progression. This indicates that the methyl does not change conformation upon excitation. The origin of the 3-methylindole spectrum has been assigned to the 1L_b electronic state, however there are several low frequency transitions that do not show clear 1L_a or 1L_b character based on 2hv data.

It has been possible to fit a barrier for the internal rotation of the methyl group based on a comparison of the excitation spectra of protonated and deuterated 3MI. See the comparison of the lower frequency regions of 3MI and 3MI- CD_3 in Figure 16. Note that the origin is intentionally saturated in order to obtain good S/N and the proper intensities for the weaker transitions. The barriers have been fit for S_0 and 1L_b states, and the 1L_a barrier can be estimated from observed splittings of transitions with 1L_a character.

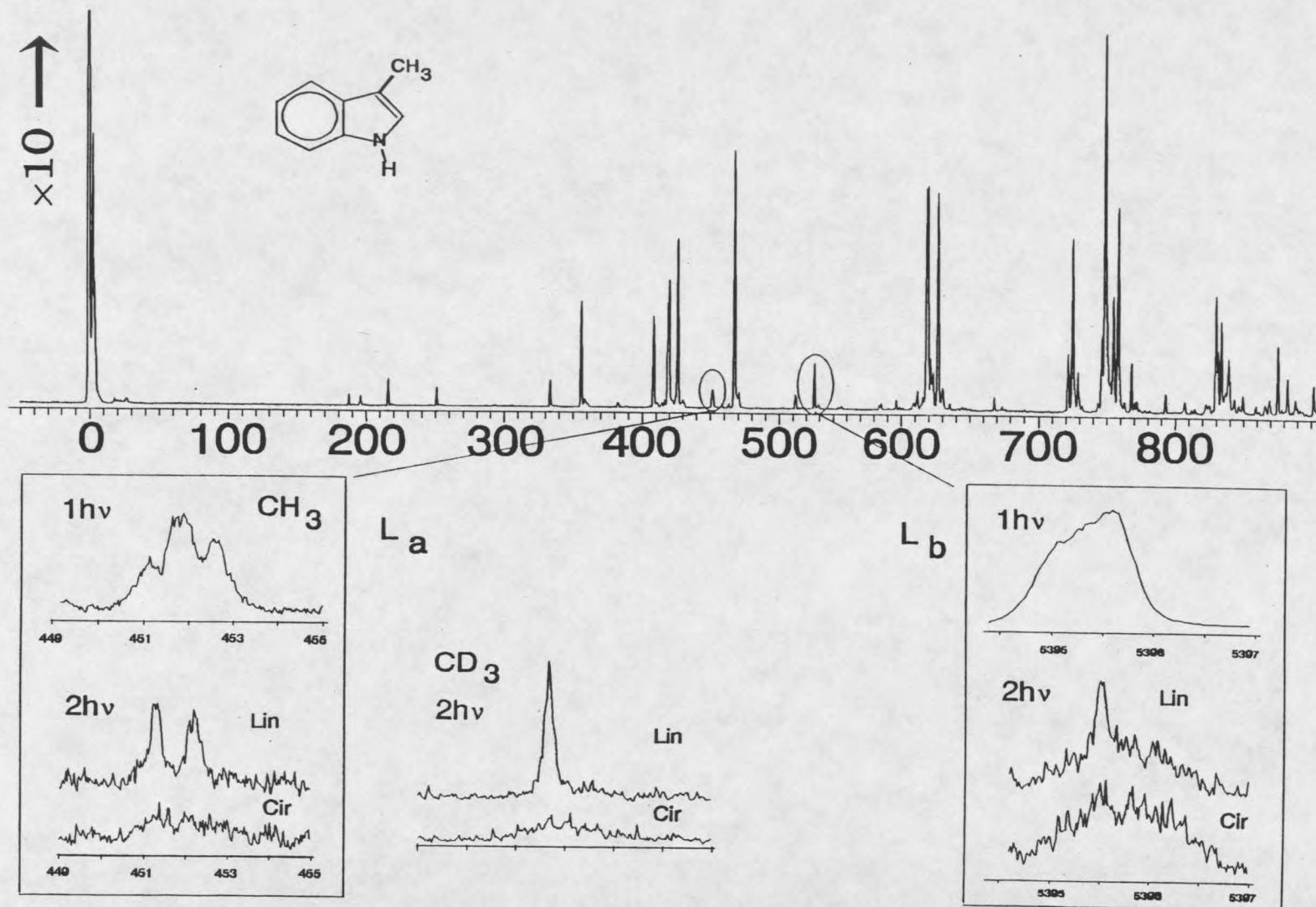


Figure 16: Comparison of the weak peaks in the low frequency region of the 3MI and 3MI-CD₃ spectra. The transitions correlate as indicated by the tie lines.

The spectrum of deuterated 3MI correlates well with the spectrum of the protonated molecule, however there are two transitions at 188 and 197 cm^{-1} in the protonated spectra that correspond with only one transition at 146 cm^{-1} in the deuterated spectrum. The 25% change in frequency is indicative that the vibrational level would be exclusively motion of the methyl hydrogens. Figure 17 shows how the methyl transitions in the CH_3 spectrum can be compared to those in the CD_3 spectrum based upon putting the spectrum on a plot of excited state combination differences (frequencies in the excitation spectrum) as a function of the pure V_3 barrier height. From these plots, the 188 cm^{-1} transition in 3MI can be assigned as $3a_1$, while the 197 cm^{-1} transition can be assigned as the $4e$. The only way to have the $3a_1$ and $4e$ torsional levels separated by 9 cm^{-1} is to have a V_3 barrier of $\sim 300 \text{ cm}^{-1}$. The internal rotational constant for CD_3 changes from CH_3 , and the same 300 cm^{-1} barrier in CD_3 would cause the $3a_1$ and $4e$ levels to coalesce into a single peak at 146 cm^{-1} because of the reduced tunneling interaction. The calculated fits and experimental results are shown in Table 5. The barrier for internal rotation in 1L_b is $V_3 = 307.6 \text{ cm}^{-1}$, $V_6 = -10.9 \text{ cm}^{-1}$, and $B = 5.30 \text{ cm}^{-1}$.

The ground state barrier for 3MI can be inferred from the origin not being split. The origin has a $0a_1-1e$ splitting that is not observable with our resolution, and does not show a sharp 9Q branch in the linearly polarized $2h\nu$ contour. The Levy group⁴⁴ has placed a value of 0.0304 cm^{-1} on the $0a_1-1e$ splitting based on high-resolution experiments. We used Levy's $0a_1-1e$ frequency of the splitting and our observed intensities of the $3a_1$ and $4e$ levels to predict the ground state barrier. There are two barriers at 258 cm^{-1} and 443 cm^{-1} which predict a 0.0304 cm^{-1} $0a_1-1e$ splitting. Since Levy's group did not state whether the $1e$ or

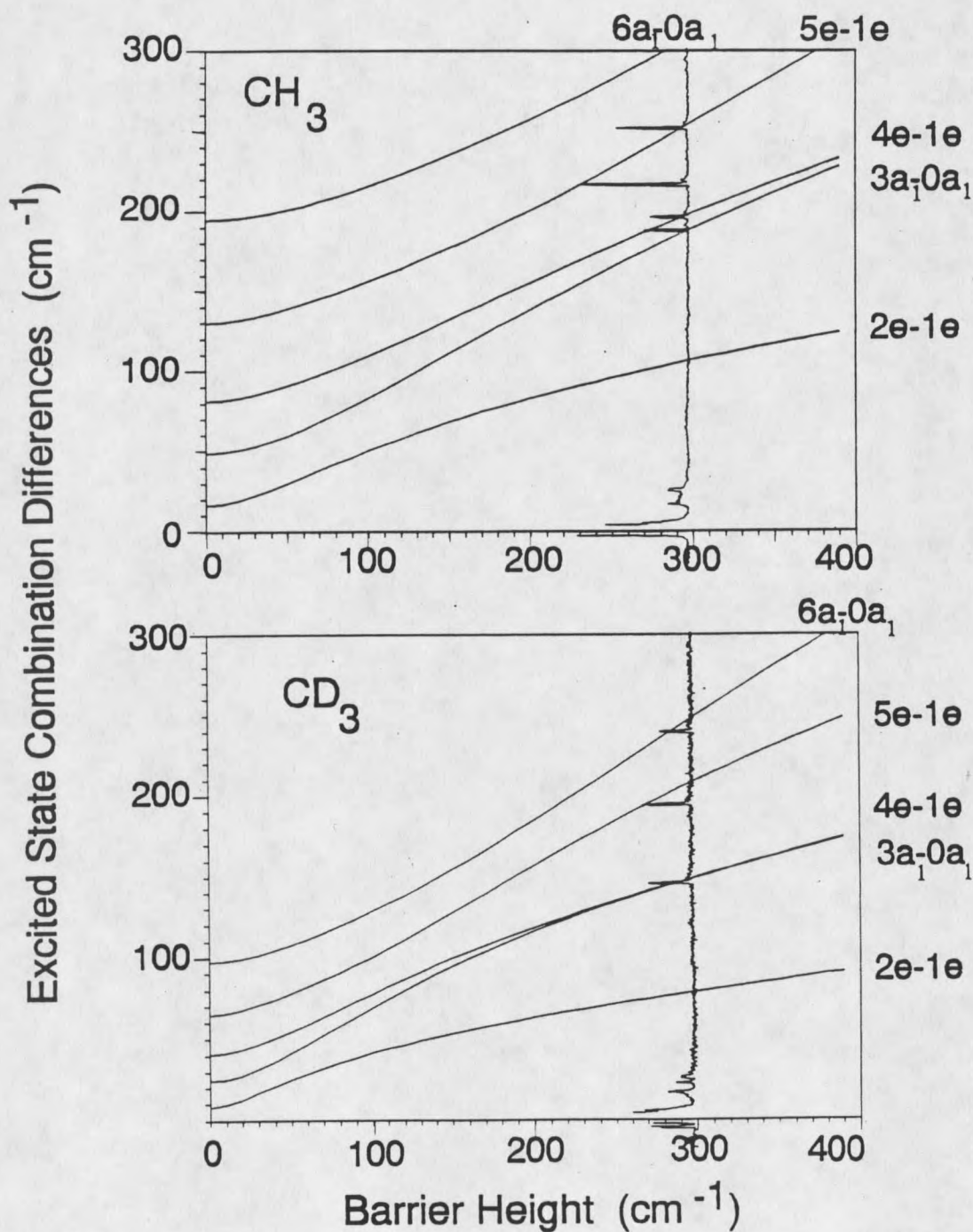


Figure 17: Plots of excited-state combination differences (same as relative frequencies) vs. a V_3 barrier height. The corresponding 3MI spectra are shown plotted to the same frequency scale indicating the assignment of the torsional transitions and the approximate barrier height.

$0a_1$ is higher in energy, both barriers must be examined. The barrier at 257.8 cm^{-1} predicts intensities for the $3a_1$ and $4e$ transitions that are significantly lower than those obtained experimentally. The higher barrier of 458 cm^{-1} fits the experimental intensities better. The calculated intensities also predict that the $1e \rightarrow 2e$, $1e \rightarrow 5e$ and $0a_1 \rightarrow 6a_1$ transitions would have intensities 1000, 30 and 10 times weaker than the $3a_1$ and $4e$ transitions. Since the $3a_1$ and $4e$ transitions only have 0.8% of the origin's intensity, it would be expected that these other transitions would be unobserved. Since there is no conformational change upon excitation, the intensity observed in the $3a_1$ and $4e$ transitions has to be generated by the barrier difference, which indicates that the 450 cm^{-1} barrier is the correct value for S_0 .

Table 5: Calculated frequencies and intensities for the 1L_b of 3-methylindole using two different ground-state barriers. ($V_3'' = 307.6 \text{ cm}^{-1}$, $V_6'' = -10.9 \text{ cm}^{-1}$ and $B' = 5.30 \text{ cm}^{-1}$.)

transition	$V_3'' = 257.8 \text{ cm}^{-1}$		$V_3'' = 443.2 \text{ cm}^{-1}$	
	frequency	intensity	frequency	intensity
$0a_1'' \rightarrow 0a_1'$	0	combined	0	combined
$1e'' \rightarrow 1e'$	-0.0304	100	0.0304	100
$1e'' \rightarrow 2e'$	103.1	6.8×10^{-5}	103.1	1.9×10^{-4}
$0a_1'' \rightarrow 3a_1'$	188.1	0.025	188.1	0.33
$1e'' \rightarrow 4e'$	196.3	0.021	196.4	0.33
$1e'' \rightarrow 5e'$	256.9	5×10^{-5}	256.9	0.011

We also have an indication of how the 1L_a electronic state affects the barrier to internal rotation. In Figure 16, there is a comparison of the one- and two-photon contours of an 1L_a and an 1L_b transitions. Note that the 1L_a transition has a resolvable $0a_1$ - $1e$ splitting in the

two-photon contour. This is not observed in the 1L_b transitions. Upon deuterating the methyl, the 1L_a transitions coalesce into one observed peak. This splitting can thus be used as a diagnostic of the electronic character of the state, however it may not be completely reliable because of the potential overlap of 1L_a and 1L_b states.

The splitting of $\sim 1 \text{ cm}^{-1}$ is indicative of a barrier of $\sim 100 \text{ cm}^{-1}$ for 1L_a . Since the 1L_a doublets are observed having nearly equal intensity, there is no change in methyl conformation in the ground and 1L_a states. The blue transition in the doublet is slightly broader in the $2h\nu$ linearly polarized contours due to the internal-overall rotation interaction, thus we assign this as the le transition. Since the barrier is several times higher in 3MI, there is less tunneling between the wells and less internal-overall rotation interactions. The implication of having the le higher in energy than the $0a_1$ in the excitation spectrum is that the barrier is smaller in the excited state than the ground state because the splitting is inversely related to the barrier height.

Comparison of the barriers obtained for the ground, 1L_a and 1L_b states for 3MI and 5MI yields several conclusions. The 1L_b state of 5MI has a barrier of approximately 80 cm^{-1} . Similar barriers are obtained for asymmetrical aromatic rings where direct steric interaction with a substituent does not occur. The barrier is also very similar to the excited state barriers calculated for the stilbene analogues discussed in the following chapters. 3MI has relatively high barriers in the ground and 1L_b electronic states. This is typical of a methyl group adjacent to a π electron containing functional group in an aliphatic system. This larger barrier is due to the asymmetry of the π system, explained in 3MI owing to the presence of a double bond on one side of the 3 position, along with a nitrogen in the five-membered

ring.⁴⁷ Further comparisons of the electronic effects on the barrier to internal rotation will be discussed in the conclusion chapter.

CHAPTER SIX

EXPERIMENTAL RESULTS: STILBENES

The stilbene molecule and its derivatives have received significant attention over the past several decades as a prototypical model for the study of reaction dynamics in the condensed phase. Stilbenes undergo cis/trans photoisomerization, and the dynamical pathway has been a point of contention for many years.⁴⁸⁻⁵⁸ A review of the current understanding of the photoisomerization of stilbenes has been written Waldeck.¹³ Stilbene is also an important molecule in organic synthesis, and is the structure of many laser dyes.⁵⁹ The feature of interest relevant to this study of electronic effects on the barrier to methyl internal rotation is the extent of the stilbene π system. Most of the previous work on electronic effects has been on single ring systems^{2-4,6-11}, while stilbene is an extended conjugated system with two phenyl rings connected by an ethylenic bond. If delocalized, the π electronic system should allow substituents on one phenyl ring to affect the π electron density on the other phenyl ring, which can then be measured by changes caused in the barrier to methyl rotation. Substitution on the ring opposite the methyl group should influence methyl barriers primarily through electronic effects, and steric interactions should be negligible.

In this study we focus on the *trans* isomer of stilbene which has a strong absorption coefficient and fluoresces strongly. This is in contrast to the fluorescence spectrum of *cis*-

stilbene, which is broad and featureless even in a jet.⁶⁰ The two isomers absorb in different frequency regions, thus small impurities of the cis-isomer should not interfere with the trans-stilbene spectrum. The jet-cold fluorescence excitation spectrum of trans-stilbene has been analyzed by Zwier⁶¹ et.al. and Ito.⁶² Trans-stilbene has been determined to be planar in both its ground and singlet excited states. The assignment of a planar stilbene is based on the one quantum forbidden nature of vibrations involving the out-of-plane motions of the phenyl rings with respect to the ethylenic plane in the isolated molecule and the symmetry of those vibrations. The planarity of trans-stilbene has been confirmed by Pratt's group using high-resolution rotational studies.⁶³

There are 78 normal modes in trans-stilbene. Three low-frequency modes can be used to identify all transitions in the first 200 cm^{-1} of the fluorescence spectrum. The two lowest frequency modes are of A_u symmetry. These modes are ν_{36} , which is the ethylenic carbon (C_e)-phenyl out-of-plane bend, and ν_{37} , the C_e -phenyl torsion. See Figure 18 for a description of the modes. Because they are both out-of-plane modes of A_u (or A'' in C_s) symmetry, they require two quanta to be allowed. Another low-frequency mode that is a dominant feature in all of the stilbene analogues is ν_{25} which has A_g symmetry and is the C_e - C_e -phenyl in-plane bend. A new skeletal mode assignment for the stilbenes is ν_{24} , which also has A_g symmetry and has been predicted by Warshel to occur at $\approx 300\text{ cm}^{-1}$. This vibration is a C_e -C-C bending motion. All mode numbers are from Warshel's QCFF- π calculations.⁶⁴

Spectral evidence suggest that the para-substituted stilbenes investigated here also retain planarity in both the ground and excited state. Table 6 shows the correlation between the C_{2h} modes for trans-stilbene with those of C_s symmetry for para substituted stilbenes. As

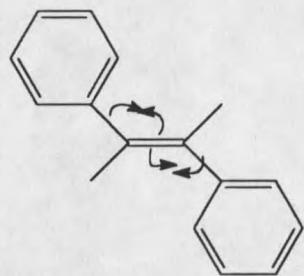
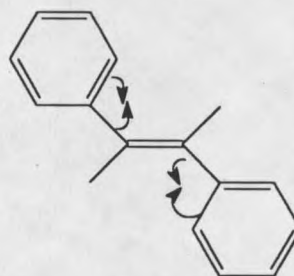
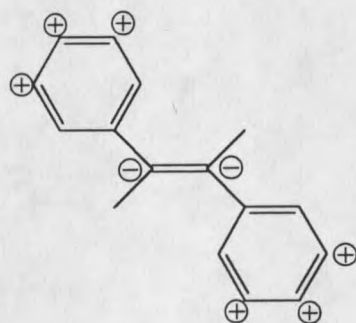
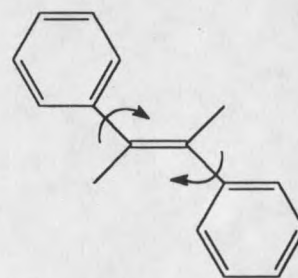
 v_{24} C₆-Phenyl Bend v_{25} Phenyl Wag v_{36} Phenyl Flap v_{37} out-of-plane
Phenyl Torsion

Figure 18: Low frequency modes of trans-stilbene.

will be further discussed in chapter seven, the meta-substituted trans-stilbenes appear to also retain their planarity in both S_0 and S_1 .

This section presents the spectra obtained for six substituted stilbenes, three of which have two observed conformers which will also be discussed. The substituents were chosen because of their electron donating or electron withdrawing properties. Their influence on the methyl group is determined by changes in the barrier to internal rotation relative to p-methyl-trans-stilbene. The experimental data includes the 1hv fluorescence excitation spectrum for each molecule, along with 2hv data and dispersed fluorescence spectra acquired to support the assignments of vibrational, electronic, and torsional transitions.

Table 6: The symmetry correlation between C_{2h} and C_s .

normal mode	molecular point group	
	C_{2h}	C_s
v36 (C_e -Ph oop bend)	A_u	A''
v37 (C_e -Ph oop twist)	A_u	A''
v25 (C_e - C_e -Ph in-plane bend)	A_g	A'

Experimental Results

p-methyl-trans-stilbene

The 1hv fluorescence excitation spectrum of p-methyl-trans-stilbene is shown in Figure 19. In this spectrum the dye laser was scanned at a rate of $0.10 \text{ cm}^{-1}/\text{sec}$, with points digitized and stored every 0.15 cm^{-1} . The S_1 origin has an absolute frequency of $31,741.0 \text{ cm}^{-1}$. The origin appears as a doublet owing to the $0a_1$ and $1e$ torsional transitions discussed

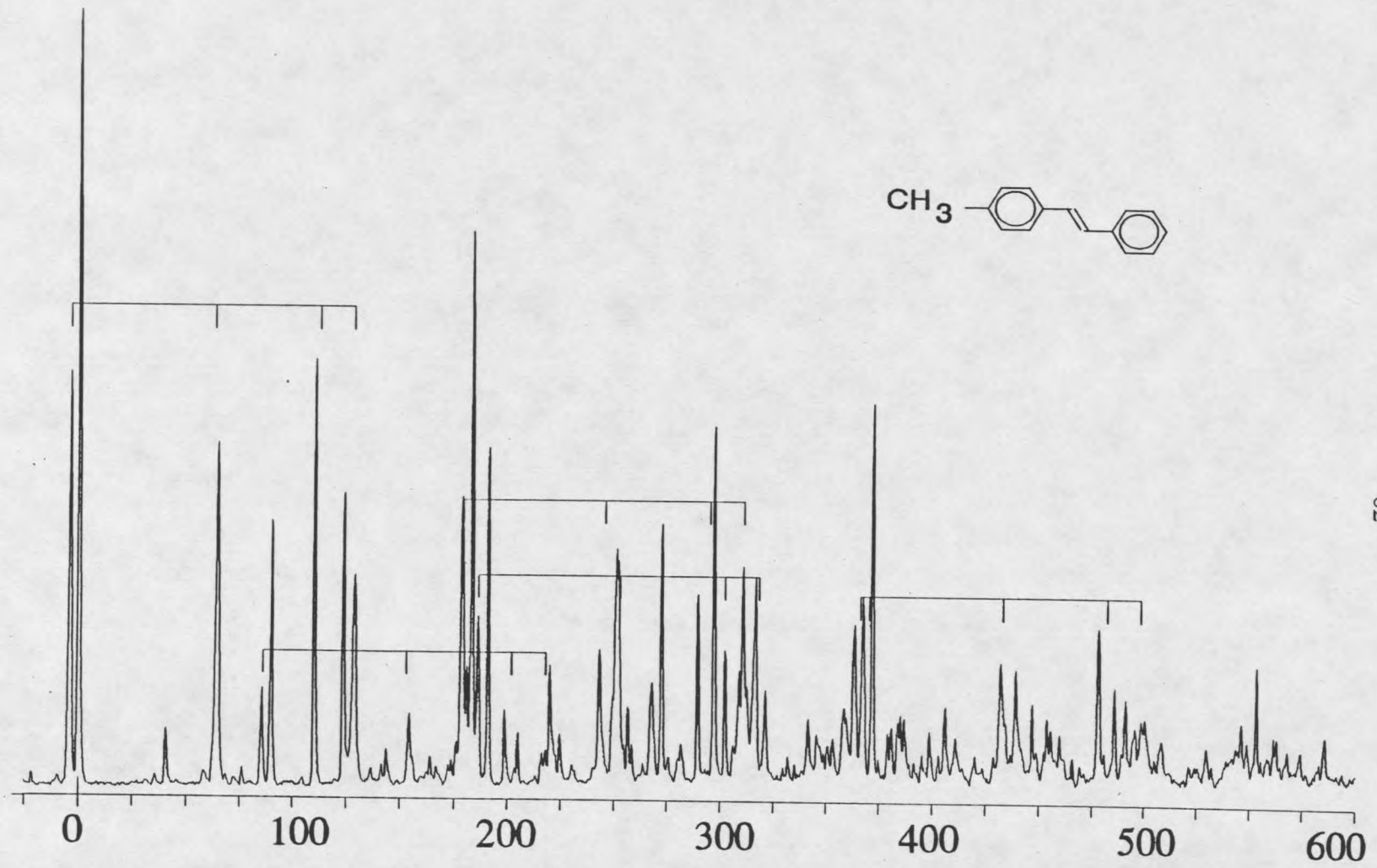


Figure 19: The $1h\nu$ fluorescence excitation spectrum of p-methyl-trans-stilbene.

in Chapter two. Here the $1e$ has a frequency -4.2 cm^{-1} less than the $0a_1$. All transitions will be reported relative in frequency to the $0a_1$ transition. The methyl rotor torsional frequencies and some skeletal vibrational frequencies for S_1 are given in Table 7. The assignment of 36_0^2 is not shown in the table and will be discussed in chapter seven. This molecule was previously studied by Spangler and Zwier¹⁴, but reexamined here because of its importance relative to the other stilbenes investigated. $2h\nu$ spectra were also taken for several transitions to see if more information could be ascertained.

Table 7: Torsional frequencies for p-methyl-trans-stilbene.

	0_0^0	37_0^2	25_0^1
$0a_1$	0 cm^{-1}	$+89.7 \text{ cm}^{-1}$	183.0 cm^{-1}
$1e$	-4.2	-4.2	-4.5
$2e$	64.2	64.5	68.1
$3a_2$	74.5		
$3a_1$	109.8	108.9	114.0
$4e$	128.7		

The barrier for S_1 as calculated from the transition frequencies is $V_3 = 150 \text{ cm}^{-1}$. The internal rotation constant used is $B' = B'' = 5.3 \text{ cm}^{-1}$. Adding a V_6 term does not improve the fit. The barrier for S_0 was found to be $\sim 28 \text{ cm}^{-1}$. Every stilbene analogue in this study has a barrier in the ground state of less than 30 cm^{-1} , and the implications of this will be discussed in Chapter seven.

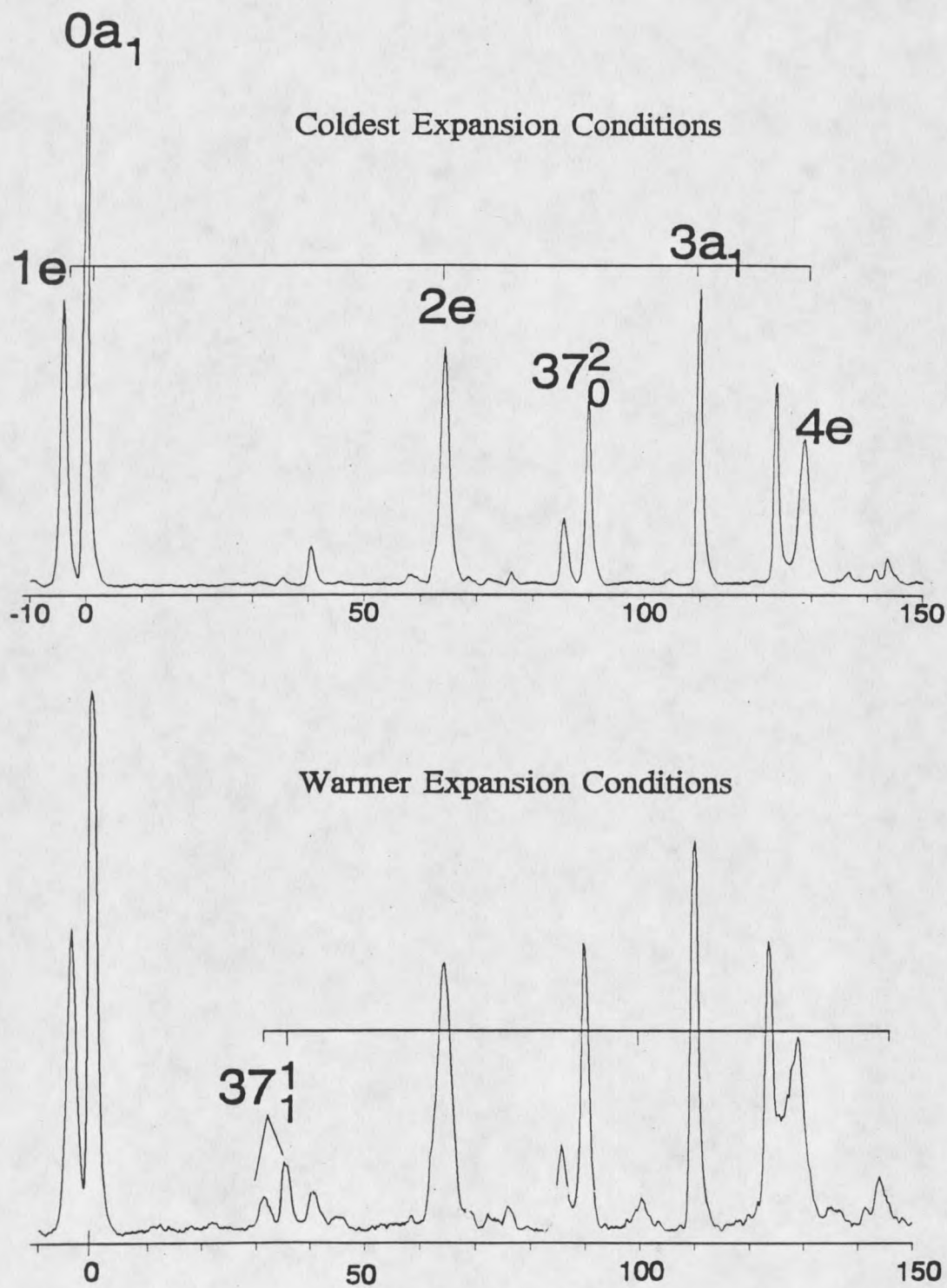


Figure 20: $1h\nu$ fluorescence excitation spectra of p-methyl-trans-stilbene under different expansion conditions.

Careful backing pressure studies were performed to allow the identification of hot bands. Figure 20 shows a comparison of the first 200 cm^{-1} taken at "warm" (1.5 barr He) and "cold" (4 barr He) expansion conditions. The bandwidths increase at lower backing pressure due to an increase in the rotational temperature of the ground state. A doublet appears with a $0a_1$ frequency of 35.1 cm^{-1} above the origin, which has two possible assignments, 37_1^1 or 36_0^2 . The transitions gain significant intensity in the warmer spectrum, thus identifying them as a hot band. The low frequency of 35.1 cm^{-1} would indicate these transitions as the hot band 37_1^1 with the other members of the torsional progression also being observed. Zwier and LHS also assigned an overlapping transition as 36_0^2 , but we have tentatively reassigned this vibration as will be discussed in the next chapter.

As mentioned above, 2hv scans were also acquired for most of the transitions with significant intensity. It was hoped that more information could be extracted from the 2hv contours, as was possible in the methylindole studies (chapter 5). Since p-methyl-trans-stilbene and the other methylindoles have C_s point group symmetry, and are near prolate tops as calculated using AMPAC in an AM1 calculation ($\kappa = -0.99029$ for p-methyl-trans-stilbene); it was expected that there could be similarities in the 2hv contours. Figure 21 shows the linearly polarized 2hv contours of the $1e-0a_1$ transitions, with the 1hv contours shown on the bottom trace for comparison purposes. The 2hv data was acquired with a point digitized every 0.03 cm^{-1} , and the spectrum shown is an average of 20 scans. The 1hv trace was taken with a point every 0.3 cm^{-1} . The $1e$ contour does have a shoulder to the red, but no strong 9Q branch. Most of the other vibrations and torsional features in this molecule were examined using 2hv linearly polarized scans, but no new information could be extracted.

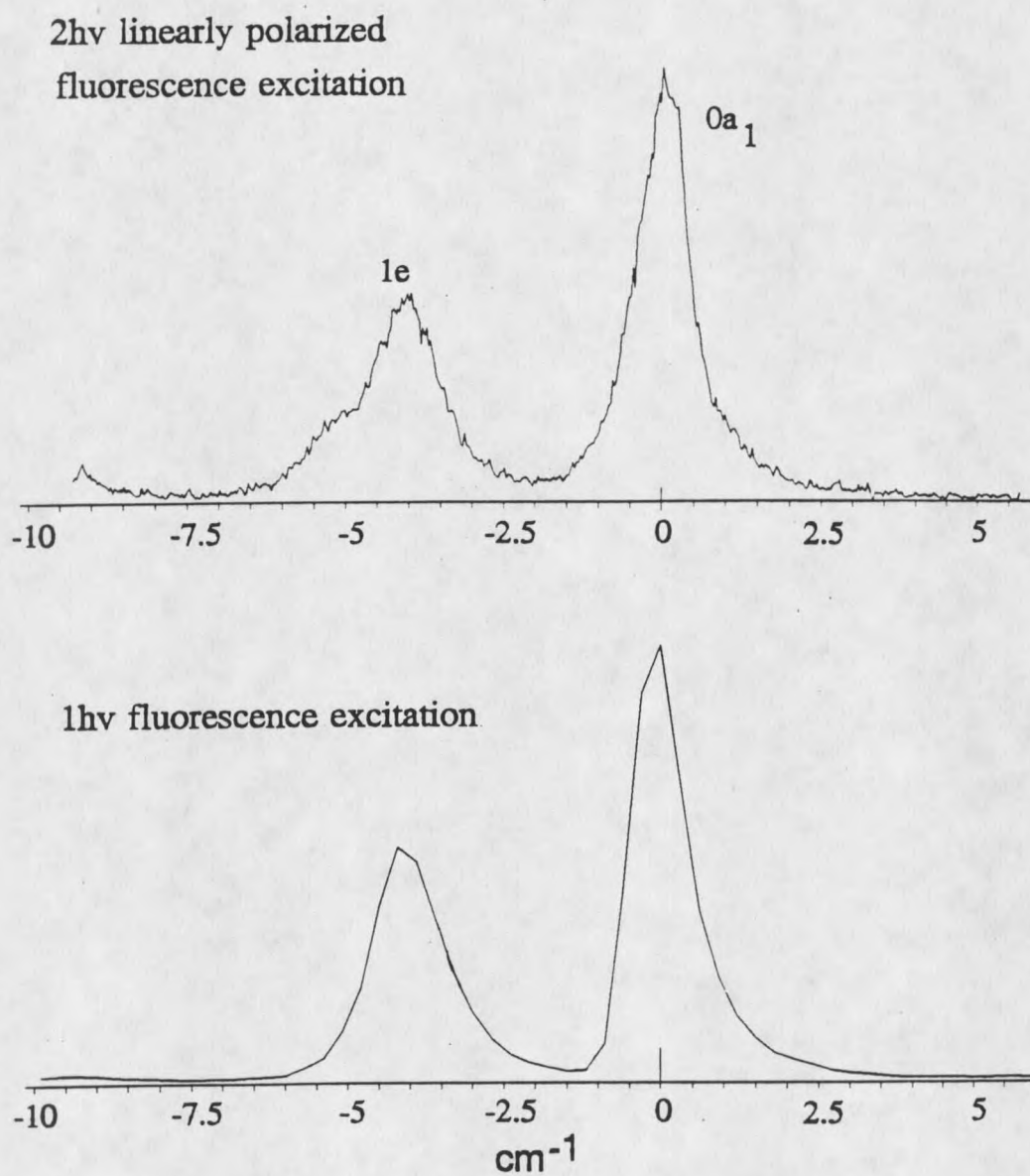


Figure 21: The linearly polarized 2hv contour of the origin of p-methyl-trans-stilbene on the top trace with the fluorescence excitation contour below.

p-methoxy-trans-stilbene

The methoxy group is a strong electron donor which makes it a good candidate for investigating the effect of substituents on a methyl rotor in an extended π system. Since no stilbenes with methoxy substitution have been previously studied, p-methoxy-trans-stilbene was investigated to understand the methoxy-stilbene vibrational structure before examining methyl rotor effects in p'-methoxy-p-methyl-trans-stilbene. Two electronic origins for p-methoxy-trans-stilbene are observed and are labeled as the A and B 0_0^0 in Figure 22. Since trans-stilbene and p-methyl-trans-stilbene each have only one observed electronic origin, the two electronic origins are likely due to the conformations of the methoxy group. The spectrum was taken with a digitized point every 0.3 cm^{-1} , and is an average of three scans. Note that the B origin appears 278 cm^{-1} above the A origin, with the absolute frequency of the A origin being $30,744.0 \text{ cm}^{-1} \pm 10 \text{ cm}^{-1}$. There are several pieces of information which indicate that the $+278 \text{ cm}^{-1}$ transition is another origin instead of being a $+278 \text{ cm}^{-1}$ vibrational level. The first indication that we are dealing with more than one electronic origin is the greatly increased congestion in the spectrum compared to p-methyl-trans-stilbene. We would not expect replacing the methyl group with a methoxy to cause such an increase in vibrational structure for such a small change in the molecular structure. The transition at $+278 \text{ cm}^{-1}$ does not behave like any identified vibrations of trans-stilbene, and a ν_{25} frequency much different than that of the first origin can be built from it. When this $+278 \text{ cm}^{-1}$ transition is identified as another electronic origin, the overall similarity of the spectra of the two conformers is readily apparent as seen in Figure 23. However, there are notable and measurable differences. The frequency of 25_0^1 is the most important of these differences as

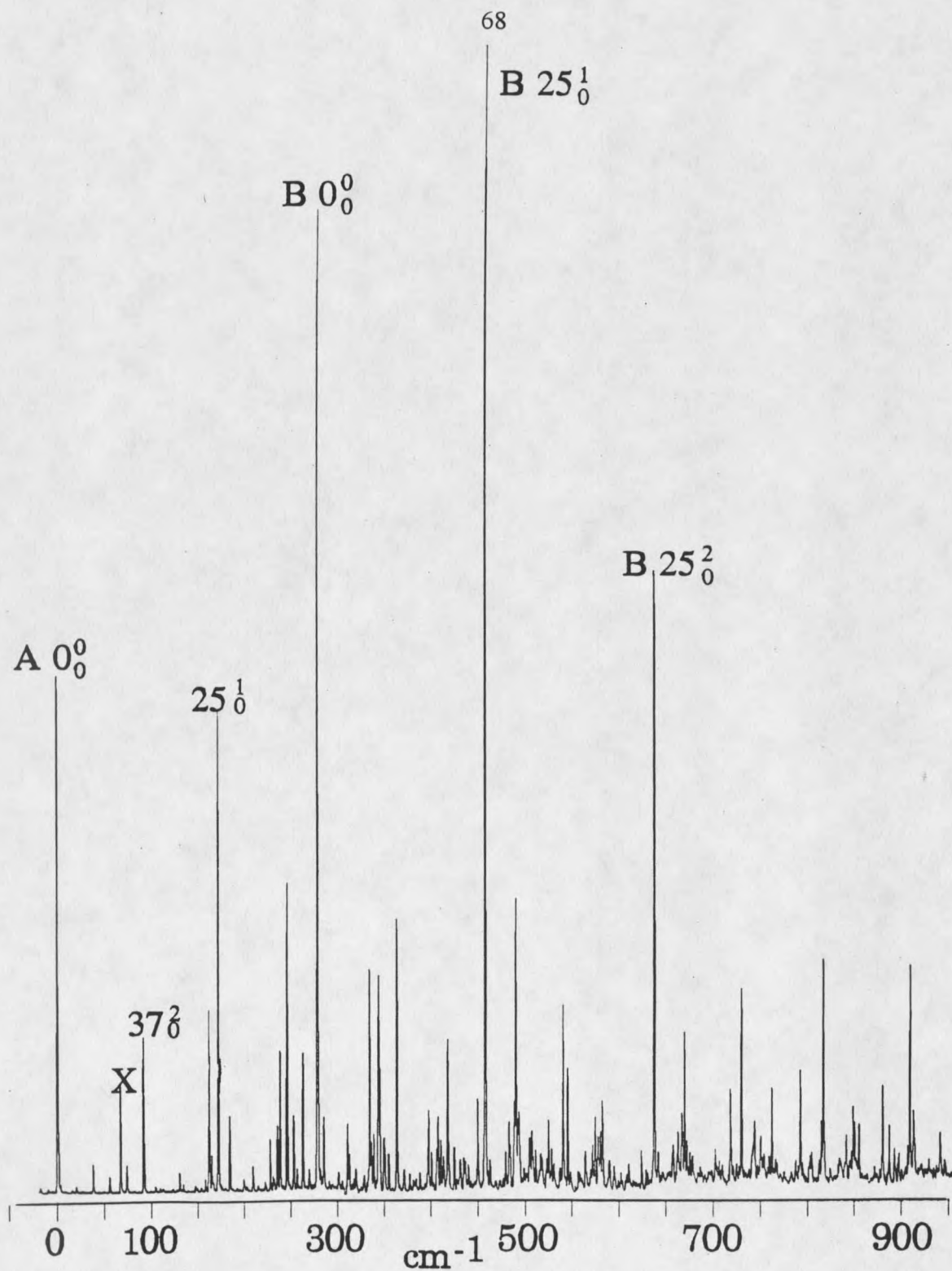


Figure 22: The 1hν fluorescence excitation spectrum of p-methoxy-trans-stilbene.

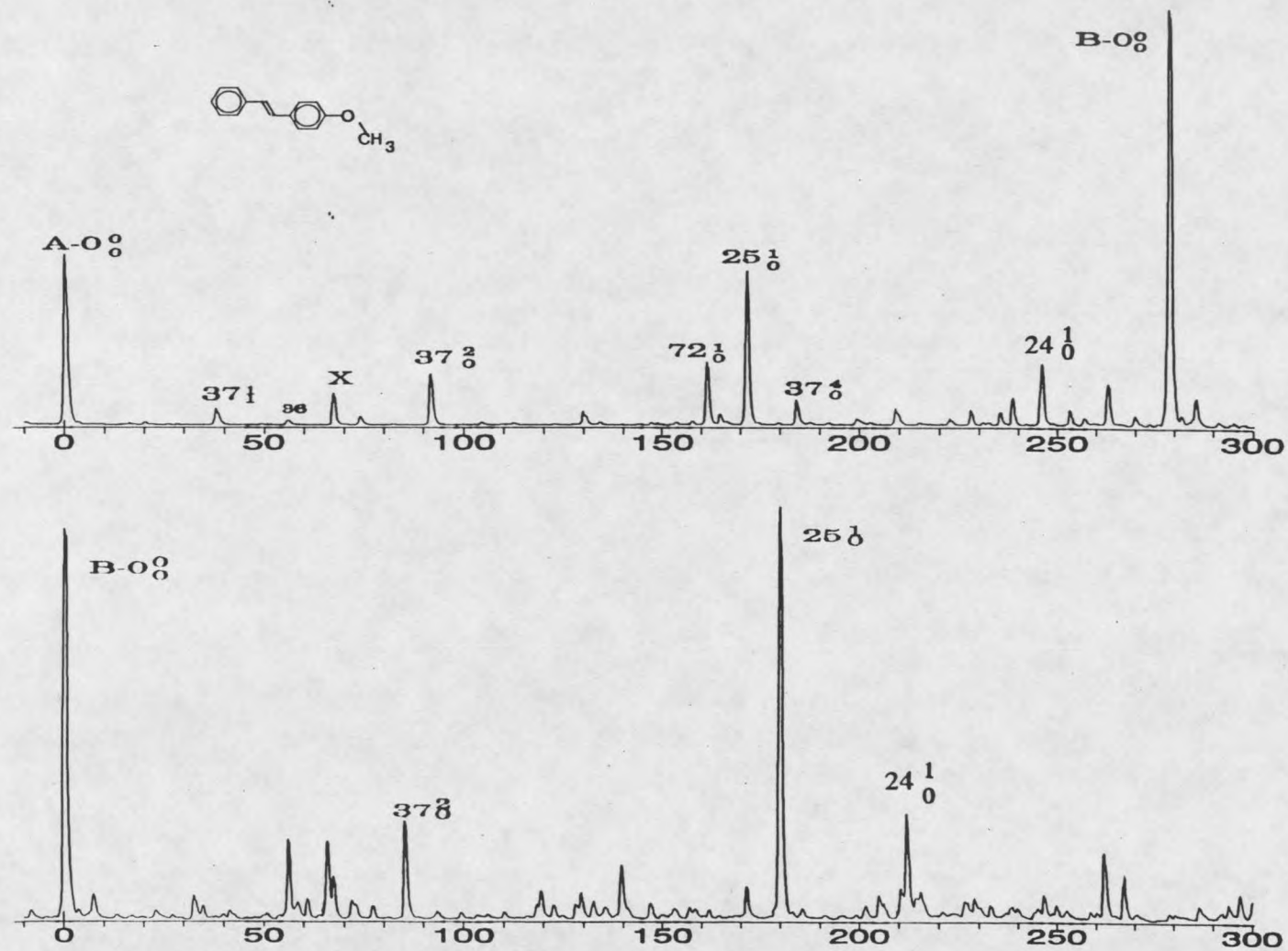


Figure 23: A vs B conformer spectra for p-methoxy-trans-stilbene.

ν_{25} appears in combination with nearly every other vibration. The frequency for 25^1_0 for the A conformer is 171.4 cm^{-1} . It increases to 179.5 cm^{-1} for the B conformer. Nearly every transition can be assigned to known fundamentals, overtones, and combinations for each conformer.

The other low-frequency vibrations also shift slightly in frequency between the conformers. Their assignments are confirmed using dispersed fluorescence as will be discussed later. 37^2 changes from 91.5 cm^{-1} for the A conformer to 85.2 cm^{-1} for the B conformer. 36^2 increases from 55.4 cm^{-1} for A to 60.0 cm^{-1} for B. Since ν_{36} and ν_{37} are of the same symmetry and are not totally symmetric, the combination band 36^137^1 is allowed and is observed at $A+73.8 \text{ cm}^{-1}$. The B 36^137^1 cannot be assigned due to congestion. P-methoxy-trans-stilbene shows a strong tendency to form helium complexes, therefore the spectrum was taken at low helium backing pressure to discriminate against He complexes. Because of the warmer conditions, several hotbands are present, including 37^1_1 at 37.8 cm^{-1} , 37^3_1 at 129.8 cm^{-1} and the combination of $37^1_125^1_0$ at 209.2 cm^{-1} for the A conformer. Once again, no hot bands are assigned for the B conformer due to spectral congestion. The assignments for the main vibrational features are shown in Table 8.

One of the most prominent features in the spectrum of p-methoxy-trans-stilbene is the absence of any methyl rotor transitions. Since the methoxy group does contain a CH_3 group, it is possible that it could contribute torsional features to the spectrum. The spectrum indicates that there is no conformation change for the methyl group upon excitation, and thus only the origin has significant intensity. There is also the possibility of a torsion of the entire methoxy group⁶⁵ which might explain the unidentified transitions at $+67 \text{ cm}^{-1}$ above each

conformer origin. Work is continuing on the identification of this transition, and it will be discussed further in chapter 7. Current spectroscopic examinations of p-hydroxy-trans-stilbene also shows a transition at $+67 \text{ cm}^{-1}$, possibly ruling out methoxy torsion.

Table 8: The major vibrational frequencies for the S_1 states of p-methoxy-trans-stilbene.

assignment	A Conformer	B conformer
36_0^2	55.4 cm^{-1}	60.0 cm^{-1}
37_0^2	91.5	85.2
$36_0^1 37_0^1$	73.8	
X	67.0	58.3, 67.2
25_0^1	171.4	179.5
37_0^4	183.9	171.0
24_0^1	245.8	211.8
$25_0^1 37_0^2$	262.8	$261.7, 267.1^a$
25_0^2	344.0	358.9
$25_0^1 24_0^1$	419.3	391.5
25_0^3	516.4	539.9

a. The assignment for B- $25_0^1 37_0^2$ involves a Fermi Resonance, as is discussed in Ch. 7.

Figure 24 shows the dispersed fluorescence from the A and B origins. By exciting the 0_0^0 , several identifying features between the conformers become apparent. Note that in the spectra presented, the laser resonance frequency has not been corrected for scattered light. The transitions at $A+20.6 \text{ cm}^{-1}$ and $B+23.5 \text{ cm}^{-1}$ are identified as 37_0^2 for each conformer. In p-methyl-trans-stilbene the frequency for the fundamental of ν_{37} in the ground state is found to be extremely low ($\approx 9 \text{ cm}^{-1}$)¹⁴ thus this assignment is likely correct. Examination of the dispersed fluorescence spectra from 37_0^2 for both conformers supports this assignment,

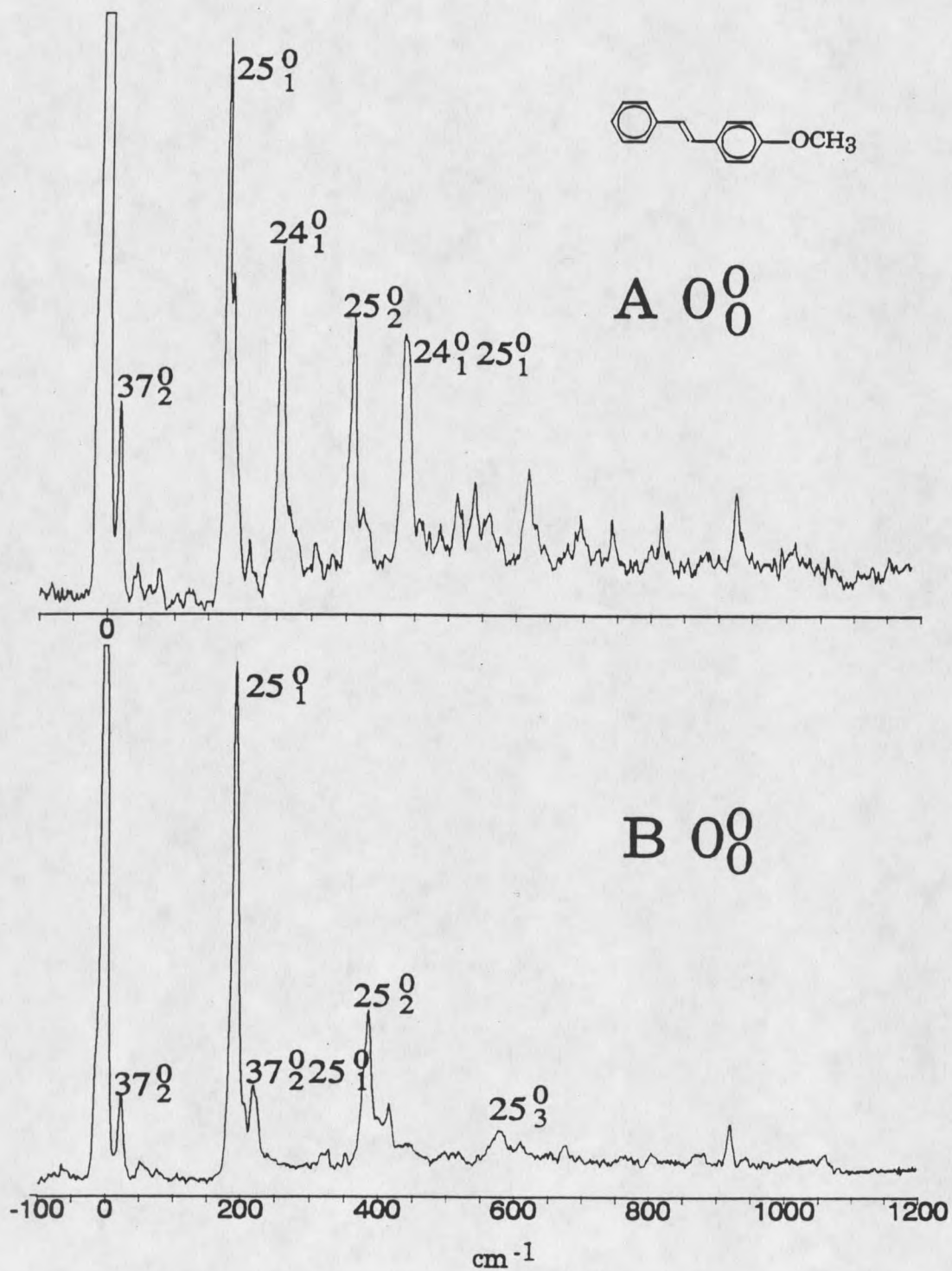


Figure 24: The dispersed fluorescence from the origins of the A and B conformers of p-methoxy-trans-stilbene.

showing a strong progression in ν_{37} as seen in Figure 25. The most intense feature in both of the spectra is 25^0_1 , having a frequency of 177.5 cm^{-1} for A and 193 cm^{-1} for B. The most striking distinction between the conformers is the appearance of a transition at $A+258 \text{ cm}^{-1}$. This is an intense vibration, and appears in combination with ν_{25} . As will be discussed later, this is tentatively assigned as ν_{24} .

P-methoxy-trans-stilbene's vapor pressure is such that most transitions with an intensity of $\approx 5\%$ of the origin's intensity could be examined via dispersed fluorescence. Since this molecule is commercially available, longer optimization periods were possible for alignment and in achieving optimal sampling conditions, a luxury not available for other stilbenes that had to be synthesized and were available in limited quantities. This also permitted longer data acquisition times enabling the study of weak transitions. The congestion in the spectrum caused by the conformers along with many low frequency transitions made dispersed fluorescence a necessary method in assigning transitions. With many of the weaker transitions the entrance slit had to be widened, sometimes up to 400μ to allow enough emission through to obtain acceptable S/N. Examination of the Franck-Condon factors is also an indication of the assignment of the transition. For example, in Figure 25, when 25^1_0 is excited and its emission dispersed, there is no transition at $+178 \text{ cm}^{-1}$, the expected frequency for 25_1 . The Franck-Condon factors do not have sufficient overlap to show intensity. The vibrations of 25_2 and 25_3 have strong intensity. Assignments of the ground and excited states were verified using the observed intensities and the frequency differences, which are dependent on the transition being excited.

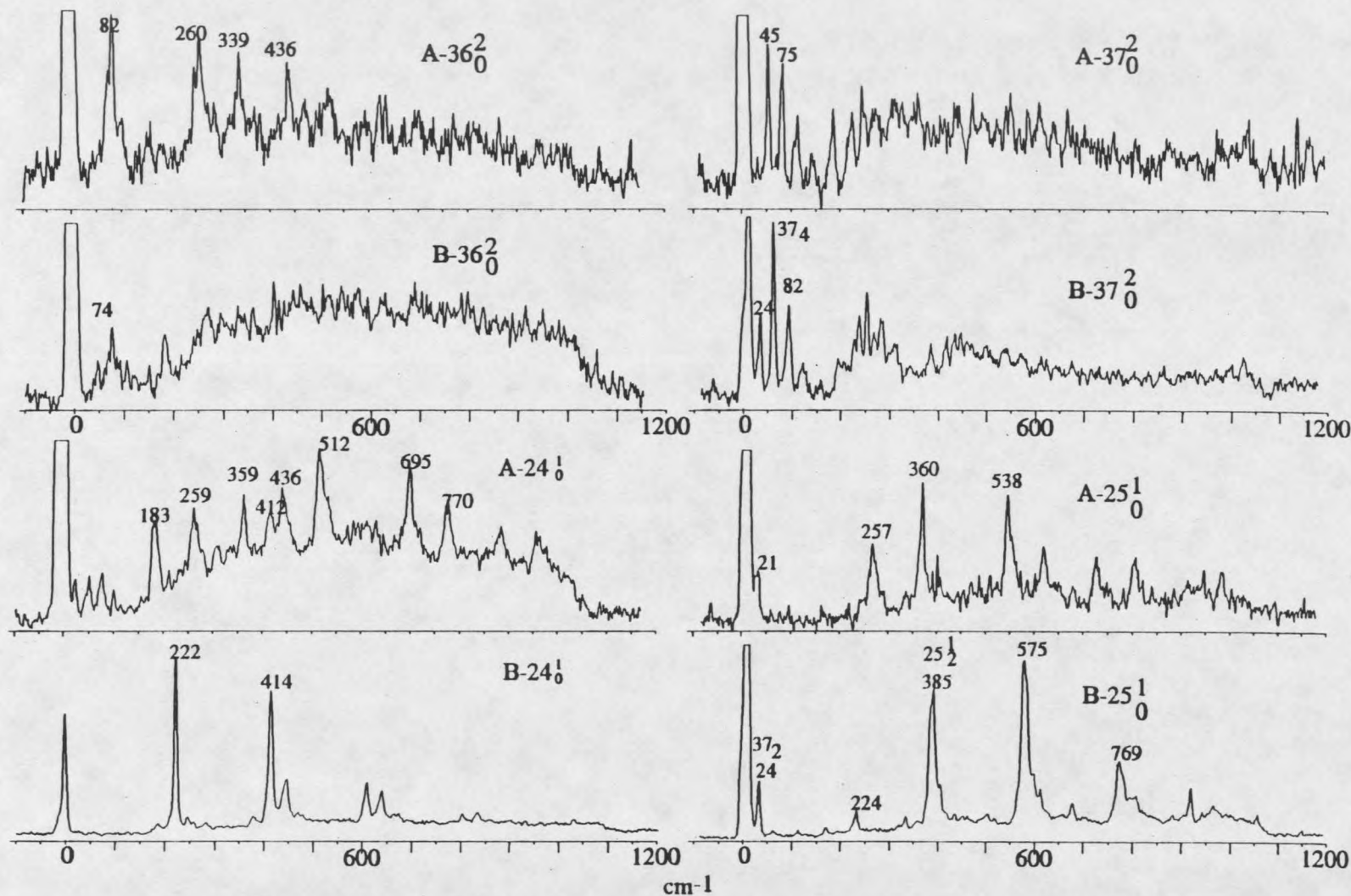


Figure 25: The dispersed fluorescence spectra of the low-frequency vibrations for the A and B conformers of p-methoxy-trans-stilbene.

There are several issues concerning this molecule that will be discussed in Chapter 7. These include the possibility of methoxy torsion, the conformation of the methoxy group for the two observed conformers, and a Fermi resonance.

p'-methoxy-p-methyl-trans-stilbene

P'-methoxy-p-methyl-trans-stilbene is a logical candidate for examination of how the electron donating capabilities of a substituent can affect the barrier to internal rotation of a methyl group over a conjugated π system. The 1hv FE spectrum, see Figure 26, is very similar to the p-methoxy-trans-stilbene spectrum discussed above in terms of the electronic and skeletal vibrational structure. The spectrum is very congested not only to the presence of the two conformers, but also to the methyl rotor structure built upon the two conformers and appearing in combination with the skeletal modes. The absolute frequency of the $A-0_0^0-0a_1$ has decreased to $30,517.4 \text{ cm}^{-1}$ upon methyl substitution, and the B origin is now $+266 \text{ cm}^{-1}$ above the A origin.

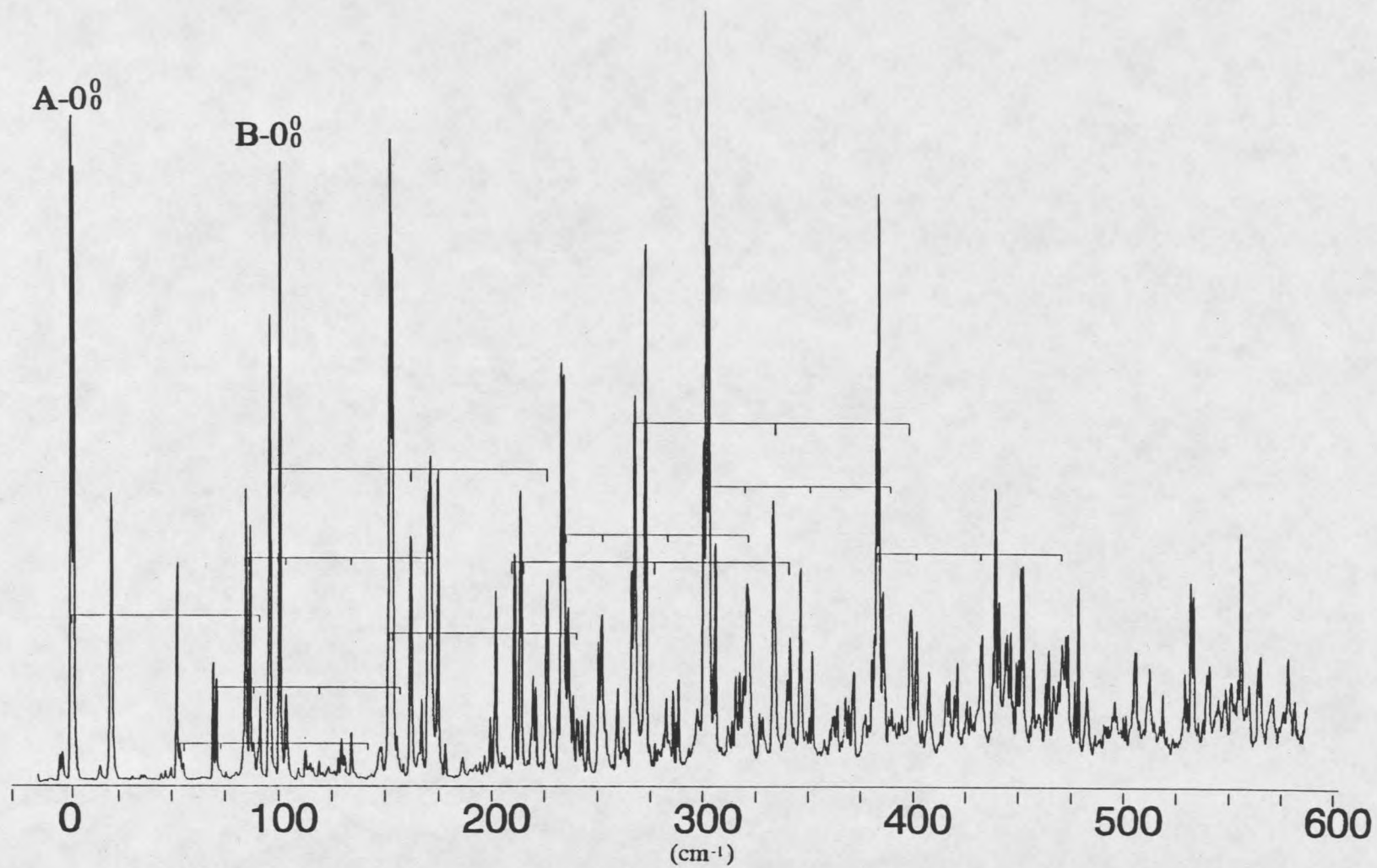
For comparison purposes, the B origin is aligned underneath the A origin in Figure 27. The lower trace contains many transitions assigned to the A conformer, complicating the assignments for the B conformer. Even though the only difference between the two origins is the conformation of the methoxy group, there are obvious frequency differences in the methyl torsional transitions between the conformers.

The splitting between the $1e-0a_1$ transitions for the A conformer is -3.2 cm^{-1} , and increases to -3.8 cm^{-1} for the B conformer, indicative of a change in the barrier to internal rotation as caused by the variations in the electron density induced by the conformation of the

methoxy group ten carbons away. For the A conformer, the $2e$ is assigned at $+46.7\text{ cm}^{-1}$, and the $3a_1$ is assigned at $+76.8\text{ cm}^{-1}$. The $4e$ and higher torsional transitions are unassigned due to their low intensity and spectral congestion. Due to the strong overlap in the spectra of the two conformers, it is difficult to make assignments for the B conformer with high confidence solely from the FE spectrum. For this reason, the assignments for the B conformer are largely based on information obtained from dispersed fluorescence. The $2e$ has increased in frequency to 48.8 cm^{-1} , and the $3a_1$ to 84.3 cm^{-1} compared to the A conformer for S_1 .

The assignment of the torsional transitions was verified using dispersed fluorescence (DF). The A conformer generally has weaker transitions and higher Franck-Condon activity making it difficult to obtain DF spectra with good S/N. Therefore the entrance slit had to be widened to $200\text{ }\mu$ for the spectra, compared to $100\text{-}150\text{ }\mu$ for the B conformer.

Several dispersed emission spectra from exciting the $A-0_0^0$ torsional levels are shown in Figure 28, including the $0a_1$, $1e$, $2e$, and $3a_1$ levels. Symmetry based selection rules state that the emission from an a_1 level must go to another a_1 level, and e to e levels. Exciting the $0a_1$ transition gives a transition at 54 cm^{-1} , which is assigned as the $3a_1$ in the ground state. This frequency is also observed in the emission following excitation of the $3a_1$ level of S_1 . A transition at 19 cm^{-1} is likely 37_2^0 . Excitation of the $1e$ for S_1 gives a transition at 21 cm^{-1} , the $2e$ for S_0 . The assignment of the $2e$ transition is more problematic, as the DF was very weak. There are two transitions in the FE spectrum for the A conformer that could be the $2e$, one at 38.0 cm^{-1} and the other at 46.7 cm^{-1} .



77

Figure 26: The 1hv FE spectrum of *p'*-methoxy-*p*-methyl-*trans*-stilbene. The conformer origins are identified with labels A and B.

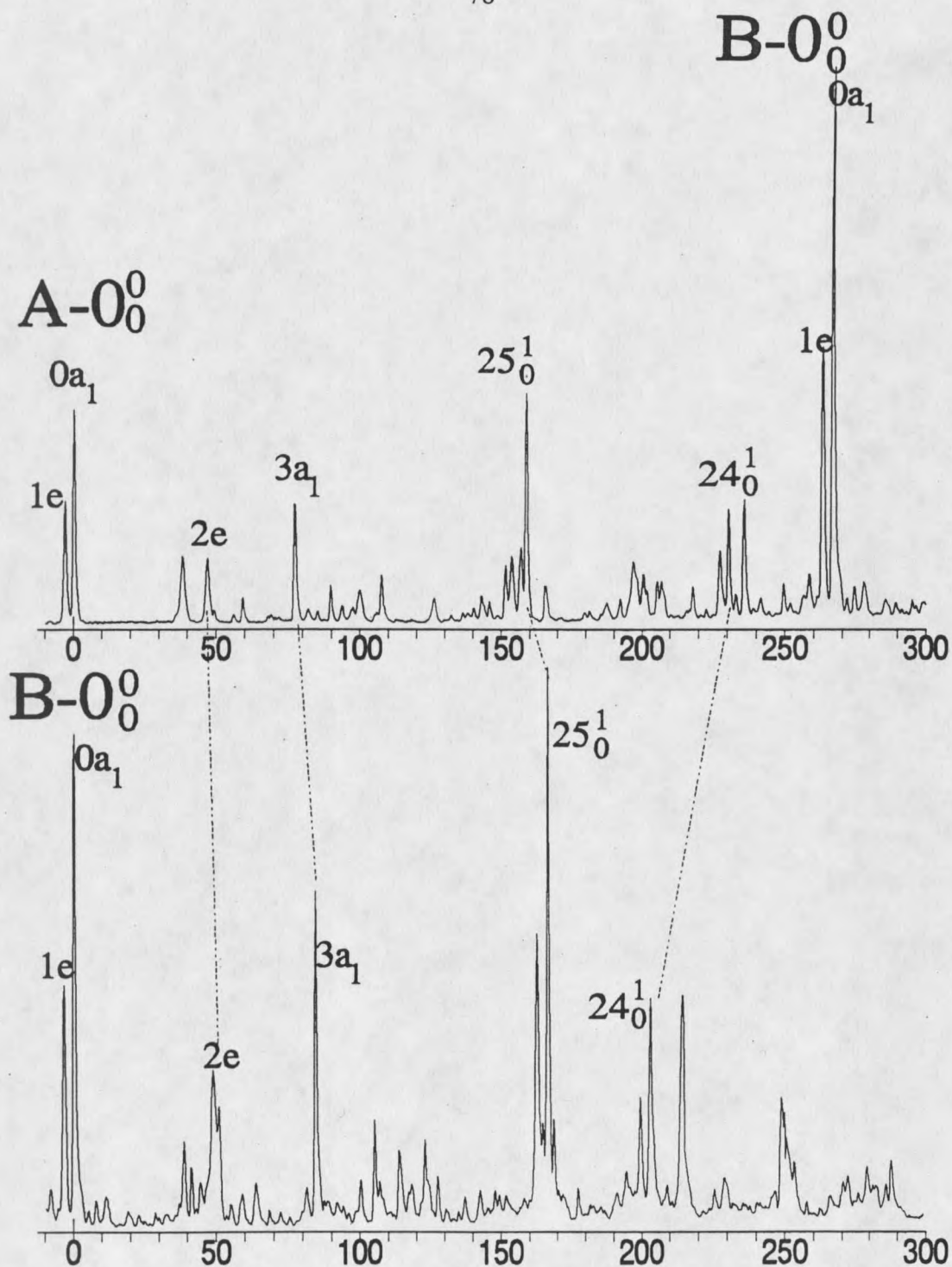


Figure 27: The first 300 cm^{-1} of the $1h\nu$ FE spectrum for each conformer. Note that the B conformer origin has been placed directly under the A origin for comparison purposes.

Based on the fact that we know the barrier is increasing between the conformers due to the $0a_1-1e$ and $3a_1$ frequencies and comparison of the observed vs. calculated intensities, we assign the $+46.7\text{ cm}^{-1}$ transition as the $2e$. Assignment of the $2e$ at 38.0 cm^{-1} does not give a calculated barrier that fits the frequencies of other torsional transitions and observed intensities well. P-methyl-trans-stilbene also has an unassigned transition at $+38.0\text{ cm}^{-1}$, and the assignment of this analogous transition will be discussed later. Frequencies for the torsional features are also confirmed by examining the DF from 25_0^1 .

The same techniques are used to assign the torsional features for the B conformer. The Franck-Condon factors for the B conformer are lower than those of the A conformer, and there may be an increased population for the B conformer. The DE spectrum of the B conformer origin indicates less vibrational activity than for the A conformer origin. Once again, the methyl barrier for S_0 is low, as indicated by the low frequency torsional features as seen in the DF in Figure 29. Emission from the B origin- $0a_1$ gives a transition at 52 cm^{-1} , the $3a_1$ in S_0 . This is verified by the emission from the B- $3a_1$, which has a S_0 frequency for $3a_1$ of 56 cm^{-1} , agreement within the resolution of the acquisition system. Excitation of the $1e$ gives a strong transition at 22 cm^{-1} , the assignment of $2e$ for S_0 . This is confirmed by dispersing the emission from the $+48.8\text{ cm}^{-1}$ transition, which has a comparable spectrum. The intensities for $4e$ and higher quanta transitions are weak, and they could not be assigned.

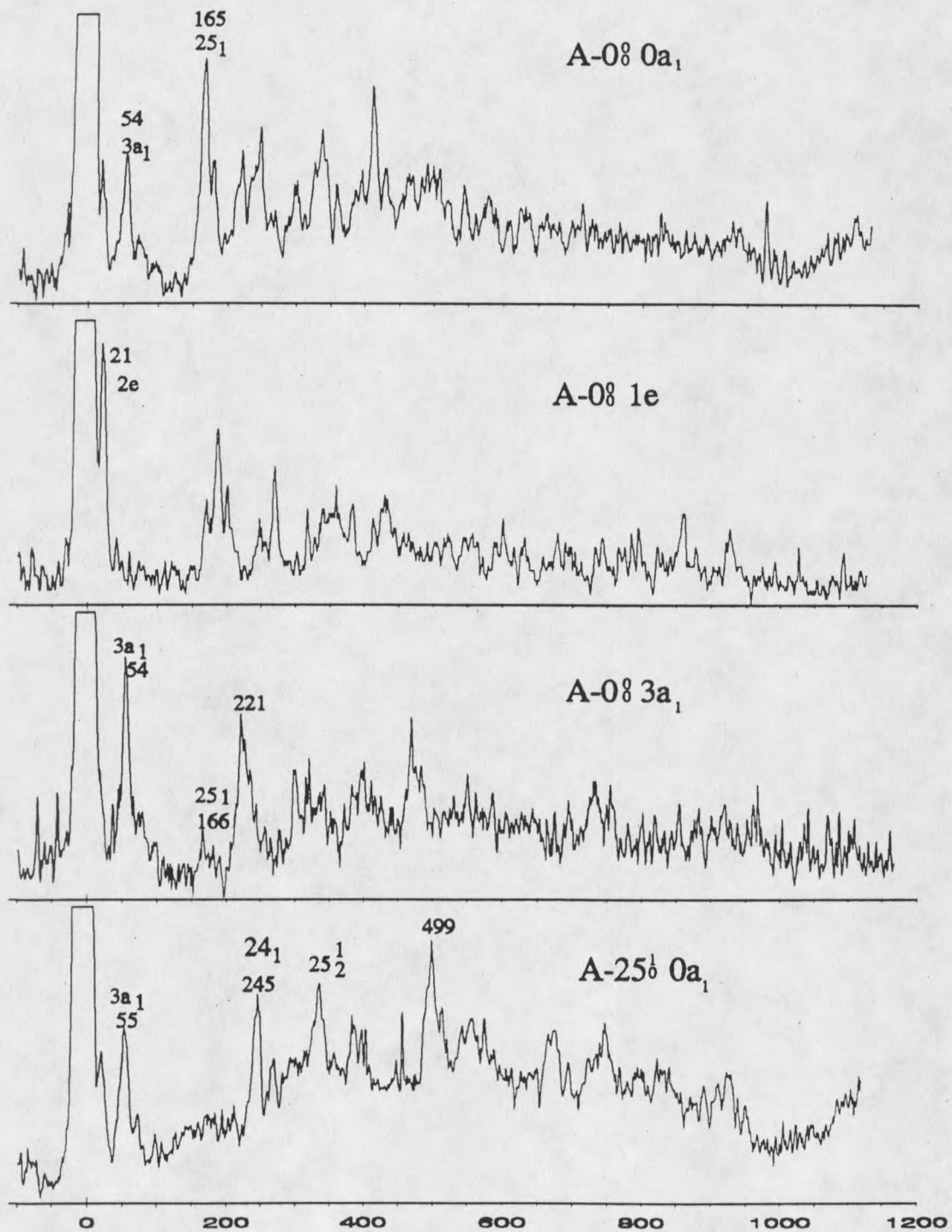


Figure 28: The DE from the A conformer torsional features of p'-methoxy-p-methyl-trans-stilbene.

Assignment of the low-frequency vibrational modes has proven to be more difficult. See Table 9 for assignment of most features. Substitution on both ends of the stilbene system may have changed some of the symmetry relationships, however, most of the vibrations are assigned and compare well to other stilbene derivatives based on a planar C_s symmetry. Once again the most prominent vibration is ν_{25} . As identified in the FE and DE spectra, the A conformer has 25^1 at 158.7 cm^{-1} , and 25_1 at 165 cm^{-1} . The ν_{25} frequency has increased for both states for the B conformer, $25^1 = 166.6 \text{ cm}^{-1}$ and $25_1 = 174 \text{ cm}^{-1}$. The ν_{24} vibration is once again a distinguishing vibration. For the A conformer, ν_{24} has a frequency in S_1 of 230.4 cm^{-1} , and a frequency in S_0 of 247 cm^{-1} . The B conformer has a ν_{24} frequency in S_1 of 203.5 cm^{-1} , and in S_0 of 216 cm^{-1} .

Assignment of 36_0^2 is tentative due to the absence of DE for this vibration. There is a transition at $A+59.4 \text{ cm}^{-1}$ that has the expected $1e-0a_1$ splitting, and this transition has a similar frequency to assigned ν_{36} frequencies in other stilbenes. For the B conformer 36_0^2 is tentatively assigned at $B+51.9 \text{ cm}^{-1}$.

Assignment of 37_0^2 is also tentative, as is the case for other para'-para-substituted stilbenes which will be discussed later. There are several weak intensity-low frequency transitions between 70 and 110 cm^{-1} that remain unassigned. None have the expected $0a_1-1e$ splitting that would be indicative of a vibrational mode, and higher torsional structure cannot be identified. The transitions are too weak to examine by DE using the current experimental methods. A transition at $A + 89.4 \text{ cm}^{-1}$ is tentatively assigned as $A-37_0^2$, based upon the frequencies of ν_{37} observed for other substituted stilbenes. The spectrum is too congested to assign 37_0^2 with any confidence for the B conformer.

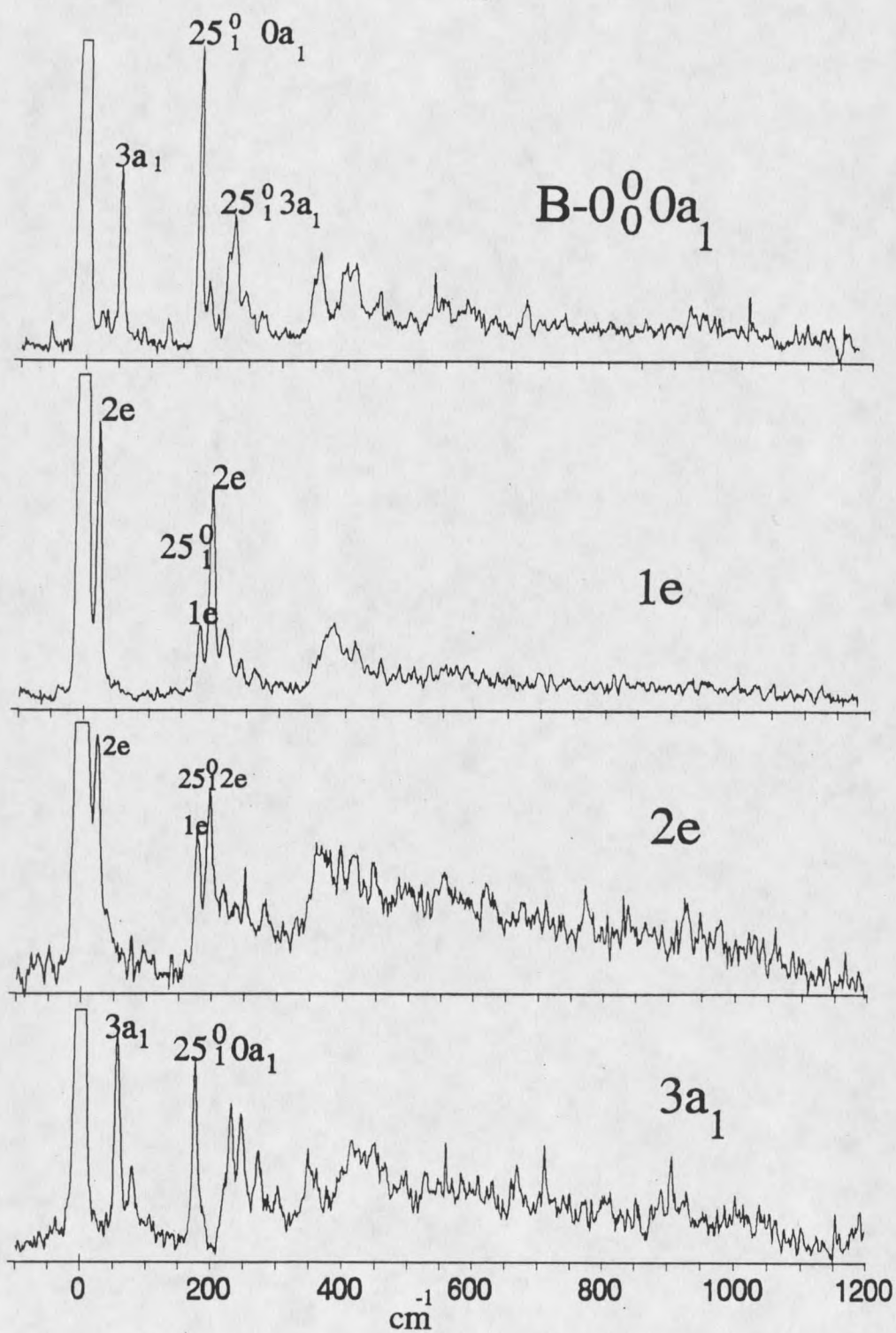


Figure 29: The DE from the $0a_1$, $1e$, $2e$, and $3a_1$ Transitions for the B Conformer of p'-methoxy-p-methyl-trans-stilbene.

The barrier to internal rotation has been fit for both conformers for S_0 and S_1 . See Table 10 for a comparison of the experimental and calculated frequencies and intensities. The barriers for the A conformer are $V_3'' = 17 \pm 2 \text{ cm}^{-1}$ and $V_3' = 91.8 \pm 1 \text{ cm}^{-1}$. The barriers for the B conformer are $V_3'' = 15 \pm 2 \text{ cm}^{-1}$ and $V_3' = 103.4 \pm 1 \text{ cm}^{-1}$. An internal rotation constant of $B = 5.30 \text{ cm}^{-1}$ was used for both electronic states. The intensity distribution for both conformers fits best with a 60° conformational change for CH_3 upon excitation. Issues regarding the barriers, vibrational assignments and conformers will be discussed further in Chapter 7.

Table 9: The torsional and vibrational frequencies for S_0 and S_1 of the A and B conformers of p'-methoxy-p-methyl-trans-stilbene. The ground state frequencies are expressed as combination differences.

assignment	A- S_0	A- S_1	B- S_0	B- S_1
$0a_1$	0 cm^{-1}	0 cm^{-1}	0 cm^{-1}	0 cm^{-1}
$1e$		-3.2		-3.8
$2e$	21	46.7	22	48.8
$3a_1$	54	76.8	52	84.3
X		38.0	37	38.6
$\nu_{36}, \nu=2$		59.4		51.9
$\nu_{72}, \nu=1$		154.2		169
$\nu_{25}, \nu=1$	165	158.7	174	166.6
$\nu_{24}, \nu=1$	247	230.4	225	203.5
$\nu_{25}, \nu=2$	335	318	357	334
$\nu_{25} + \nu_{24}$	412		399	636
$\nu_{25}, \nu=3$	499	476	526	767

Table 10: The experimental and calculated frequencies and intensities for the A and B conformers in S_1 for *p'*-methoxy-*p*-methyl-*trans*-stilbene.

torsional level	experimental frequency	calculated frequency	experimental intensity	calculated intensity
A-0a ₁	0	0	0.3082	0.342
A-1e	-3.2	-3.6	0.2169	0.207
A-2e	49.9	43.1	0.1749	0.234
A-3a ₁	76.8	78.4	0.1961	0.159
A-4e	107.6	102	0.1039	0.057
B-0a ₁	0	0	0.3384	0.3588
B-1e	-3.8	-4.0	0.186	0.2265
B-2e	48.8	47.2	0.2630	0.2356
B-3a ₁	84.3	84.5	0.2126	0.179

p'-chloro-*p*-methyl-*trans*-stilbene

The halogens are the next class of substituents to be examined for the stilbenes. The halogens are exceptions to the general rules of substituents for aromatic compounds.⁶⁶ Halogens are strongly electronegative, withdrawing electron density from the carbon atom through the sigma bond. At the same time the nonbonding electrons on the halogens donate electron density through pi bonding. The carbon-halogen bond is strongly polarized, with the carbon atom being at the positive end of the dipole. This polarization draws electron density away from the benzene ring, making it less reactive toward electrophilic substitution. The electron density throughout the conjugated system should be affected, and the barrier to internal rotation of the methyl group will be shown to be influenced by halogen substitution.

The halogenated stilbenes included in this study are p'-chloro-p-methyl-trans-stilbene, p'-chloro-m-methyl-trans-stilbene, and p'-fluoro-p-methyl-trans-stilbene.

P'-chloro-p-methyl-trans-stilbene was a molecule synthesized by several people⁶⁷ in the chemistry department, and all work was completed with less than 500mg of sample. The 1hv fluorescence excitation spectrum is shown in Figure 30. The absolute frequency of the $0a_1$ transition of the origin is $31,224.3 \text{ cm}^{-1}$. The spectrum shown had a point taken every 0.2 cm^{-1} , with a backing pressure of 1.0 bar helium. Helium complexes are still observed at this low pressure and higher backing pressures gave a spectrum extremely congested with multiple complexes. Even with the complex contribution reduced, the spectrum of this molecule becomes congested by 200 cm^{-1} due to combination bands.

The spectrum is very similar to p-methyl-trans-stilbene, but there is a shift in the torsional features. The $1e-0a_1$ splitting is -3.45 cm^{-1} . $2e$ is assigned at 50.1 cm^{-1} , and $3a_1$ at 85.1 cm^{-1} . $4e$ is tentatively assigned at 106.8 cm^{-1} , a transition that has the characteristic e broadening and is near the calculated $4e$ frequency. Higher members of the torsional progression cannot be identified due to lack of intensity and spectral congestion.

The assignments of the torsional transitions are supported by DF. Due to stronger fluorescence and improved alignment techniques for the CCD and monochromator, the origin's $1e$ and $0a_1$ DF spectra contain no significant scattered light due to the laser resonance, nearly all of the intensity is due to fluorescence. As shown in the top spectrum in Figure 31, excitation of the $0a_1$ transition gives the frequency of $3a_1$ for S_0 of 54 cm^{-1} . This is supported by excitation of the $3a_1$ level which also gives a transition at 55 cm^{-1} . The transition observed

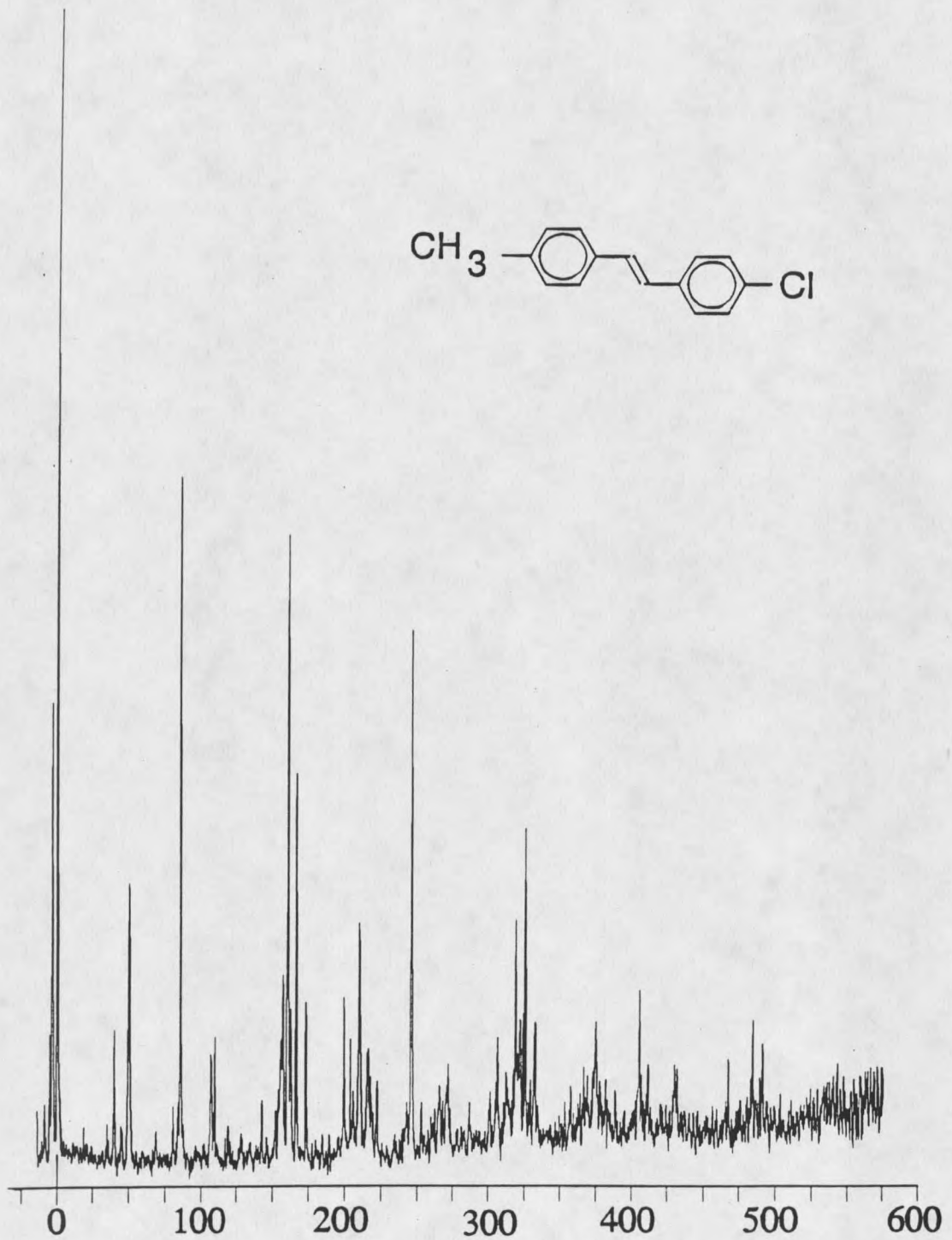


Figure 30: The 1h ν FE spectrum of p'-chloro-p-methyl-trans-stilbene.

in the $0a_1$ spectrum at 22 cm^{-1} is either due to excitation of the $1e$ due to spectral overlap, or more likely, the frequency of 37_2 for S_0 . The assignment of ν_{37} in both states is still tentative as it is not readily identified in the excitation spectrum. If the 22 cm^{-1} transition is indeed 37_2^0 , its low intensity is consistent with the lack of a strong 37_0^2 band in the excitation spectrum.

Excitation of the $1e$ yields the expected e progression in the ground state with a frequency of 21 cm^{-1} for $2e$ in the ground state. Assignment of $2e$ in the excitation spectrum was initially tentative as there are two transitions near the expected frequency of $2e$, similar to the low-frequency regions in other stilbene analogues. These are at 39.8 cm^{-1} and 50.1 cm^{-1} . Both transitions are broader than the assigned a_1 levels, characteristic of e levels. Based on the intensities of the transitions and frequencies of the rest of the torsional structure, the transition at 50.1 cm^{-1} is assigned as the $2e$. The dispersed fluorescence is fairly weak, but gives a peak at 21 cm^{-1} for the $2e$ of S_0 .

The 39.8 cm^{-1} transition appears to be analogous to $\sim 40\text{ cm}^{-1}$ transitions present in other methylated stilbenes. There are several low frequency transitions that remain unassigned that could be other members of an e only progression of this vibration.

37^2 remains unassigned as discussed above, as does ν_{36} . The $3a_1$ transition has shoulders that could be 37_0^2 . Other members of their torsional progressions are unaccounted for. The most prominent vibration is once again 25^1 , with its $0a_1$ at $+159.9\text{ cm}^{-1}$, and its $1e$ at 156.6 cm^{-1} . The Franck-Condon factors for ν_{25} show intensity out to three quanta in the excited state. The first 600 cm^{-1} of the spectrum was acquired as after this point it is very congested. In the ground state, as can be seen in Figure 31, the frequency for 25_1 is 169 cm^{-1} , 25_2 is 345 cm^{-1} , and 25_3 is 514 cm^{-1} . If the progression in ν_{25} is harmonic it would be

expected to be at 507 cm^{-1} . The excited state for ν_{25} is slightly anharmonic as is the case for several other stilbenes, however, we cannot be confident with the degree of anharmonicity in S_0 since the resolution is $\approx 6\text{ cm}^{-1}$ and anharmonicity typically lowers the frequency.

By analogy with the ν_{24} frequencies in the other stilbenes, we assign the transition at 222 cm^{-1} in S_1 as 24_0^1 for p'-Cl-p-Me-trans-stilbene. The torsional progression can also be assigned for this skeletal mode. In the ground state, 24_1 has a frequency of 258 cm^{-1} .

Table 11: The experimental and calculated frequencies/intensities for p'-chloro-p-methyl-trans-stilbene. ($V_3 = 104.3\text{ cm}^{-1}$, $V_6 = 4.9\text{ cm}^{-1}$, 60° conformation change.)

assignment	experimental frequency	calculated frequency	experimental intensity	calculated intensity
$0a_i$	0 cm^{-1}	0	.3241	.2983
$1e$	-3.45	-3.46	.1686	.1555
$2e$	50.1	49.4	.2618	.2656
$3a_i$	85.0	84.8	.1835	.2405
$4e$	106.8	107.8	.0619	.0758
$5e$		155		

The barrier to internal rotation for the methyl group has been fit for both S_0 and S_1 . The barrier for S_0 is $V_3'' = 25.0\text{ cm}^{-1}$ with no contribution from V_6 . The internal rotation constant is $B'' = B' = 5.4\text{ cm}^{-1}$. The first excited state fit is $V_3' = 104.3\text{ cm}^{-1}$ with a small contribution of $V_6' = 4.9\text{ cm}^{-1}$. Based on the observed intensities in both states, it was found that a 60° conformational change occurs for the CH_3 . See Table 11 for the experimental and calculated frequencies and intensities of the methyl rotor transitions in the excited state. The

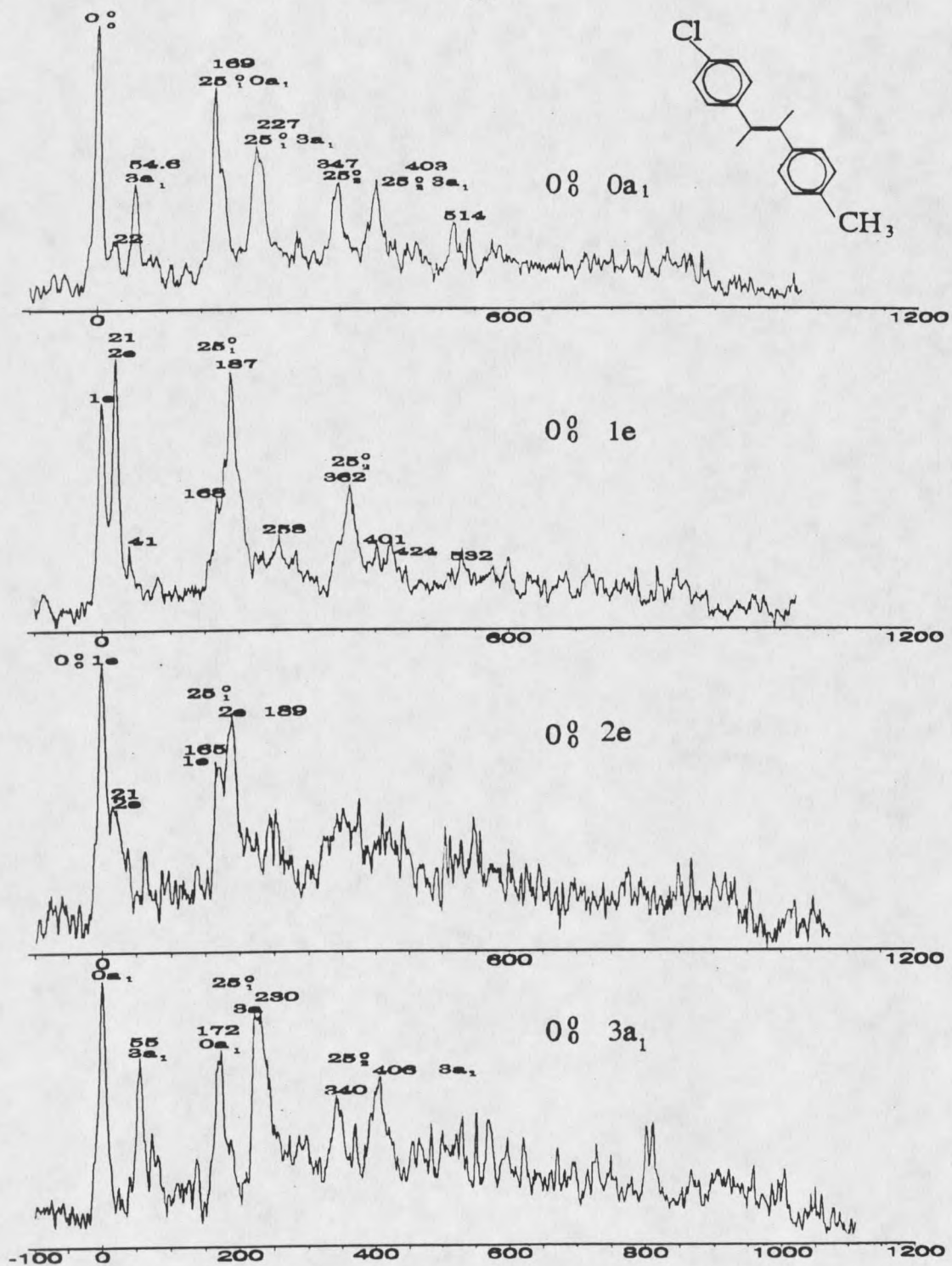


Figure 31: The DE of the 0° methyl rotor structure for p'-chloro-p-methyl-trans-stilbene.

fits for the ground state are not shown as they are very comparable to the ground states of all of the other presented stilbene analogues.

p'-fluoro-p-methyl-trans-stilbene

The next compound examined is p'-fluoro-p-methyl-trans-stilbene. Since fluorine is the most electronegative element, there should be some effect felt by the methyl group ten carbons away. The similarity between the p'-chloro- and p'-fluoro-p-methyl-trans-stilbene is striking, however, there are some subtle differences brought upon by mass affects and/or changes in the electron density. See Figure 32 for the 1hv fluorescence excitation spectrum of p'-fluoro-p-methyl-trans-stilbene. The absolute frequency of the origin $0a_1$ is $31,585.3 \text{ cm}^{-1}$.

The barrier to internal rotation for the methyl group has been slightly altered upon the substitution of a fluoro group for the chloro group. In the excitation spectrum, the $1e$ is -3.6 cm^{-1} from the $0a_1$. The $2e$ is assigned at 49.4 cm^{-1} , however, there is once again the "X" transition at 40.5 cm^{-1} . The $3a_1$ is now at 82.6 cm^{-1} . The $4e$ level is assigned at 106.3 cm^{-1} . There are several other unexplained transitions in the first 150 cm^{-1} of the spectrum.

The assignment of the torsional levels of the excited state is supported by the dispersed fluorescence from each transition. The $0a_1$ and $1e$ spectra contain no significant scattered light due to the laser. See Figure 33. Excitation of the $0a_1$ and $3a_1$ transitions yield a frequency of 54 cm^{-1} for $3a_1$ in S_0 . The $2e$ is identified at 21 cm^{-1} . Also included in the figure is the DE from the X and $2e$ transitions. They are very similar in the fact that they both appear to be of e character. The calculated intensities from exciting the $2e$ transitions

and dispersing the emission better match the spectrum from the 49.4 cm^{-1} level, supporting the $2e$ assignment. Calculations were also performed using the X frequency as the $2e$ transition in calculating the S_1 methyl rotor barrier, however, neither the frequencies or intensities fit the data as well.

The barrier for the ground state of p'-fluoro-p-methyl-trans-stilbene is calculated to be 27.8 cm^{-1} . This low barrier is very similar to all of the other stilbene analogues presented. The barrier for S_1 is slightly lower than the one calculated for p'-chloro-p-methyl-trans-stilbene, showing that there is a slight effect upon changing the chloro for the fluoro group. The change in barrier is likely brought upon by the change in electronegativity between chlorine and fluorine. The barrier for S_1 is calculated using 49.4 cm^{-1} level as the $2e$ level, resulting in $V_3 = 100.5 \text{ cm}^{-1}$, $V_6 = 12 \text{ cm}^{-1}$ and $B' = 5.4 \text{ cm}^{-1}$. The experimental and calculated frequencies are shown in Table 12.

Table 12. The calculated and experimental torsional frequencies for p'-fluoro-p-methyl-trans-stilbene. ($V_3 = 100.5 \text{ cm}^{-1}$, $V_6 = 12 \text{ cm}^{-1}$).

assignment	experimental frequency	calculated frequency
$0a_1$	0 cm^{-1}	0 cm^{-1}
$1e$	-3.6	-3.6
$2e$	49.4	49.4
$3a_1$	82.6	82.6
$4e$	109.9	110.4

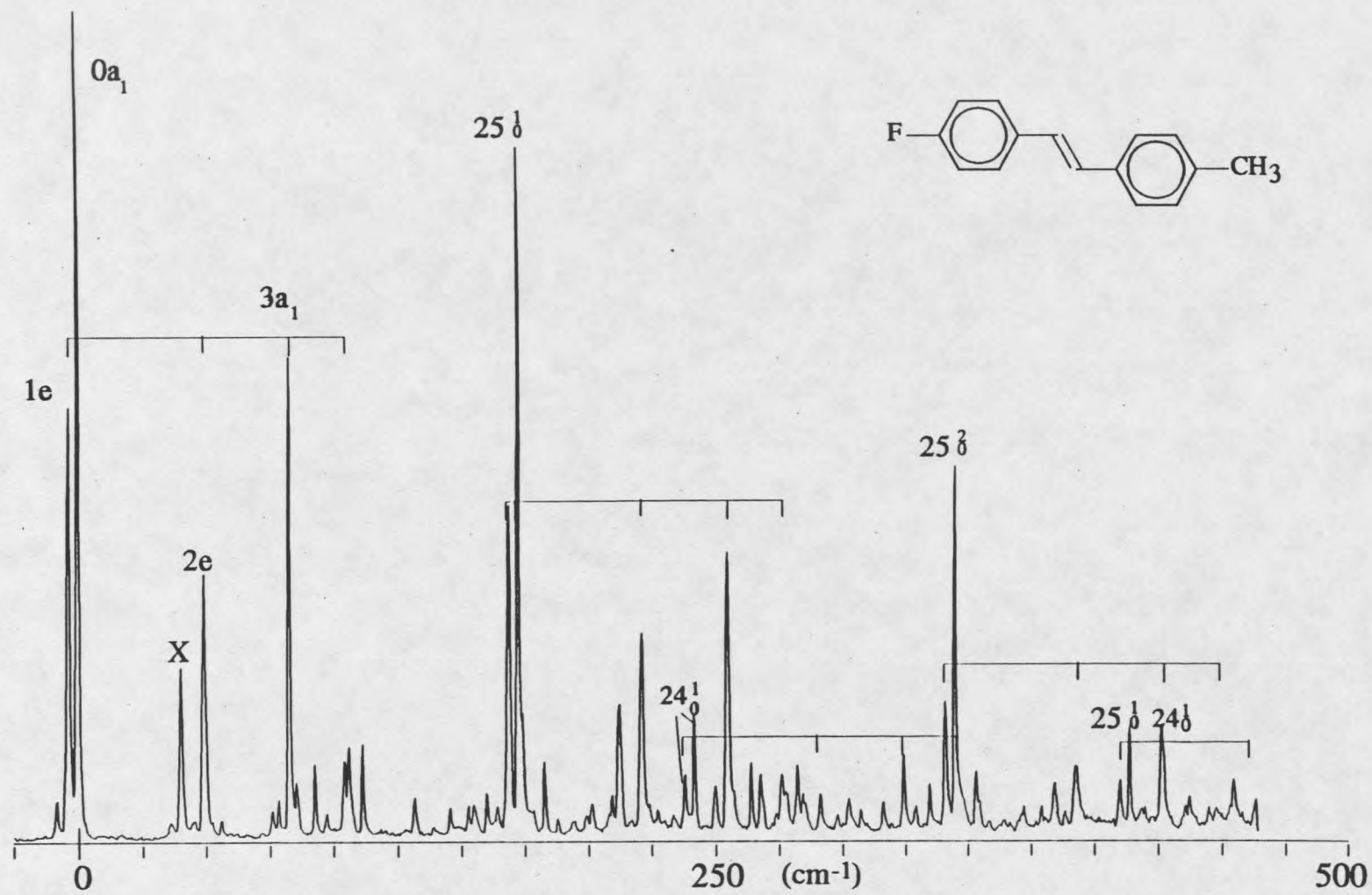


Figure 32: The 1hv FE spectrum of p'-fluoro-p-methyl-trans-stilbene.

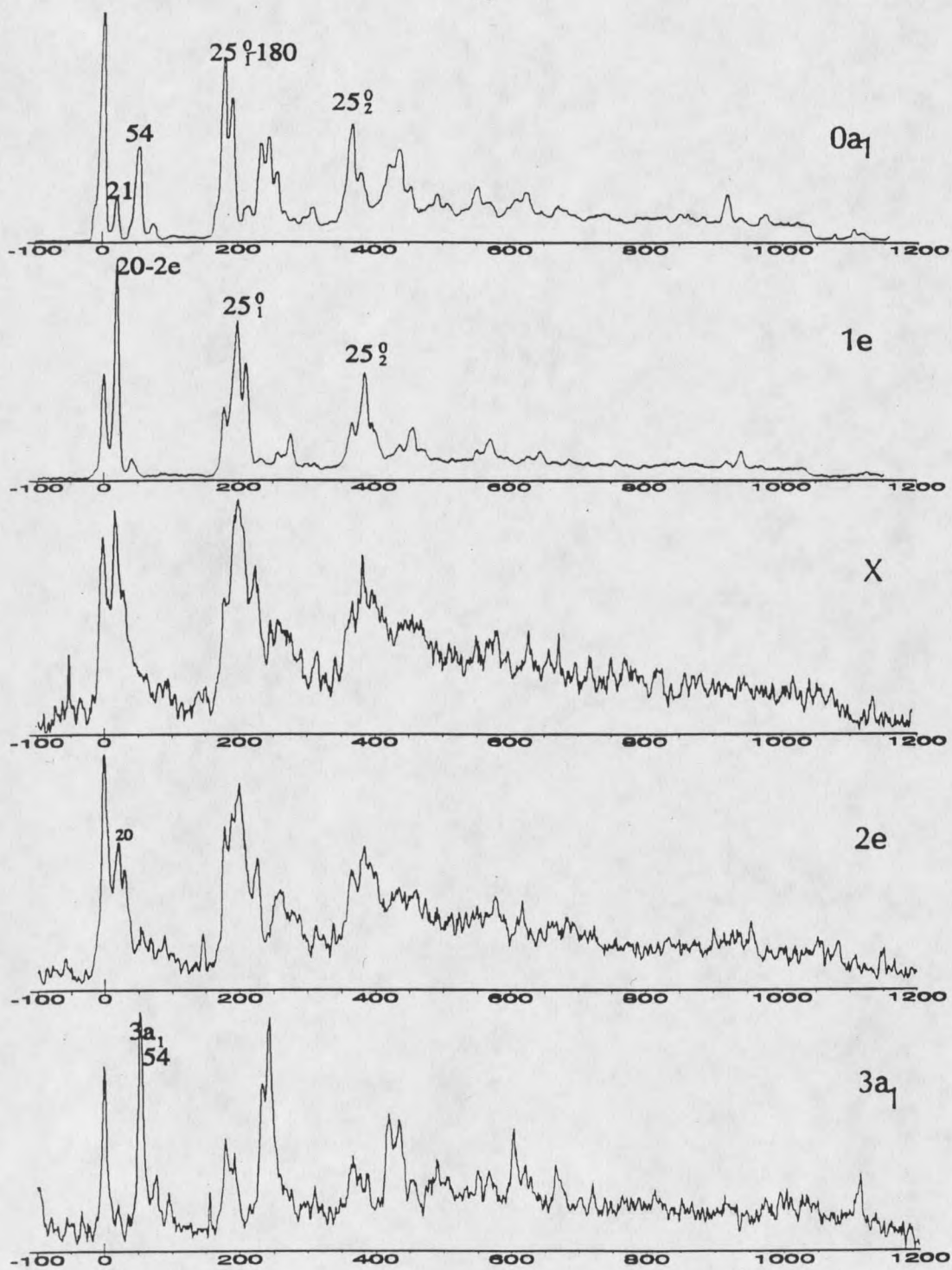


Figure 33: The DF of the rotor levels for p'-fluoro-p-methyl-trans-stilbene.

